Aus dem Leibniz-Institut für Molekulare Pharmakologie (FMP) Berlin

DISSERTATION

Photoinactivation of Glutamate Receptors by Genetically Encoded Unnatural Amino Acids

zur Erlangung des akademischen Grades

Doctor of Philosophy (PhD)

vorgelegt der Medizinischen Fakultät
Charité – Universitätsmedizin Berlin

von

Viktoria Klippenstein

aus Orlowka, Kirgisistan

Datum der Promotion: 30.05.2015

Contents

List of figures and tables

Abbreviations

A	Alanine
(aa)RS	(Aminoacyl-) tRNA-synthetase
ad.	adde
AMPA	α-amino-3- hydroxyl-5-methyl-4-isoxazole-propionate
ATD	Amino-terminal domain
ATP	Adenosine 5′-triphosphate
AzF	*p*-Azido-L-phenylalanine
BSA	Bovine serum albumin
Bst	*Bacillus stearothermoühilus*
BzF	*p*-Benzoyl-L-phenylalanine
C	Cysteine
CA1	Cornu ammonis 1
CMV	Cytomegalovirus
CNIH	Cornichon
CTD	Carboxyl-terminal domain
CTZ	Cyclothiazide
D	Aspartic acid
D1	Upper lobe of the LBD
D2	Lower lobe of the LBD
DDM	Dodecylmaltoside
DNA	Deoxyribonucleic acid
DNQX	6,7-Dinitroquinoxaline-2,3-dione
dNTP	Deoxynucleotide mix
DSMZ	Deutsche Sammlung von Mikroorganismen und Zellkulturen
E. coli / *Ec*	*Escherichia coli*
EF	Elongation factor
(e)GFP	(Enhanced) green fluorescent protein
EGF(R)	Epidermal growth factor (receptor)
EPSC	Excitatory postsynaptic current

et al.	et (and) alii (others)
ER	Endoplasmatic reticulum
F	Phenylalanine
F1 / F2	Flanking primers 1 / 2
FBS	Fetal bovine serum
FTIR	Fourier transform infrared
G	Glycine
GABA	γ-Aminobutyric acid
Glu	Glutamate
GPCR	G-protein coupled receptor
GRB2	Growth factor receptor-bound protein 2
GST	Glutathione S-transferase
h	Hours
HEK-293(T)	Human embryonic kidney-293(T) cells
5-HT_{3A}R	Serotonin-gated receptor
IF	Initiation factor
(i)GluR	(Ionotropic) glutamate receptor
IRES	Internal ribosome entry site
I_{ss}	Steady-state current
IV	Current-voltage
LacZ	Lactose operon
LBD	Ligand-binding domain
L	Leucine
Leu	Leucyl-
LTD	Long-term depression
LTP	Long-term potentiation
M	Methionine
m1 / m2	Mutagenic primers 1 / 2
MEM	Minimum essential medium
min	Minutes
Mj	*Methanococcus jannaschii*

mRNA	Messenger RNA
ms	Milliseconds
MTS	Methane thiosulfonate
MW	Molecular weight
nAChR	Nicotinic acetylcholine receptors
NEM	N-ethyl-maleimide
NMDA	*N*-methyl-D-aspartate
ORF	Open reading frame
overlap PCR	Overlap polymerase chain reaction
PDB	Protein data bank
PEI	Polyethylenimine
PLL	Poly-L-lysine
Pyl	Pyrrolysyl-
Q	Glutamine
R	Arginine
RBP1	Retinol binding protein 1
RF	Peptide release factor
RNA	Ribonucleic acid
rpm	Revolutions per minute
RR	Rectification ratio
RT	Room temperature
s	Seconds
S	Serine
SOC	Super optimal broth with catabolite repression
SV40	Simian virus 40
TAA	Ochre stop codon
TAG	Amber stop codon
TARP	Transmembrane AMPA receptor regulatory proteins
TGA	Opal stop codon
T_m	Melting temperature
TMD	Transmembrane domain

tRNA	Transfer RNA
Trp	Tryptophanyl-
Tyr	Tyrosyl-
U	Unit
UAA	Unnatural amino acid
UV	Ultraviolet
(*v/v*)	Volume / volume
WT	Wild-type
(*w/v*)	Mass / volume
Y	Tyrosine

Abstract (English)

Ionotropic glutamate receptors (iGluRs) are ubiquitous in the mammalian brain and the AMPA-subtype is essential for fast, glutamate-activated postsynaptic currents. In the framework of this study, photoactive unnatural amino acid (UAA) crosslinkers as *p*-Benzoyl-L-phenylalanine (BzF, also known as Bpa) or *p*-Azido-L-phenylalanine (AzF) were incorporated site-specifically into AMPA receptors expressed in mammalian cells. Incorporation was performed via genetically encoded UAA mutagenesis using specific orthogonal tRNA / tRNA-synthetase pairs. This approach has been shown to be a powerful extension of site-directed mutagenesis, which has allowed systematic structure-function studies of a range of ion channels, however, its application to ligand-gated ion channels as the glutamate receptors has been sparse. The aim of this study was the extension of the use of UAAs in photoinactivation of AMPA receptors. The establishment and thorough characterization of UAA photocrosslinking in AMPA receptors has been a fundamental part of the study. Methodologically, UV-driven photocrosslinking was detected by means of rapid perfusion outside-out patch-clamp electrophysiology, and assessed by biochemical experiments.

Electrophysiological measurements revealed, that receptors rescued by incorporation of AzF or BzF within the lower ligand-binding domain (LBD) interface had nearly invariably similar properties to wild-type (WT) channels and were expressed at similar levels. BzF incorporation at these subunit interfaces within the LBD allowed photocrosslinking of subunits, which was induced by UV irradiation at 365 nm from a mercury lamp. Photoinactivation was characterized by peak current reduction of ~90% within ~10 seconds of cumulative UV exposure. BzF incorporation led to selective and potent UV-driven photoinactivation of both homomeric (GluA2) and heteromeric (GluA2:GluA1) AMPA receptors. State dependence of trapping at two sites in the lower lobe of the LBD is consistent with deformation of the LBDs as well as intersubunit rearrangements during AMPA receptor desensitization.

These experiments demonstrate, that UAAs are a useful tool for exploring structural rearrangements of the AMPA receptor and suggest relevant applications of photoinactivation of glutamate receptor ion channels in native systems.

Abstract (German)

Ionotrope Glutamatrezeptoren (iGluRs) gehören zu einer der häufigsten Rezeptorfamilien in unserem Gehirn, wobei der AMPA-Subtyp mit seiner Erzeugung von glutamat-aktivierten elektrischen Strömen in der Postsynapse eine zentrale Rolle bei der Signalübertragung zwischen Nervenzellen spielt. Im Rahmen dieser Arbeit wurden photoaktive unnatürliche Aminosäuren wie *p*-Benzoyl-L-phenylalanin (BzF, auch bekannt als Bpa) oder *p*-Azido-L-phenylalanin (AzF) positions-spezifisch innerhalb von AMPA-Rezeptoren eingebaut, die in Säugetierzellen (HEK-293) exprimiert wurden. Der Einbau erfolgte über die so genannte genetisch-kodierte unnatürliche Aminosäure-Mutagenese, die auf die Verwendung spezifischer orthogonaler tRNA / tRNA-Synthetase-Paare beruht. Die Nutzung unnatürlicher Aminosäuren hat sich in früheren Studien als eine leistungsstarke Erweiterung der herkömmlichen positions-spezifischen Mutagenese bewiesen und erlaubte systematische Struktur-Funktions-Studien an einer Reihe von Ionenkanälen. Ihre Anwendung auf Liganden-gesteuerte Ionenkanäle, wie etwa der Glutamatrezeptoren, war jedoch bislang spärlich. Das Ziel dieser Studie bestand darin, die Nutzung von unnatürlichen Aminosäuren auf AMPA-Rezeptoren zu übertragen und dadurch ihre Photoinaktivierung auszulösen. Die Etablierung sowie gründliche Charakterisierung der Photoinaktivierung von AMPA-Rezeptoren mittels unnatürlicher Aminosäuren war ein grundlegender Bestandteil der Studie. Die Rezeptorphotoinaktivierung wurde methodisch mittels elektrischer Stromableitungen aus “outside-out patches” nach rascher Glutamatperfusion untersucht und die Ergebnisse wurden durch biochemische Experimente bestätigt.

Die elektrophysiologischen Messungen haben ergeben, dass die unnatürlichen Aminosäuren AzF und BzF erfolgreich in die untere Ligandenbindedomäne (LBD) des Rezeptors eingebaut wurden, wobei die mutierten AMPA-Rezeptoren ähnliche kinetische Eigenschaften wie die Wildtyp (WT)-Ionenkanäle zeigten. Der orts-spezifische Einbau von BzF in die LBD erlaubte eine Vernetzung von Rezeptoruntereinheiten, welche durch eine UV-Bestrahlung bei 365 nm aus einer Quecksilberlampe induziert wurde. Die Photoinaktivierung zeichnete sich durch eine 90%ige Reduzierung der Amplitude des abgeleiteten Stromes innerhalb von ~10 Sekunden kumulativer UV-Belichtung aus. Der Einbau von BzF führte zu einer selektiven UV-ausgelösten Photoinaktivierung sowohl in homomeren (GluA2) als auch in heteromeren (GluA2:GluA1) AMPA-Rezeptoren. Dadurch konnten verschiedene funktionale Zustände des Rezeptors

eingefangen werden, die der vorausgesagten Verformung der LBDen, sowie der strukturellen Umlagerungen während der AMPA-Rezeptor-Desensibilisierung, entsprachen.
Die präsentierten Ergebnisse zeigen, dass unnatürliche Aminosäuren hervorragend dazu geeignet sind, strukturelle Änderungen von AMPA-Rezeptoren zu untersuchen und dementsprechend die Anwendung der Photoinaktivierung auf native Systeme übertragen werden könnte.

1 INTRODUCTION

1.1 Structural and functional properties of ionotropic glutamate receptors (iGluRs)

1.1.1 Physiological relevance of iGluRs

Fast excitatory synaptic transmission in the mammalian central nervous system is mediated by ionotropic glutamate receptors (iGluRs). The family of iGluRs comprises three major classes – the AMPA (*α*-amino-3-hydroxyl-5-methyl-4-isoxazole-propionate), kainate, and NMDA (*N*-methyl-D-aspartate) subtypes, all ligand-gated ion channels, named after their eponymous high-affinity agonists, and defined by their physiological properties (Collingridge & Lester, 1989; Dingledine et al., 1999; Traynelis et al., 2010). In addition, another subfamily of iGluRs has been described based on sequence homology – the orphan subunits delta1 and delta2. (Yamazaki et al., 1992; Araki et al., 1993; Lomeli et al., 1993; Schmid & Hollmann, 2008; Ryu et al., 2012).

The different subtypes of the iGluR family are expressed at ~70–80% of brain synapses. During excitatory neurotransmission, binding of presynaptically released glutamate results in ion channel pore opening and a transduction of an electrical signal, causing postsynaptic depolarization and generation of excitatory postsynaptic currents (EPSCs; Traynelis et al., 2010). Thus, the AMPA receptor density within the active zone contributes to activity-dependent processes as long-term potentiation (LTP, strengthening of synapses), or long-term depression (LTD, weakening of synapses), which may form the cellular basis for cognitive functions such as learning and memory (Malinow & Malenka, 2002; Shepherd & Huganir, 2007).

Dysregulation of the glutamatergic cycle, including glutamate metabolism, glutamate release from presynaptic vesicles, receptor signalling, and re-uptake of the neurotransmitter, can have impact on numerous neuronal dysfunctions. Vesicle packaging and glutamate release can be perturbed by stress or psychotropic drugs (Musazzi et al., 2010). Malfunction of fast glutamate removal from the synaptic cleft can have neurotoxic effects (Hardingham et al., 2002; Leveille et al., 2008). Decreased glutamate activity in limbic, cortical, and hippocampal brain structures involving AMPA and NMDA receptors has been described to be associated with schizophrenia (Rubio et al., 2012; Menniti et al., 2013). Further neurological and psychiatric disorders affected

by iGluRs include brain ischemia (Choi & Rothman, 1990; Johnston et al., 2001; Al Rahim & Hossain, 2013), mood disorders (Alt et al., 2006), Alzheimer´s disease (Butterfield & Pocernich, 2003), and amyotrophic lateral sclerosis (Spalloni et al., 2012). Furthermore, psychostimulants such as cocaine induce long-term changes in glutamatergic neurotransmission by increased AMPAR function (Bellone & Lüscher, 2006; Bowers et al., 2010). Thus, understanding of the glutamate receptor structure and function is not only crucial for the understanding of brain functions including learning and memory, but also of various diseases.

1.1.2 The structure and function of the AMPA receptor subfamily

The first glutamate receptor subunit, GluK1, was cloned in 1989 (Hollmann et al., 1989). 17 further GluR subunit genes were subsequently cloned, which formed a fundamental starting point for future studies of glutamate receptor structure, function, and physiology (Boulter et al., 1990; Keinänen et al., 1990; Sakimura et al., 1990; Moriyoshi et al., 1991; Meguro et al., 1992). Despite functional differences, all iGluR classes share a common structural design. All are integral membrane-proteins built up of four subunits (>900 amino acids each). Each subunit contains a large extracellular part, formed by the amino-terminal domain (ATD) and the ligand-binding domain (LBD), a transmembrane domain (TMD), and an intracellular carboxyl-terminal domain (CTD; Traynelis et al., 2010).

Functional receptors can be homomeric (Boulter et al., 1990; Sommer et al., 1992; Rosenmund et al., 1998), but all classes of iGluRs preferentially form heteromeric complexes of tetramers in their native environment, with different combinations of GluA1-4 for AMPA, GluK1-K5 for kainate, and GluN1/N2A-D/GluN3A-B for NMDA receptors, thus decorating receptor complexes with various biophysical properties (Christensen et al., 2004; Lu et al., 2009; Paoletti et al., 2013). Receptors assemble from subunits within the same receptor class (Hollmann & Heinemann, 1994; Laube et al., 1998). The assembly of tetramers occurs in the endoplasmatic reticulum (ER) and proceeds in two steps – (*i*) the dimerization of two subunits, followed by (*ii*) the dimer-of-dimers formation (Ayalon & Stern-Bach, 2001; Schorge & Colquhoun, 2003; Shanks et al., 2010). Heteromeric subunit combinations vary depending on the brain region and the developmental state (Shepherd & Huganir, 2007). For example, at mature hippocampal excitatory synapses, AMPA receptors predominantly form heteromers between GluA2 and

GluA1 (which represents ~80% at CA1 synapses and ~95% of extrasynaptic AMPA receptors), or GluA2 and GluA3 respectively (Wenthold et al., 1996; Lu et al., 2009). Heteromers between GluA2 and GluA4 are also formed, but mainly in immature neurons of the hippocampus (Zhu et al., 2000).

The first structural information about the subunit arrangement of AMPA receptors derived from isolated LBDs (Armstrong et al., 1998). To date, ~120 high-resolution structures of the soluble AMPA receptor LBDs and six structures of the ATDs were solved providing insights into the dimeric organization of these domains (Kuusinen et al., 1999; Armstrong & Gouaux, 2000; Sun et al., 2002; Armstrong et al., 2006; Jin et al., 2009). The dimeric arrangement of the four subunits has been further supported by electron-microscopy studies (Tichelaar et al., 2004; Nagakawa et al., 2005). The first, and up to now, only full-length structure of an AMPA receptor was described in 2009 (**Figure 1 A**; PDB 3KG2; Sobolevsky et al., 2009). It represents an antagonist-bound (closed pore) homomeric rat GluA2 receptor with a 3.6 Å resolution. It confirmed, in accordance to previous studies, that both the ATDs and the LBDs are organized as two-fold symmetrical dimer-of-dimers, and revealed an unexpected symmetry mismatch of these dimer pairs between the ATD and the LBD. Dimer pairs form between subunits A/B and C/D in the ATD, and subunits A/D and B/C in the LBD (**Figure 1 B & C**). The extracellular two-fold symmetry dissolves within the TMD, which shows a four-fold symmetric arrangement (**Figure 1 D**). The swap of partners within dimers of the ATD and LBD was further functionally confirmed for GluK2 receptors (Das et al., 2010).

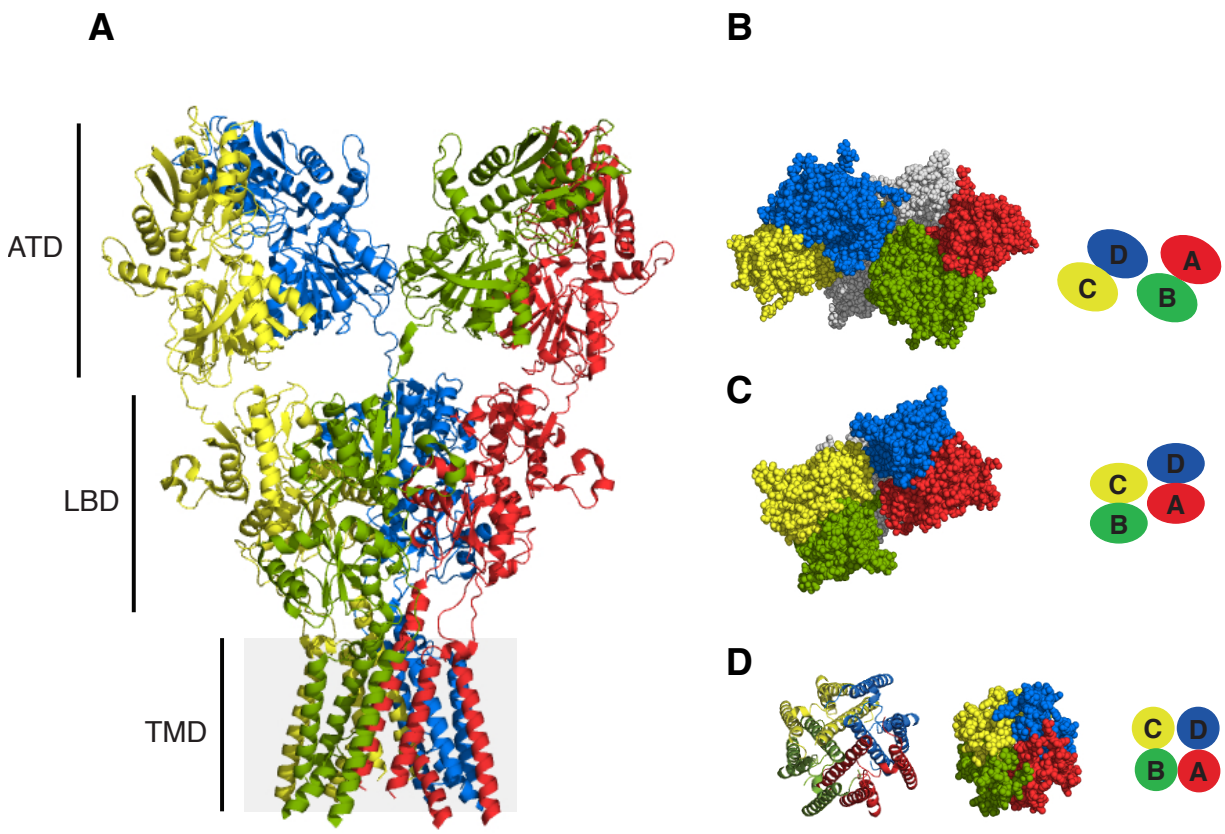

Figure 1 Full-length structure of the homomeric GluA2 receptor (PDB 3KG2; Sobolevsky et al., 2009). Each of the four subunits is shown in a different colour. (**A**) Side-view of the full-length GluA2 structure. The location of the ATD, LBD, and TMD within the tetrameric protein is labelled. The C-terminal domain is missing. (**B**) The four ATDs are shown as *spheres* from the top to illustrate the two-fold symmetric dimer organization between subunits C/D and A/B. The dimer-of-dimers arrangement is additionally shown schematically. (**C**) Accordingly to panel *B*, the four LBDs of one tetramer are shown as *spheres* from the top. At this level, partners within dimers are swapped with the subunits B/C and A/D forming dimeric arrangements. (**D**) A helical, spherical, and schematic representation of the TMD. The two-fold symmetry is dissolved within the TMD, whose subunits are arranged four-fold symmetrical.

A schematic representation of a single GluA2 subunit is shown in **Figure 2**. Until now, little is known about the function of the AMPA receptor ATDs. It is the most divergent domain within the iGluR family and was suggested to participate in the initiation of dimeric assemblies of subunits (in particular during the formation of heteromeric receptors) and trafficking (Ayalon et al., 2005; Clayton et al., 2009; Jin et al., 2009). In NMDA receptors, the ATDs contain binding sites for polyamines, protons, zinc ions, and ifenprodil, compounds, which have no effect at the ATDs of AMPA receptors (Paoletti & Neyton, 2007). The LBDs are organized as clamshell-like structures that are formed by the two polypeptide segments S1 and S2. The clamshell consists of two globular domains – D1 that forms the upper lobe and D2 that forms the lower lobe (Stern-Bach et al., 1994). AMPA receptor agonists bind to the LBD clamshells triggering the closure of the clamshell and a subsequent opening of the ion channel pore (Armstrong & Gouaux, 2000). The TMD of all glutamate receptor ion channel subtypes shows homology to an inverted K^+ channel, illustrating their evolutionary ancestry (Panchenko et al., 2001; Kuner et al., 2003). Three hydrophobic membrane-spanning helices (M1, M3, M4) of each subunit contribute to the formation of the ion channel with M2 forming the pore loop (Wollmuth & Sobolevsky, 2004). The M3 helix is thought to be the pore-lining domain that forms the ion permeation barrier and contains the selectivity filter (Sobolevsky et al., 2009). Interestingly, the M4 helix is absent in K^+ channels. It is assumed that it performs fundamental functions, since M4 truncations produce non-functional AMPA or NMDA receptors (Schorge & Colquhoun, 2003; Salussolia et al., 2011). The pore of AMPA receptors can be blocked by intracellular polyamines including spermine and spermidine (Bowie & Mayer, 1995; Koh et al., 1995; Williams, 1997). The CTD of iGluRs is exposed to the cell interior, where it interacts with a range of PDZ-domain proteins in neurons. It is critical for receptor trafficking and localization at the postsynapse (Sheng & Sala, 2001; Ziff, 2007; Anggono & Huganir, 2012). Deletion of the CTD does not impair the tetramerization and functionality of either AMPA or NMDA receptors in HEK cells, oocytes, or within their native environment (Puddifoot et al., 2009; Salussolia et al., 2011; Granger et al., 2013).

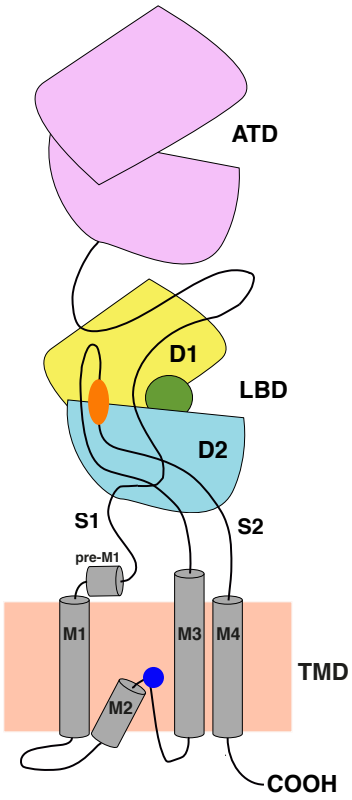

Figure 2 Schematic representation of the glutamate receptor subunit topology. The ATD is shown in *violet*. The two segments, S1 and S2, form the upper (D1; *yellow*) and lower (D2; *light blue*) lobe of the LBD. Glutamate (*green*) binds at the clamshell between D1 and D2. The TMD part (*grey*) of the receptors contains the helices M1, M3, and M4. M2 forms the pore loop and contains the Q/R editing site (*blue circle*). The location of the flip/flop splice region is indicated as an *orange oval*.

A range of molecular mechanisms including alternative splicing and RNA editing diversify the biophysical properties of AMPA receptors. Alternative splicing at a region within the fourth membrane domain of each subunit in AMPA receptors results in flip and flop splice variants (Sommer et al., 1990). These modifications lead to distinct receptor properties, such as different desensitization and deactivation kinetics (Mosbacher et al., 1994), differences in AMPA receptor trafficking (Coleman et al., 2006), and variable sensitivity to allosteric regulation of desensitization by cyclothiazide (CTZ; Partin et al., 1995; 1996; Sun et al., 2002). Around 99% of native GluA2 subunits are RNA-edited. This posttranscriptional process replaces a glutamine

residue (Q) by an arginine (R) in the pore region at the so-called Q/R editing site (Q607R; Hollmann et al., 1991; Sommer et al., 1991). This modification has a great impact on the receptor´s Ca^{2+}-permeability (Hollmann et al., 1991; Burnashev et al., 1992), controls receptor release from the ER (Greger et al., 2002), and might promote the tetramerization of AMPA receptors (Greger et al., 2003). At the postsynapse, AMPA-type receptors are functionally fine-tuned by a range of interacting auxiliary subunits. The major classes of interacting proteins include the TARP family (transmembrane AMPA receptor regulatory proteins; Chen et al., 2000; Nicoll et al., 2006; Milstein et al., 2007), the cornichon homologs (CNIH-2 and CNIH-3; Schwenk et al., 2009), CKAMP44 (von Engelhardt et al., 2010), and 21 further proteins that were recently identified by high-resolution proteomics (Schwenk et al., 2012).

In the framework of this study, the main focus was set on the investigation of the LBD lobe movements during receptor activation. An introduction on the current knowledge of AMPA receptor LBD mobility during gating is given in the following section.

1.1.3 Mobility of the AMPA receptor LBDs during gating

The LBDs of AMPA receptors are highly mobile domains undergoing large conformational changes during the gating process. Structural information has been provided by various studies offering snapshots of AMPA receptor domains in the apo, active, or the desensitized state. However, for studying the dynamic mobility of AMPA receptors during activation, complementary electrophysiological studies are essential. Several functional studies gave insight into the rearrangements of the LBDs during the different conformational states accompanying receptor activation (Armstrong et al., 2006; Plested & Mayer, 2009; Sobolevsky et al., 2009; Pøhlsgaard et al., 2011). Within a dimer of subunits, two LBDs are arranged in a back-to-back fashion with the clamshells pointing in opposite directions (Armstrong & Gouaux, 2000; Sun et al., 2002; **Figure 3 A**). Binding of agonists between the D1 and D2 lobes induces a closure of the LBD globular domains, whose extent depends on the efficacy of the agonist (Armstrong et al., 1998; Sun et al., 2002; Jin et al., 2002; 2003). In one proposed model (**Figure 3 A**), the D2 lobes move towards D1 by ~21° upon binding of full agonists such as glutamate or AMPA. This conformational change triggers the ion channel gate to open (Armstrong & Gouaux, 2000). This open state represents an energetically unstable conformation (Lau & Roux, 2011), resulting in a

rapid transition into a deactive or a desensitized state. Deactivation involves a rapid unbinding of the agonist following re-opening of the clamshells and a subsequent closure of the ion channel pore (Armstrong et al., 2006). The desensitized state is characterized by pore closure of the ion channel with persistent binding of the agonist. The non-conducting desensitized state involves additional conformational rearrangements at the level of the LBD dimer. Crosslinking studies suggest, that the D1 lobe undergoes a ~14° rotation towards D2, resulting in a disruption of the D1-D1 interface, whereas the D2 lobes move closer together (Sun et al., 2002; Armstrong et al., 2006; Plested & Mayer, 2009). A further proposed model of structural LBD rearrangements during receptor desensitization showed an unexpected large separation of the GluK2 LBD dimers into four distinct domains (Schauder et al., 2013; **Figure 3 B**). As identified by single-particle cryoelectron tomography on full-length GluK2 receptors, this conformational change is much more pronounced than assumed before, raising the possibility of the existence of different intermediate states during receptor desensitization.

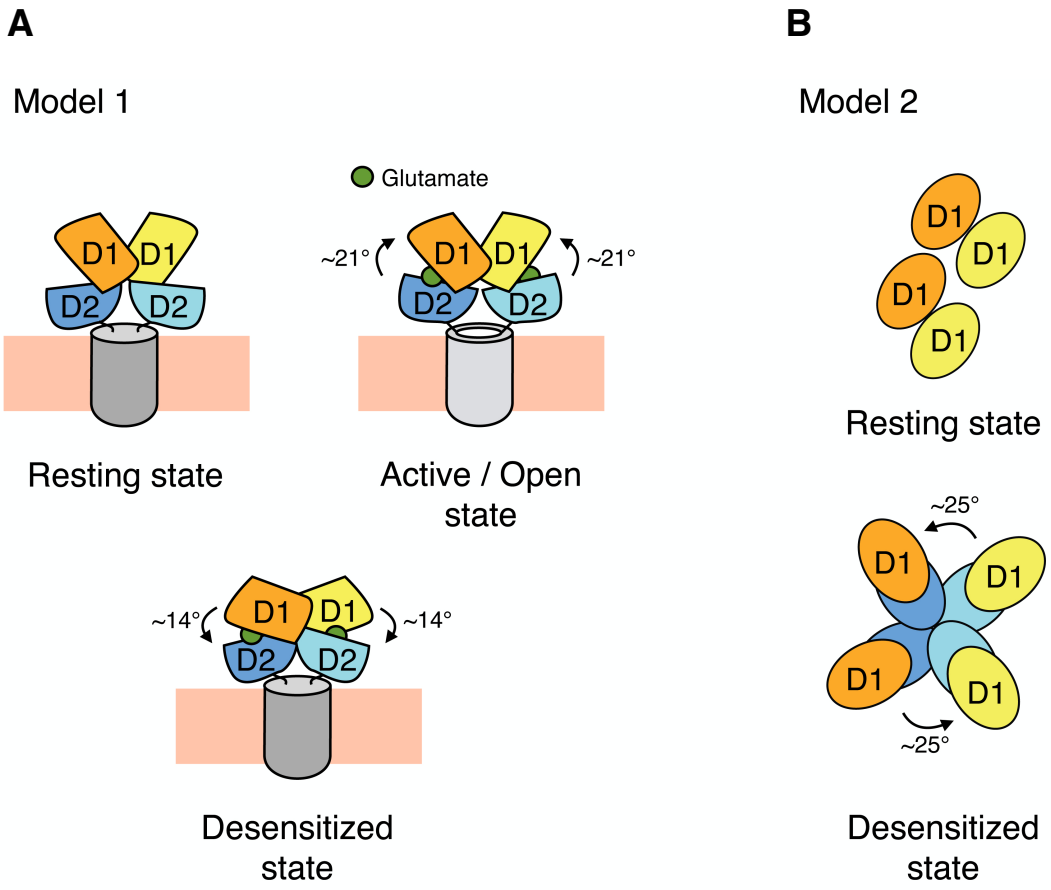

Figure 3 Representation of the two proposed models of glutamate receptor LBD mobility during gating. The upper (D1) and lower (D2) lobes of the LBDs are labelled correspondingly. The ATD is omitted for clarity. (**A**) Diagram of one AMPA receptor dimer from the side. The TMD is represented by a cylinder (*grey*). Three distinct conformations during AMPA receptor gating are shown: the resting, active, and the desensitized state. In the resting state, the ion channel is closed (*dark grey*). According to the model of Armstrong et al. (2006) and Plested & Mayer (2009), the binding of a full agonist as glutamate (*green*) induces conformational changes within the LBD dimer, represented by the movement of the D2 domains towards D1 by ~21°. This rearrangement drives the ion channel to open (*light grey*). Following movement of D1 towards D2 by ~14° disrupts the D1 interface resulting in receptor desensitization, a non-conducting conformation (*dark grey*). (**B**) The LBDs of all four subunits are shown from the top for the resting and the desensitized state. Cryoelectron tomography (as shown by Schauder et al., 2013) revealed a dimeric organization of the GluK2 LBDs in the resting state (the D2 lobes are omitted for clarity), and a full separation of the four subunits at the LBD level during desensitization (by ~25°).

Disruption of the D1–D1 interface during desensitization was confirmed by probing methane thiosulfonate (MTS) accessibility on cysteines placed along the D1 interface (Armstrong et al., 2006). The introduction of cysteines at specific sites at the lower LBD interface resulted in state-dependent intermolecular crosslinking in the desensitized state, which correlated with the predicted LBD lobe mobility during receptor activation by structural analysis (Armstrong et al., 2006; Plested & Mayer, 2009). Furthermore, it revealed that the LBD domains are also mobile in the resting state in the absence of the agonist, as shown by effective disulfide trapping in this functional condition (Plested & Mayer, 2009). Further studies have provided insight into dynamics of LBD subunit interfaces during gating using cysteine mutagenesis in the cognate kainate receptors (Weston et al., 2006a; 2006b; Das et al., 2010) and NMDA receptors (Furukawa et al., 2005). The desensitized state of AMPA receptors can be blocked by either specific mutations, such as the L483Y mutation (Stern-Bach et al., 1998; Sun et al., 2002), or positive allosteric modulators such as CTZ (Sun et al., 2002). Both stabilize the active state, providing valuable tools to isolate active states during glutamate receptor gating. Analysis of LBD structures of the AMPA- or DNQX-bound L483Y mutant, as well as of the complex between GluA2 and CTZ in the presence of glutamate, provided great information about the importance of the stability of the D1–D1 interface during gating (Sun et al., 2002). The GluA2 L483Y mutation in generated knock-in mice was homozygously lethal. However, heterozygous mice were viable, but had a range of neurological deficits including seizures and died usually in postnatal week three (Christie et al., 2010). This result shows that AMPA receptor desensitization is of large importance for brain development.

In general, desensitization has been described for many ligand-gated ion channels that contribute to fast synaptic transmission (Jones & Westbrook, 1996). However, its clear physiological role in the brain is not resolved yet. There is only little evidence, that EPSC-inducing synapses, which are characterized by a rapid clearance of glutamate from the synaptic cleft, are kinetically influenced by desensitizing AMPA receptors to a large extent (Hjelmstad et al., 1999; DiGregorio et al., 2007). Several studies have suggested an important function of receptor desensitization in synaptic depression (Trussell et al., 1993; Rozov et al., 2001), during saturating concentrations of glutamate, AMPA, or quisqualate in the brain (Kiskin et al., 1986; Mayer & Vyklicky, 1989), during high glutamate release frequencies (Trussell & Fischbach, 1989; Otis et al., 1996a; 1996b), or neuronal computation (Rothman et al., 2009).

Despite the great physiological importance of AMPA receptors, fundamental functional processes as the structural rearrangements of their LBDs following activation are still not fully resolved. Numerous existing structural and functional studies gave insights into the LBD movements during receptor activation, however, a detailed picture is lacking. To expand the conventional methodological repertoire to study movements of proteins, photoactivatable UAA groups were site-specifically introduced to AMPA receptors, which allowed trapping of distinct functional states.

1.2 Expansion of the genetic code by introducing UAAs to proteins

1.2.1 The standard genetic code

The standard genetic code was cracked following the discovery that the information for the synthesis of the amino acid phenylalanine is contained in the triple uracil codon (UUU; Nirenberg et al., 1962). This finding was crucial for the understanding of the mechanism of protein biosynthesis. The genetic code is shared by all forms of life. It consists of 64 nucleotide triplets (codons), each encoding one of the standard group of 20 amino acids, including the three stop codons TAG (Amber), TGA (Opal), and TAA (Ochre). The synthesis of proteins involves (*i*) a messenger RNA (mRNA), which is transcribed from a DNA sequence and carries the genetic information in the form of codons; (*ii*) ribosomes, which assemble from two subunits to form the site of translation (30S/50S subunits in prokaryotes, 40S/60S in eukaryotes); (*iii*) tRNAs, which are decorated with their appropriate amino acid and contain an anticodon complementary to a codon on the mRNA; and (*iv*) aminoaminoacyl-tRNA-synthetases (aaRSs), enzymes that drive the aminoacylation of correct tRNAs at their 3`-terminal adenosine (Watson, 1964; Woese et al., 2000; Rodnina & Wintermeyer, 2009). A range of factors tightly controls the different phases of translation, including initiation factors (IFs), elongation factors (EFs), and peptide release factors (RFs; Kozak, 2005; Rodnina & Wintermeyer, 2009; Myasnikov et al., 2009; Loh & Song, 2010). Two non-canonical amino acids, selenocysteine and pyrrolysine, have been recently added to the standard group of 20 amino acids (Srinivasan et al., 2002; Ambrogelly et al., 2007). These amino acids are co-translationally incorporated at the Opal and Amber stop codons in archaea and eubacteria, in response to specific mRNA sequences (Longstaff et al., 2007), or specific

translation elongation factors (Fagegaltier et al., 2000). Despite this natural expansion of the genetic code and numerous post-translational modifications including methylation, acetylation, glycosylation, ubiquitylation, or phoshorylation (Walsh et al., 2005), the natural repertoire of amino acid variations is limited. Introduction of amino acids that are not specified by the standard genetic code diversifies functional properties of proteins and adds novel characteristics that are not available in nature. Such amino acids are called unnatural or non-canonical amino acids and carry synthetically modified, unique side chains. UAAs can be introduced to any kind of protein, regardless of its type, size, quantity, or location (Wang et al., 2007). Also, there are nearly no restrictions in the choice of UAA substitutions (Beene et al., 2003; Wang et al., 2006), except for the less efficient incorporation of D-amino acids compared to their L-type counterparts (Ellman et al., 1991; Dedkova et al., 2003).

1.2.2 Nonsense codon suppression to site-specifically introduce UAAs to proteins – a short overview

Different chemical and molecular approaches have been implemented within the last three decades to introduce UAAs into polypeptide chains or proteins in the effort to artificially expand the standard genetic code. At present, the primary technique that utilizes the site-specific introduction of UAAs into proteins expressed in living cells, is the suppression of nonsense codons by specific tRNAs (Beene et al., 2003). Nonsense codons are stop codons that are not suppressed by one of the 20 common amino acids (Wang et al., 2007). Traditionally, Amber stop codons are used. Compared to other nonsense codons, these are the least-used stop codons (7%) in *Escherichia coli* (*E. coli* or *Ec*) and *Saccharomyces cerevisiae*. Also, the Amber stop codon occurs in the lowest frequency in mammalian cells (in *Homo sapiens*: TAG: 23%, TAA: 30%, TGA: 47%; Wang et al., 2006; Liu et al., 2007). Efficient suppression of an Amber codon introduced prematurely in the open reading frame (ORF) results in a functional full-length protein. In cases where the introduced stop codon is not suppressed effectively, truncated proteins are generated due to termination of protein synthesis (Saks et al., 1996).

Peter Schultz and colleagues were the first to develop a general method to specifically incorporate single amino acid groups into proteins at an introduced Amber codon site (Noren et al., 1989; Noren et al., 1990). Yeast-evolved phenylalanine-specific suppressor tRNAs were

synthesized *in vitro* by means of run-off transcription, chemically aminoacylated with phenylalanine, and added to an *in vitro* (cell-free) protein synthesis reaction of *E. coli* β-lactamase-DNA carrying the Amber codon. This *in vitro* approach that is restricted to short peptides of 50-100 amino acids (Liu & Schultz, 2010), has been the prevalent approach to modify proteins for many years and contributed largely to our current knowledge of utilizing UAAs to expand the genetic code.

The transfer of the technique to proteins expressed in intact cells, in particular *Xenopus laevis* oocytes, by the labs of Dennis A. Dougherty and Henry A. Lester, has opened up new vistas in the work with UAAs (Nowak et al., 1995; Nowak et al., 1998). This approach relies on the microinjection of chemically-acylated Amber suppressor tRNAs into oocytes, along with an Amber-codon-containing mRNA that is selectively suppressed by a single UAA. Microinjection has been extensively used for functional studies on a range of ion channels including nicotinic acetylcholine receptors (nAChR; Nowak et al., 1995; 1998; Kearney et al., 1996; Miller et al., 1998; Dougherty, 2000; Li et al., 2001), potassium channels (England et al., 1997; Tong et al., 2001; Pless et al., 2011; 2013), NMDA receptors (Ye et al., 2013), proline (Lummis et al., 2005a), GABA (Chang & Weiss, 2002; Lummis et al., 2005b; 2011; 2012; Padgett et al., 2007), or serotonin-gated ion channels (5-HT_{3A}Rs; Beene et al., 2002; 2004). Other membrane proteins extensively studied in *Xenopus* oocytes belong to the GPCRs protein family (G-protein coupled receptors; Turcatti et al., 1996; Torrice et al., 2009). Although chemical acylation of tRNAs is a flexible method, since the same suppressor tRNA can theoretically be decorated with any desired UAA, it has the disadvantage of lacking regeneration *in vivo* (in living cells), thus limiting the amount of the synthesized protein (Sakamoto et al., 2002; Wang et al., 2006; Wang et al., 2007).

More recently, genetic techniques for UAA incorporation into proteins have developed rapidly. This approach is based on the *in vivo* synthesis of components required for protein translation. The genetically encoded introduction of UAAs has been applied in this study and is discussed more detailed in the following section.

1.2.3 Genetically encoded UAA mutagenesis

To genetically encode UAAs, a set of stop codon suppression components must be introduced into the cell. This includes genes encoding (*i*) a protein of interest carrying a site-specifically introduced nonsense codon, (*ii*) an orthogonal suppressor tRNA, specifically engineered to be aminoacylated with the desired UAA, (*iii*) a specific orthogonal tRNA-synthetase; and sufficient amounts of the UAA within the cell (**Figure 4**). Following *in vivo* synthesis, the tRNA is charged with the UAA by its cognate tRNA-synthetase and suppresses the introduced Amber stop codon on the mRNA encoding the desired protein, resulting in a site-specific introduction of the non-natural group.

Genetic evolution of orthogonal tRNA / tRNA-synthetase pairs has allowed highly efficient introduction of UAAs into proteins of bacteria (Liu & Schultz, 1999; Wang et al., 2001; Chin & Schultz, 2002; Farrell et al., 2005; Neumann et al., 2008; Wang et al., 2010), yeast (Edwards & Schimmel., 1990; Edwards et al., 1991; Chin et al., 2003a; 2003b; Huang et al., 2008), mammalian cells (see **Table 1**), and into a series of whole-cell organisms – the nematode *Caenorhabditis elegans* (Greiss & Chin, 2011; Parrish et al., 2012), the arthropod *Drosophila melanogaster* (Bianco et al., 2012), and neurons of living mice (Kang et al., 2013).

For high-fidelity UAA-incorporation, specifically-engineered tRNA / tRNA-synthetase pairs must be orthogonal within the host cell or organism in order to avoid crosstalk with endogenous pairs. An orthogonal tRNA must not be aminoacylated by any endogenous tRNA-synthetases, but is only substrate to its cognate orthogonal synthetase. Equally, an orthogonal synthetase must not aminoacylate any endogenous tRNA with endogenous amino acids, but rather catalyze aminoacylation of the orthogonal tRNA with its specific UAA at its active site (Wang et al., 2006; Chin, 2014). On the other hand, both components must retain compatibility with the biosynthetic machinery of the host cell. To ensure the orthogonal nature of tRNA / tRNA-synthetase pairs, both components are evolved from species of separate branches of life (Wang & Schultz, 2001; Wang et al., 2007).

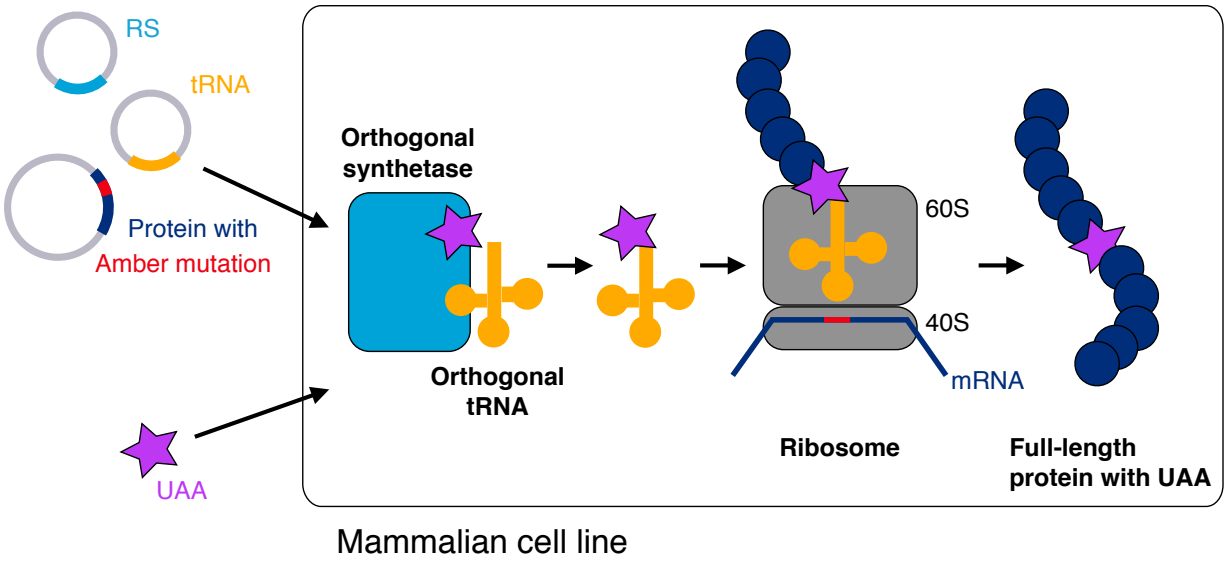

Figure 4 Genetically encoded UAA mutagenesis in mammalian cells. A gene encoding a protein of interest (*dark blue*) and containing an introduced Amber stop codon (TAG, *red*) is co-transfected with vectors carrying genes for the orthogonal tRNA (*yellow*) / tRNA-synthetase (*light blue*) pair into a mammalian cell line. The cells are incubated in the presence of the UAA (*purple asterisk*) in the growth medium and are taken up by an endogenous amino acid transport system. After *in vivo* expression, the orthogonal RS attaches the UAA to its complementarily orthogonal tRNA. In the ribosome (*grey*), which consist of the two subunits 60S and 40S, the information encoded in the mRNA is translated into a polypeptide sequence. The UAA is incorporated in response to the Amber codon on the mRNA by the complementary anticodon (CUA; *not shown*) on the suppressor tRNA. After release from the ribosome, the full-length polypeptide, site-specifically carrying the UAA, folds into a functioning protein (modified from Chin, 2014).

To engineer orthogonality, synthetases and tRNAs are subjected to an evolutionary selection process. The first orthogonal tRNA / tRNA-synthetase pairs designed for the use in *E. coli* were selected from large *Methanococcus jannaschii* (*Mj*) mutant $tRNAs^{Tyr}$ and mutant Tyrosyl (Tyr)-RSs libraries (~10^9 variants) by the Schultz lab (Wang et al., 2001). The archeal *Mj*$RNAs^{Tyr}$ / TyrRS pair differed in its identity elements from its bacterial counterpart, and thus the crossreactivity between these two pairs was little. To further reduce the recognition of *Mj*$RNAs^{Tyr}$ by *Ec*RSs and of *Ec*$RNAs^{Tyr}$ by *Mj*RSs, along with an increase of specificity for the UAA of choice, libraries of *Mj* mutant suppressor tRNAs and synthetases passed through

repeated rounds of positive and negative selections in the presence or absence of their cognate counterpart. Antibiotic resistance genes and genes encoding lethal proteins with introduced Amber codons served as selection markers. Mutant tRNA-synthetases can, where possible, also be generated based on crystal structures of the synthetase (or on those of available homologues), and be directly applied to the host cell of interest (Wang et al., 2001; Wang & Schultz, 2001; 2004; Wang et al., 2006).

High incorporation efficiencies using the genetic method could be easily achieved in *E. coli* or yeast. However, genetic encoding of UAAs in mammalian cells posed a challenge, since their tRNA genes differ, in regard of transcription and following modification, from those of prokaryotes (Wang et al.,2006). Genes encoding eukaryotic tRNAs possess two internal promoters, the A- and B-box sequences, a feature needed for transcription by the RNA polymerase III. Also, their 3`-CCA is not encoded genetically, but appended enzymatically (Li et al., 2002; Wang et al., 2006). Generating an additional A-box in an *Ec*RNA^{Tyr} did not lead to a functional tRNA for applications in mammalian cells. Luckily, in contrast to *E. coli*, the tRNA^{Tyr} from *Bacillus stearothermophilus* (*Bst*) naturally contains the promoter sequence of an A- and B-box, and is effectively charged by the *Ec*TyrRS, making it an ideal tRNA / synthetase pair (Sakamoto et al., 2002). Orthogonal pairs for the use in mammalian cells are usually evolved in tRNA / tRNA-synthetase libraries in yeast and subsequently adapted to mammalian cell systems (Chin et al., 2003b); or can, equally to the engineering process in *E. coli*, be designed based on existing structures to create orthogonal pairs with altered specificity directly in mammalian cells (Sakamoto et al., 2002; Zhang et al., 2004).

In mammalian cells, first effective orthogonal suppressors to be described, were combinations of a modified *Bst*RNA^{Trp} and a TrpRS or a *Bst*RNA^{Tyr} and a *Ec*TyrRS pair (Sakamoto et al., 2002; Chin et al., 2003a; Zhang et al., 2004). Currently, the *Bst*RNA^{Tyr} / *Ec*TyrRS pair is the predominant one for sufficient nonsense codon suppression of proteins in mammalian cells. Using this pair, various types of UAAs including fluorescent (Sakamoto et al., 2002; Hino et al., 2006; Liu et al., 2007; Wang et al., 2007a), photoactivatable (Hino et al., 2005; 2006; Liu et al., 2007; Wang et al., 2007a; Ye et al., 2008; Takimoto et al., 2009; Ye et al., 2009; Ye et al., 2010; Grunbeck et al., 2011; Hino et al., 2011; Coin et al., 2011; Grunbeck et al., 2012; Naganathan et al., 2013; Huber et al., 2013; Zhu et al., 2014), redox-active (Zhang et al., 2004), or bioconjungative groups (Liu et al., 2007; Takimoto et al., 2009) have been incorporated. Another

very common orthogonal pair for the use in mammalian cells is the PylRS / $tRNA^{Pyl}$ pair from *Mj*, *Methanosarcina mazei* (*Mm*) and *barkeri* (*Mb*). It has been used to introduce a range of L-lysine derivates (Mukai et al., 2008; Chen et al., 2009; Groff et al., 2010) or Norbornene (Lang et al., 2012).

Further strategies to maximize the efficiency of UAA incorporation include variations in the choice of promoters to drive the expression of bacterial tRNAs, modifications of the 3´-flanking sequence, or tendemly repetitions of tRNA genes on the expression vectors (noted in **Table 1**).

Table 1 Overview of relevant studies employing genetically encoded stop codon suppression in proteins expressed in mammalian cells. The abbreviations not introduced before are listed alphabetically. **Apa**: *p*-Acetyl-L-phenylalanine; **Boc-lysine**: N^{ε}-*tert*-Butyloxycarbonyl-L-lysine; **Cmn**: 4,5-dimethoxy-2-nitrobenzyl-cysteine; **Cyc-lysine**: N^{ε}-Cyclopentyloxycarbonyl-L-lysine; **DanAla**: Dansylalanine; **EGF(R)**: Epidermal growth factor (receptor); **FTIR**: Fourier transform infrared; **GRB2**: Growth factor receptor-bound protein 2; **GST**: Glutathione S-transferase; **Ipa**: *p*-Iodo-L-phenylalanine; **IY**: 3-Iodo-L-tyrosine; **5-HTPP**: 5-Hydroxy-L-tryptophan; **LacZ**: Lactose operon; **Mpa**: *p*-Methoxy-L-phenylalanine; **Ome**: *o*-Methyl-L-tyrosine; **ONBK**: *o*-Nitrobenzyl-oxycarbonyl-N^{ε}-L-lysine; **Ppa**: *p*-Propargyloxy-L-phenylalanine; **tmdPhe**: *p*-Trifluoromethyl-diazirinyl-L-phenylalanine; **Z-lysine**: N^{ε}-Benzyloxycarbonyl-L-lysine

UAA	**tRNA / tRNA-synthetase pair**	**Matter of investigation**	**Reference**
IY	*Ec*TyrRS / *Bst*RNA^{Tyr} & *Ec*TyrRS / *Ec*RNA^{Tyr}	Design and comparison of the tRNA / RS pairs in Ras and EGFR	Sakamoto et al., 2002
5-HTPP	*Bst*TrpRS / $tRNA^{Trp}$	Design and optimization of the tRNA / RS pair for Opal codon suppression in the bacteriophage T4 fibritin	Zhang et al., 2004
BzF	*Ec*TyrRS / *Bst*RNA^{Tyr}	Photocrosslinking of Grb2 to EGF and to endogenous proteins	Hino et al., 2005
IY, BzF	*Ec*TyrRS / *Bst*RNA^{Tyr}	Efficiency of Amber suppression in LacZ & photocrosslinking of Grb2 to endogenous proteins	Hino et al., 2006
Mpa, Apa, BzF, Ipa, AzF, Ppa	*Ec*TyrRS & *Bst*RNA^{Tyr}	Optimization of the tRNA / RS pair using GFP37TAG & mass spectrometry analysis	Liu et al., 2007

UAA	**tRNA / tRNA-synthetase pair**	**Matter of investigation**	**Reference**
BzF, DanAla, Ome	*Ec*TyrRS & *Ec*RNA^{Tyr} (H1 promotor & human 3`-flanking sequence)	Investigating the fast inactivation of a potassium channel in HeLa cells & genetically encoding of GFP in neurons	Wang et al., 2007
Apa, BzF	*Ec*TyrRS & *Bst*RNA^{Tyr} (human 5`-leader sequence)	Optimization of the tRNA / RS pair in two GPCRs & derivazation of Apa with a hydrazide-fluorophor	Ye et al., 2008
Acetyl-, Boc-, Z-lysine	*Mm*PylRS / tRNA^{Pyl}	Testing different tRNA promotors (U6, T7) and engineering of RSs to incorporate different pyrrolysine analoges into the genes of GRB2 and LacZ	Mukai et al., 2008
AzF, BzF, Ome, Ppa	*Ec*TyrRS & *Bst*RNA^{Tyr}	Mutational engineering of a RS specific to improve the recognition by the tRNA in eGFP; photocrosslinking of GST-AzF dimers	Takimoto et al., 2009
AzF	*Ec*TyrRS & *Bst*RNA^{Tyr} (human 5`-leader sequence)	Screening for optimal RS variants & monitoring movements of GPCR helices by FTIR difference spectroscopy	Ye et al., 2009
Cyc-lysine, ONBK	*Mm*PylRS / tRNA^{Pyl} (U6 promoter)	Confirmation of orthogonality of the RS / tRNA pair to incorporate Cyc-lysine into RBP1; engineering of a RS specific for ONBK using eGFP; photolysis of ONBK upon UV	Chen et al., 2009
AzF	*Ec*TyrRS & *Bst*RNA^{Tyr} (human 5`-leader sequence)	Monitoring movements of GPCR helices by FTIR difference spectroscopy	Ye et al., 2010
photocaged N^{ε}-methyl-lysine	*Mm*PylRS / tRNA^{Pyl} (U6 promoter)	UV-induced photolysis of the UAA within eGFP	Groff et al., 2010
photocaged lysine	*Mb* & *Mm*PylRS / tRNA^{Pyl}	Activation of a kinase by light-induced uncaging	Gautier et al., 2010
AzF, BzF,	*Ec*TyrRS & *Bst*RNA^{Tyr} (human 5`-leader sequence)	Mapping ligand-binding sites on GPCRs	Grunbeck et al., 2011

UAA	**tRNA / tRNA-synthetase pair**	**Matter of investigation**	**Reference**
tmdPhe, BzF	*Ec*TyrRS & *Bst*RNA^{Tyr}	Comparing photocrosslinking properties of BzF and tmdPhe between GRB2 and EGF; identification of further binding partners of GRB2 using mass spectrometry	Hino et al., 2011
AzF	*Ec*TyrRS / *Ec*RNA^{Tyr}	Studying the ligand-receptor interaction between a GPCR and different ligands	Coin et al., 2011
BzF, DanAla	*Ec*TyrRS / *Ec*RNA^{Tyr} (H1 promoter)	Tracking optical changes of a phosphatase voltage-sensitive domain in neural stem cells	Shen et al., 2011
BzF	EcTyrRS & BstRNA^{Tyr} (human 5`-leader sequence)	Mapping ligand-binding sites on GPCRs	Grunbeck et al., 2012
Norbornene	*Mb* & *Mm*PylRS / tRNA^{Pyl}	Site-specific labelling of an EGFR with different tetrazine-fluorophores	Lang et al., 2012
AzF	*Ec*TyrRS & *Bst*RNA^{Tyr} (human 5`-leader sequence)	Trapping of GPCR-ligand complexes; labelling of low-abundance GPCRs with fluorescent or peptide-epitope derivates	Naganathan et al., 2013
Apa, AzF, BzF	*Ec*TyrRS & *Bst*RNA^{Tyr} (human 5`-leader sequence)	Bioorthogonal labelling of luciferase and a GPCR with a fluorophor	Huber et al., 2013
Cmn	*Ec*LeuRS & *Ec*RNA^{Leu} (H1 promoter)	Design of a photoactivatable, inwardly rectifying potassium channel (PIRK) in HEK cells, neurons, and *in vivo* (mouse neocortex)	Kang et al., 2013
AzF, BzF	*Ec*TyrRS & *Bst*RNA^{Tyr} (human 5`-leader sequence)	UV-induced photoinactivation of homomeric and heteromeric AMPA receptors with BzF in the LBD	Klippenstein et al., 2014
AzF, BzF	*Ec*TyrRS & *Bst*RNA^{Tyr} (human 5`-leader sequence)	Investigation of ATD interfaces in NMDA receptors with different subunit compositions in oocytes, HEK cells, and neurons	Zhu et al., 2014

1.2.4 The photoactive UAAs *p*-Benzoyl-L-phenylalanine (BzF or Bpa) and *p*-Azido-L-phenylalanine (AzF)

In this chapter, the focus is set on two photocrosslinkers, AzF and BzF, whose photochemistry has been comprehensively studied in a range of previous studies, and which were applied for receptor photoinactivation in this study.

The first general use of BzF in biological systems was described in 1973 (Galardy, 1973), followed by its use as a photoactivatable UAA for site-specific incorporation into a 17-residue Calmodulin-binding peptide chain by means of solid-phase peptide synthesis (*in vitro*) in order to photolabel protein-peptide interactions (Kauer et al., 1986). This study was crucial for the opening of an entire novel sphere in studying protein-peptide interactions (Dorman & Prestwich, 1994). Further substrate photoaffinity labelling studies based on solid-phase peptide synthesis using BzF and AzF followed (Miller & Kaiser, 1988; Shoelson et al., 1993; Kurose et al., 1994). The first *in vitro* attempt to suppress Amber stop codons for the introduction of BzF to proteins was reported in 1994 (Cornish et al., 1994). The incorporation efficiency into a T4 lysozym was described to be over 50%, which however, resulted in a catalytically inactive protein. The further use of the genetic approach has allowed efficient incorporation of AzF and BzF into various proteins of bacteria (Chin et al., 2002a; 2002b; Kirshenbaum et al., 2002; Chin & Schultz, 2002; Farrell et al., 2005; Mori & Ito, 2006; Wang et al., 2010; Sato et al., 2011), yeast (Chin et al., 2003a; 2003b; Huang et al., 2008; Young et al., 2009; Lee et al., 2009; Palzer et al., 2013; Berg et al., 2014), oocytes (Garcia et al., 2007; Ye et al., 2013), and mammalian cells (see **Table 1**) to study protein-protein, peptide-ligand, or DNA-protein interactions. Other studies in mammalian cell lines have used benzophenone tethered to cysteines (BPMTS, benzophenone-4-carboxamidocysteine methanethiosulfonate) that was introduced to the inactivation gate and the voltage sensor in sodium and potassium channels (Horn et al., 2000; Ding & Horn, 2001).

Typical techniques to study protein-protein interactions are yeast two-hybrid systems (Fields & Song, 1989; Drees, 1999) or protein arrays (MacBeath, 2002; Zhu & Snyder, 2003). These approaches, however, give only insight into protein interaction networks *in vitro*, outside their cellular context, leaving the question open as to whether they are representative of the protein complexes within the cell (Hino et al., 2005). Genetic encoding of UAAs can be directly applied to living cells or organisms overcoming these difficulties (Wang et al., 2007). In this context, a

major advantage to apply photoactive UAAs to proteins *in vivo*, in particular the usage of the UAAs AzF and BzF, is their covalent character excluding kinetic-based dissociation of unstable complexes or dissociation of noncovalently associated proteins during affinity purification or cell lysis. Thus, in principle a more detailed picture of the protein interaction network within the cell is provided (Chin & Schultz, 2002; Hino et al., 2005; Hino et al., 2011).

1.2.4.1 Photocrosslinking of BzF

The UV-driven reaction of covalent BzF-crosslinking is illustrated in **Figure 5**. Upon UV exposure at 350-365 nm, BzF adopts a short-lived triplet excited state of 80-120 µs. The resulting ketone diradical can subsequently react with geometrically-accessible C–H bonds to form a covalent adduct (Kauer et al., 1986; Galardy et al., 1973; Dorman & Prestwich, 1994; Ding & Horn, 2001; Tanaka et al., 2008). The photoactive ketone group of BzF preferentially reacts within 3.1 Å with its crosslinking target, usually an α-carbon of a neighbouring peptide backbone. The covalent crosslink is generated via two steps – (*i*) hydrogen abstraction creating alkyl and ketyl free radicals with a lifetime much shorter than that of the triplet state, followed by (*ii*) recombination of these radicals. In the presence of an abstractable hydrogen, the lifetime of the triplet state is decreased by factor 100 and the planarity of the benzophenone ring during the triplet state favours the reactivity of the ketone group. In the absence of an H-atom donor within the triplet state lifetime, the crosslinking reaction can fail. In this case, BzF efficiently drops back in its initial state and can be excited again, which is one of the major advantages of this crosslinker. Thus, activation cycles by UV can be repeated, until a crosslinking-beneficial conformation is present (Dorman and Prestwich, 1994; Ding & Horn, 2001; Tanaka et al., 2008). A negligible possibility of BzF photodestruction due to oxidation of one of the radicals has also been described. In this case, BzF looses its ability to be activated again (Dorman & Prestwich, 1994; Horn et al., 2000).

Although C–H backbones have been shown to be the most eligible crosslinking partners, even in the presence of water or other nucleophiles, further hydrogen donors as methylene groups of lipids or amino acid side chains have the ability to react with the ketone group of BzF. The reactivity order of preference has been described as follows: C–H > NCH > SCH > methine > $C{=}CCH_2$ > CH_2 > CH_3. Notably, reactive binding partners are C_γ–H of leucine, C_β–H of valine,

and CH_2 groups next to heteroatoms in lysine, arginine, and methionine. Aromatic or vinylic / ethenylic C–H bonds are not thought to be hydrogen atom donors (Dorman & Prestwich, 1994; Tanaka et al., 2008). In general, BzF is a chemically more stable photocrosslinker compared to diazo esters, aryl azides, and diazirines (Kauer et al., 1986; Dorman & Prestwich, 1994; Lee et al., 2009). Advantageously, it absorbs at longer wavelengths (365 nm) that do not induce damage of proteins or nucleic acids. Among the few disadvantages of BzF, bulkiness and hydrophobicity can be named (Galardy et al., 1973; Dorman & Prestwich, 1994; Chin & Schultz, 2002).

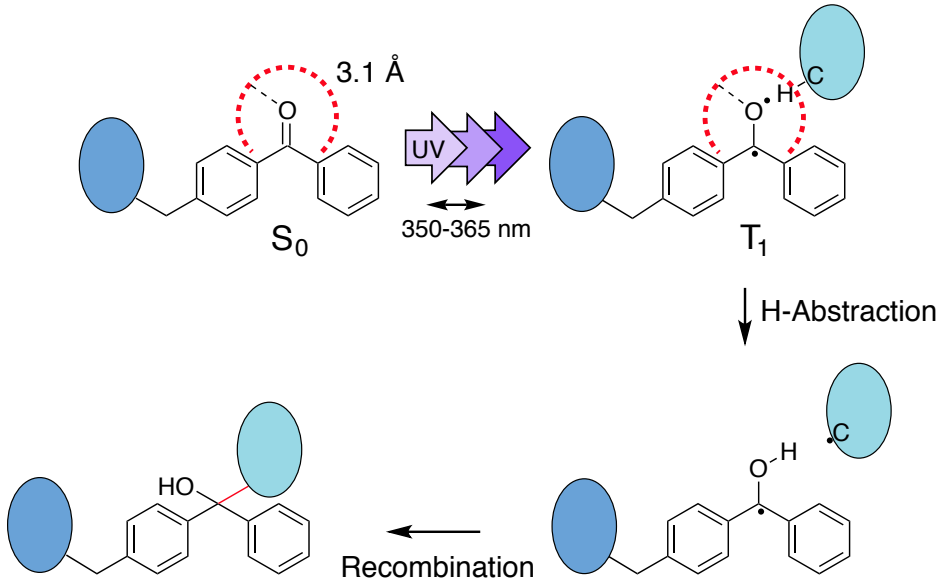

Figure 5 Photocrosslinking reaction pathway of BzF. BzF is site-specifically introduced to a polypeptide chain (shown as a *dark blue oval*). Its photoreactive ketone group, which is stable at the ground state (S_0), preferentially crosslinks to C–H bonds within 3.1 Å (the radius is indicated in *red*). Upon absorption of a photon at 350-365 nm, the ketone group is excited into the triplet excited state (T_1). In the presence of an abstractable hydrogen from neighbouring polypetide chains (*light blue*), the alkyl and ketyl free radicals recombine to produce a covalent crosslink (modified from Ding & Horn, 2001).

1.2.4.2 Photocrosslinking of AzF

Compared to BzF, AzF shows a more diverse crosslinking reaction pathway (**Figure 6**). Activation of the photoreactive azide group at 254-400 nm induces a loss of dinitrogen (N_2) and the formation of a short-lived (~1 ns) excited state with free radicals. This generated nitrene is able to form an irreversible crosslink with various chemical groups (Schwyzer & Caviezel, 1971; Escher & Schwyzer, 1974). Nitrene groups can insert into neighbouring active hydrogens of either C–H bonds or primary amines (N–H bonds). In the absence of an adequate interacting partner, the reactive nitrene fails to recombine and expands its ring into a less reactive but more stable dehydroazepine intermediate (ketenimine). Once rearranged into a ketenimine, the crosslinking efficiency decreases producing nonspecific crosslinking products. Ketenimine reacts with either nucleophiles as amines ($R–NH_2$) or water, or inserts into hydrogens, generating nonspecific crosslinks (R–H; Knowles, 1972; Keana & Cai, 1990; Thermo Fisher Scientific, Inc., Handbook, 2009; Tanaka et al., 2008). Photodamage of biomolecules is also more likely when using AzF, because its maximum excitation wavelength is shorter compared to BzF (below 310 nm; Kurose et al., 1994; Chin et al., 2002b; Tanaka et al., 2008). Several studies, however, have shown that the azide group can also be equally activated with longer wavelengths (up to 400 nm; Takimoto et al., 2009; Berg et al., 2014). Nonspecific reaction effects are also found when using AzF, even in the absence of UV illumination, an effect that could arise from higher sensitivity of azide groups towards ambient daylight (Grunbeck et al., 2011).

Despite its known limitations as a photocrosslinker, AzF has been extensively used for site-specific fluorescent labelling of proteins. Azide groups can be chemically coupled to various bioorthogonal groups (Kiick et al., 2002; Kolb & Sharpless, 2003; Agard et al., 2004; Yanagisawa et al., 2008), overcoming limitations of conventional labelling methods implying cysteines (Davis & Chin, 2012; Naganathan et al., 2013). Another advantage of AzF is its infrared activity that allows studying conformational changes of proteins by means of FTIR, as previously described for GPCRs (Ye et al., 2009; 2010).

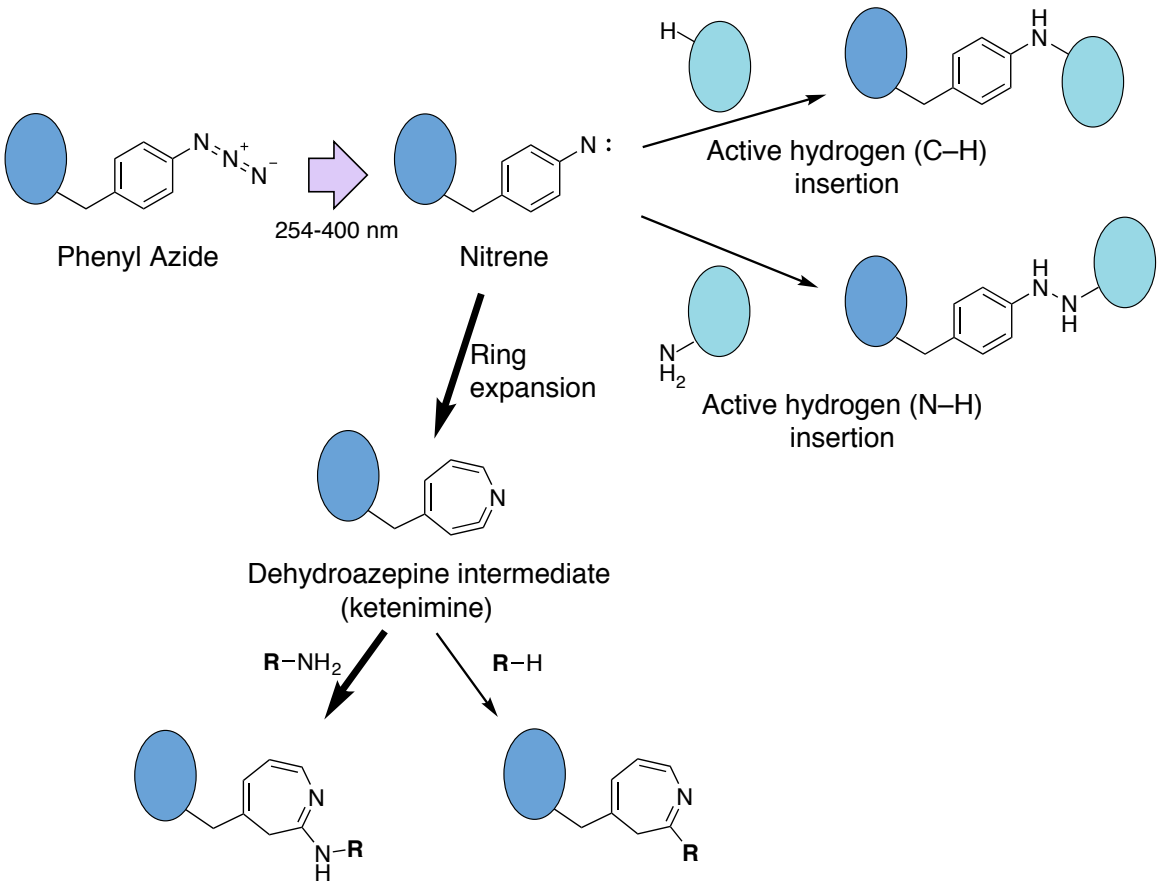

Figure 6 The multiple reaction pathways of AzF. AzF is site-specifically introduced to a polypeptide chain (shown as a *dark blue oval*). Illumination between 254 and 400 nm activates the photosensitive azide group of AzF resulting in a short-lived nitrene radical formation. In the presence of favourable partner, the reactive nitrene can insert into active hydrogens of a neighbouring polypeptide (*light blue*) to produce a specific covalent photocrosslink. In the absence of proper reaction candidates, the nitrene expands its ring forming a ketenimine. Ketenimines can further react with polypeptides or proteins (R) that contain nucleophilic (R–NH_2) or active hydrogen (R–H) groups. The bold arrows highlight the dominant pathway of AzF (modified from Thermo Fisher Scientific, Inc., Handbook, 2009).

2 METHODS AND MATERIALS

2.1 Cell culture

2.1.1 Buffers and solutions

The molecular weight (MW; equivalent to g/mol) is indicated for all chemicals. Unless otherwise stated, chemicals were purchased from Carl Roth (Karlsruhe, Germany) or Sigma Aldrich GmbH (Taufkirchen, Germany), with the highest purity available. The ethanol was typically not denatured.

Minimum essential medium (MEM) complete

MEM was supplemented with 10% fetal bovine serum (FBS superior) and 5% penicillin / streptomycin. All ingredients were purchased from Biochrom AG / Merck Millipore (Berlin, Germany). MEM complete was stored at +4°C for maximum four weeks.

Polyethylenimine (PEI) solution for transfection

PEI (linear 25 kD; Polysciences, Inc., Eppelheim, Germany) was dissolved to a final concentration of 1 mg/ml in milliQ H_2O. To facilitate dissolving, the solution was heated up to 50°C. The pH was adjusted to 7.0 with NaOH and the solution was filtered through a 0.2 µm Nylon filter (NALGENE™; Fisher Scientific, Schwerte-Geisede, Germany). Aliquots were stored at –20°C.

Kynurenic acid solution

The kynurenic acid solution contained (in mM): 50 kynurenic acid sodium salt (MW 229.17; Abcam Biochemicals, Cambridge, UK), 100 $MgCl_2$ (pH 7.45). The solution was filter-sterilized using a 0.22 µm Nylon filter (NALGENE™). Aliquots were stored at –20°C.

UAA-supplemented cell culture media

p-Benzoyl-L-phenylalanine (BzF; MW: 269.3; Bachem Holding AG, Bubendorf, Switzerland) was dissolved in 1 M HCl. *p*-Azido-L-phenylalanine (AzF; MW: 206.1; Chem-Impex International, Inc., Wood Dale, IL, USA) was dissolved in 1 M NaOH. The dissolved UAAs were immediately added to prewarmed (37°C) MEM complete in a final concentration of 1 mM for BzF and 0.5 mM for AzF. Media supplemented with UAAs were adjusted to pH 7.3 and sterilized using a 0.22 µm PVDF filter (Millex®-GV; Merck Millipore, Schwalbach, Germany) The protocols were adopted from Hino et al. (2006) and Ye et al. (2009).

2.1.2 Cell lines and cultivation

GluA2 receptors were overexpressed in HEK-293 (human embryonic kidney) cells for electrophysiological recordings or in HEK-293T cells for Western blotting. HEK-293T cells express the large T antigen SV40 (simian virus 40), which enhances the cell proliferation rate and thus upregulates the expression level (Moens et al., 1997; Li et al., 2012). Both cell lines were purchased from the Leibniz Institute DSMZ (Deutsche Sammlung von Mikroorganismen und Zellkulturen GmbH, Braunschweig, Germany). For long-term storage, the cells were cryopreserved in a DMSO-free freezing medium (Recovery™ Cell Culture Freezing Medium; Life Technologies GmbH, Darmstadt, Germany) in liquid nitrogen at –196°C. Before use, the cell cultures were thawed in a water bath (37°C) for 2-3 min, collected in MEM complete, centrifuged for 5 min at 500 x g, resuspended in cell culture medium, and plated onto 25 cm^2 flasks. Cells were maintained in MEM complete at 37°C and 5% CO_2. They were split twice per week. For splitting, the confluent cell monolayer was washed with sterile 1 x PBS (Biochrom AG / Merck Millipore), followed by an incubation in 0.05% Trypsin / 0.02% EDTA in PBS (Biochrom AG / Merck Millipore) for 3 min at 37°C. Detached cells were collected in 10 ml MEM, centrifuged at 500 x g for 5 min, resuspended in culture medium, and plated on new flasks containing fresh MEM complete in a dilution of 1:5-1:8. Cells between passages five and 30 were used for electrophysiology and Western blotting. All dishes and flasks for cell cultivation were purchased from NUNC™ / Thermo Fisher Scientific (Schwerte, Germany).

2.1.3 Preparation of Poly-L-lysine (PLL) coated cover slips

For electrophysiological recordings, cells were plated on 10 mm glass cover slips (Hartenstein, Würzburg, Germany). Before use, the cover slips were sonicated in 70% ethanol for 15 min in sterile 50 ml Falcon tubes (Sarstedt, Nümbrecht, Germany), and stored afterwards in 99% ethanol at room temperature (RT). After flame sterilization, the cover slips were covered with a drop of a 0.01% PLL solution (in milliQ H_2O) for 15 min in order to achieve effective coating. Afterwards, they were rinsed twice in 1 x PBS and placed into sterile 3.5 cm dishes. HEK cells were plated onto the coated cover slips in a 1:80-1:100 dilution from a 25 cm^2 flask. This ensured a 60-70% confluency on the day of transfection.

2.1.4 Transfection and UAA incubation

The HEK cells were transfected 24 h after splitting. For electrophysiological recordings, a total amount of 3 µg DNA (1 µg/µl) was transfected per 3.5 cm dish. For Western blotting, 10 cm dishes were used, and the total amount of transfected DNA was scaled-up to 21 µg. For transfections, the DNA:PEI ratio was 1:3 (*v/v*). For transfections of 3.5 cm dishes, the DNA was added to 250 µl of a serum- and antibiotics-free cell culture medium, followed by addition of 9 µg PEI. The mix was vortexed, incubated at RT for 30-40 min, and transferred afterwards dropwise on the dish. The transfection medium was replaced 6 h after transfection with MEM complete. If required, the medium was supplemented with 0.5 mM AzF or 1 mM BzF, as previously described. To avoid glutamate-mediated excitotoxicity, a final concentration of 1 mM kynurenic acid solution was added to the cell culture medium. Kynurenic acid is a competitive antagonist of AMPA receptors, and thus prevented receptor overactivation by glutamate secreted during cell cultivation. This ensured cell viability despite receptor overexpression (Prescott et al., 2006).

For electrophysiological and biochemical experiments on homomeric receptors, three vectors were co-transfected: (*i*) the GluA2 wild-type or Amber mutant subunit; (*ii*) the orthogonal tRNA-synthetase; and (*iii*) the orthogonal tRNA. Transfections were performed in a mass ratio of 4:1:1. Wild-type controls were always co-expressed on the same tRNA / tRNA-synthetase-containing background, unless otherwise stated. For recordings of heteromeric receptors, four vectors were

co-transfected: (*i*) the rat GluA1 (Q) subunit; (*ii*) the edited form of GluA2, A2 Q607R_IRES_eGFP-Y40TAG, carrying an Amber mutation; (*iii*) the tRNA; and (*iv*) the tRNA-synthetase. The DNA mass ratio (GluA1:GluA2) was typically 1:1, if not differently stated.

2.2 Molecular biology

2.2.1 Expression vectors

Vectors encoding AMPA receptor subunits

Rat GluA2 subunits were expressed from a bicistronic BiQG pRK5 expression vector. The flip splice variant of the subunit, unedited at the Q/R site and with G at the R/G site, was used for overexpression of homomeric receptors. The endogenous TAG stop codon of GluA2 was edited to the Opal stop codon (TGA) in order to prevent incorporation of UAAs. Amber stop codons were introduced by overlap PCR at a series of positions within the LBD: L483, A665, M721, G725, S729, and Y768. eGFP was expressed from an Internal Ribosome Entry Site (IRES) immediately following the GluA2 coding sequence. Initially, a wild-type gene for eGFP was used, which was later modified via introduction of a Y40TAG mutation to act as a reporter of cells that were competent for rescue of Amber codons. The following natural substitution GluA2 mutants were designed: L483F, L483Y, S729Y. The pRK5 vector contained a cytomegalovirus (CMV) promotor for protein expression in mammalian cell lines and ampicillin-resistance for selective bacterial transformations.

For recordings of heteromeric receptors, an unedited rat GluA1 (Q; without a fluorescent marker) expressed from the pcDNA 3.1 (+) vector was used, and the edited form of GluA2, A2 Q607R_IRES_eGFP-Y40TAG (QR), with introduced Amber mutations at the M721, G725, and S729 sites within the LBD.

For Western blotting, GluA2 wild-type or Amber mutant subunits with three cysteines deleted (3 x Cys (–); C190A, C436S, C528S), and carrying a C-terminal FLAG-tag were used (Lau et al., 2013).

Amber suppressor tRNA / tRNA-synthetase pairs specific for AzF and BzF

Orthogonal Amber suppressor pairs specific for BzF and AzF, previously validated for use in

mammalian cells, were obtained from Thomas Sakmar (Rockefeller University, NY, USA; Ye et al., 2008; 2009). The synthetases were specific for either AzF or BzF and drove suppression of Amber codons by aminoacylating their cognate exogenous mutant tRNA with the appropriate UAA. They derived from an *E. coli* Tyr-synthetase gene and contained the following point mutations: Y37G, D182G, and L186A within the BzF-synthetase gene; and Y37L, D182S, F183M, and L186A within the AzF-synthetase gene. The RS variants were cloned into a pcDNA3.1(+) / neo expression vector and contained a C-terminal FLAG-tag. The Amber suppressor tRNA derived from the *Bst* $tRNA^{Tyr}$ (*Bst*-Yam) and could be charged with both AzF and BzF. The expression cassette was expressed from a pSVBpUC vector and contained: (*i*) a 5′ leader sequence from the human $tRNA^{Tyr}$ gene; (*ii*) the *Bst* $tRNA^{Tyr}$ gene sequence with a CUA anticodon; and (*iii*) a 3′-terminal transcription termination sequence.

Vector encoding mCherry

The fluorescent protein mCherry was expressed from a pmCherry-N1 vector (Clontech Laboratories, Inc., Saint-Germain-en-Laye, France) and was used as a transfection control.

2.2.2 Buffers and solutions

50 x TAE buffer

The 50 x TAE stock solution contained (in M): 2 Tris base (MW: 121.14), 1 acetic acid (MW: 60.05), 0.1 $Na_2EDTA \bullet 2\ H_2O$ (MW: 372.2). The pH was adjusted to 8.5.

Super optimal broth with catabolite repression (SOC) medium

The SOC medium contained: 0.5% (*w/v*) Bacto-yeast extract, 2% (*w/v*) Bacto-tryptone, 10 mM NaCl, 2.5 mM KCl, 10 mM $MgCl_2 \bullet 6\ H_2O$, 10 mM $MgSO_4 \bullet 7\ H_2O$. All ingredients were dissolved in milliQ H_2O in the absence of magnesium. After autoclaving, the magnesium reagents were added under sterile conditions. The pH was usually between 6.8 and 7. SOC medium stocks were stored at –20°C.

2.2.3 Site-directed mutagenesis

2.2.3.1 Preparation of primers

Mutagenic and flanking primers were designed using the MacVector software (MacVector, Inc.; Cambridge, UK). Primers for site-directed mutagenesis and sequencing were purchased from Biomers GmbH (Ulm, Germany). The lyophilized primers were dissolved in endotoxin-free 1 x TE buffer (Macherey & Nagel, Düren, Germany) and stored at –20°C.

2.2.3.2 Overlap polymerase chain reaction (PCR)

Site-directed mutations were introduced using overlap PCR, a two-step reaction PCR (Aiyar et al., 1996). Specific mutagenic primers (m1 and m2) and flanking primers (F1 and F2) were used to insert Amber mutations or natural substitutions. The process of overlap PCR mutagenesis is shown schematically in **Figure 7**. In the first step, intermediate PCR products were generated by the F1/m2 and m1/F2 primer pairs that contained an overlapping region with the mutation site of interest. The two separate PCR products were used as templates for a second PCR reaction directed by the flanking primers F1 and F2. The Phusion Polymerase with its appropriate buffer was purchased from Thermo Fisher Scientific, dNTPs were obtained from KAPA Biosystems (Wilmington, MA, USA). The PCR was run in the Flex Cycler PCR machine (Analytik Jena, Jena, Deutschland).

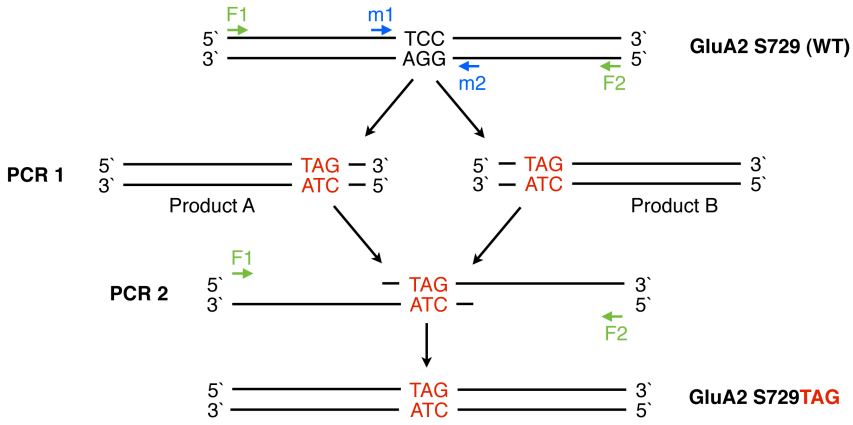

Figure 7 Schematic representation of the overlap PCR process. The Amber codon insertion at the GluA2 site S729 is shown as an example. Mutagenic (*blue*) and flanking primers (*green*) were used to replace the codon for serine (TCC) at position S729 within a WT GluA2 subunit by an Amber stop codon (*red*). Intermediate PCR products amplified by the F1/m2 and m1/F2 primer pairs were generated (first round of PCR). Both products contained an overlapping region with the introduced Amber mutation. The two fragments were mixed in the second round of the PCR in order to amplify the full insert using the flanking primers F1 and F2. The generated PCR product carried the S729TAG mutation.

The PCR reaction mixes were prepared as follows:

<u>First step of PCR:</u>

Template DNA	10 ng
F1 or F2 (25 µM)	1 µl
m2 or m1 (25 µM)	1 µl
dNTP (10 mM)	1 µl
5 x Phusion Buffer HF	10 µl
Phusion Polymerase (2 U/µl)	0.5 µl
H_2O (milliQ) *ad.* 50 µl	

<u>Second step of PCR:</u>

PCR product 1	10 ng
PCR product 2	10 ng
F1 (25 µM)	2 µl
F2 (25 µM)	2 µl
dNTP (10 mM)	2 µl
5 x Phusion Buffer	20 µl
Phusion Polymerase	1 µl
H_2O (milliQ) *ad.* 100 µl	

The primer annealing temperature was calculated with the MacVector software from the melting temperature (T_m) of the primer pair used. The template was denatured for 3 min at 94°C followed by 35 cycles of the following PCR program:

denaturation	94°C	30 s
primer annealing	depending on the primers used	30s
primer extension	72°C	30 s/kb (depending on the fragment length)
final extension	72°C	5 min

2.2.3.3 Agarose gel electrophoresis and gel extraction of the PCR products

The amplified PCR products were separated on 1% agarose gels (SeaKem®LE Agarose; Lonza, Rockland, USA) that were supplemented with ethidium bromide (1:10000 of a 1% stock solution). The separation of DNA fragments was carried out in 1 x TAE buffer at 80-120 V. A 6 x DNA loading dye (Thermo Fisher Scientific) was used. The DNA fragment size was determined using the following markers: the 1 kb DNA ladder (ranging from 250 to 10000 bp; O`Gene Ruler; Thermo Fisher Scientific) or a 100 bp marker (ranging from 100 to 1500 bp; produced by the Plested lab). The DNA fragments were visualized by a UV lamp (Peqlab Biotechnologie GmbH, Erlangen, Germany) and extracted from agarose gels using the Innu PREP Gel extraction kit (Analytik Jena) as described by the manufacturer.

2.2.3.4 Enzymatic digestion of the PCR products

Products of the second PCR contained specific restriction sites for insertion into the GluA2 pRK5 expression vector. Both the template vector and the second PCR product were cut using the same enzymatic single cutters prior ligation. Enzyme-specific restriction buffers were purchased from New England Biolabs GmbH (NEB; Frankfurt am Main, Germany). Bovine serum albumin (BSA) was added to the digestion reactions if required.

The restriction reaction was prepared as follows:

Template (host) vector	2 µg
or second PCR product (insert)	1.5-2.5 µg
Restriction enzyme A	5-10 U (Units)
Restriction enzyme B	5-10 U
100 x BSA	0.5 µl
10 x NEB buffer	5 µl
H_2O (milliQ) *ad.* 50 µl	

The mixes for DNA restriction were vortexed shortly and spun down. Depending on the restriction enzymes used, the restriction samples were incubated for ~2 h at their favoured temperature (most of the enzymes used were active at 37°C). Digested fragments (host vector and inserts) were separated on 1% agarose gels and extracted as described above.

2.2.3.5 Dephosphorylation of the host vector

Vector backbones were dephosphorylated following restriction in order to prevent re-ligation. Hereby, 1 U of Fast Alkaline Phosphatase (Fast AP; Thermo Fisher Scientific) was used per 1 µg DNA. The mix was incubated for 10 min at 37°C, followed by inactivation of the enzymes at 75°C for 5 min.

2.2.3.6 Ligation

The insert was ligated into the host vector using a T4 ligase (1 Weiss U / µl) with its appropriate buffer (Thermo Fisher Scientific). The ratio between the plasmid and the insert was usually 1:3. 50 ng of the dephosphorylated vector backbone were used for the ligation. The amount of the insert was calculated from the following equation (Erdmann et al., 2005).

$$\text{amount}_{\text{insert}}\,(\text{ng}) = (50\ \text{ng} / \text{size (bp)}_{\text{vector}}) * \text{size (bp)}_{\text{insert}}$$

The reaction batch was prepared as follows:

Template	50 ng
Insert	calculated amount (ng)
10 x T4 ligation buffer	2 µl
T4 ligase	1 µl
H_2O (milliQ) *ad.* 20 µl	

The samples were vortexed, spun down, and incubated for 45 min at RT. To inactivate the T4 ligase, the tubes were subsequently placed on the heater (65°C) for 10 min. A control reaction without inclusion of the insert-DNA was prepared additionally.

2.2.3.7 Transformation into competent *E. coli* cells

Competent *E.coli* cells for transformations were prepared from the Nova Blue strain using the Roti®-Transform kit. The cell aliquots were stored at –80°C until use. 2 µl of the ligation sample were added to 80 µl of competent *E.coli* cells and incubated for 20 min on ice. A heat shock at 42°C for 40 s allowed creation of pores into the bacterial cell membrane and thus introduction of the DNA. The competent cells were transferred into sterile 13 ml Falcon tubes (Sarstedt), 100 µl of the SOC medium were added, and the mix was shaken for 30-45 min at 37°C in the incubator. Afterwards, the cells were transformed on ampicillin-containing agar plates (Lennox; the final concentration of ampicillin was 100 µg/ml) and the clones grew at 37°C overnight. The control ligation sample (in the absence of the insert) was expected to result in a colony-free plate.

2.2.3.8 DNA Mini- and Midi-preparations

LB medium (Luria / Miller; the final concentration of ampicillin was 100 µg/ml) was inoculated with isolated bacteria clones for DNA Mini- or Midi-preparations. The samples were shaken at 200 rpm at 37°C overnight. The DNA was isolated from bacterial cells using the innu PREP Plasmid Mini- or Midi-Kit (Analytik Jena) as described by the manufacturer.

2.2.3.9 Analysis of the mutated DNA

To confirm a succeeded ligation of the mutated insert into the host vector, the plasmid DNA was cut with restriction enzymes as used for the digestion prior ligation, and separated on 1% agarose gels.

Following DNA-preparations, the received DNA concentrations were determined using a spectrophotometer (IMPLEN Nano Photometer; München, Germany). The ratio of absorbance at

260 and 280 nm was used to assess the DNA purity. A ratio of 1.8 qualified the plasmid DNA for further use.

The sequence of the entire amplified region was confirmed by double-strand sequencing using the flanking primers from the PCR reaction. The sequencing samples were prepared as follows:

DNA (200 ng)	1 µl
Primer (5 µM)	1 µl
milliQ H_2O	5 µl

The sequencing was performed by the group of Prof. Dr. Thomas Jentsch. Prior sequencing, the DNA went through a PCR reaction in the presence of a BigDye® Terminator Cycle Sequencing kit (v1.1; Life Technologies GmbH) to allow detection by the sequencing machine. Following purification on Sephadex G-50 chromatography medium (superfine; GE Healthcare Europe GmbH, Freiburg, Germany), the samples were mixed with Hi-Di™-Formamide (Life Technologies GmbH), and sequencing was carried out in an AB Prism 3730 DNA Analyzer (Applied Biosystems, Darmstadt, Germany).

2.2.3.10 Plasmid preparation for archiving

5 µl of plasmid DNA (1 µg/µl) were mixed with 2.32 µl of endotoxin-free 1 x TE buffer and 17.68 µl of 99% ethanol. For precipitation, 1 µl of 3 M sodium acetate was added followed by centrifugation at maximum speed (~14000 rpm) for 20 min. The pellet was washed with endotoxin-free 70% ethanol, dissolved in 50 µl 1 x TE buffer, and stored at –20°C.

2.3 Electrophysiological recordings

2.3.1 Solutions

The osmolarity of all extra- and intracellular solutions was determined in the cryoscopic osmometer (Gonotec GmbH, Berlin, Germany) using a 300 mOsm calibration standard (Osmomat 030-M-RS; Gonotec GmbH).

Ringer solution

The 10 x external Ringer solution contained (in mM): 150 NaCl, 0.1 $MgCl_2$ (MW 203.3), 0.1 $CaCl_2$ (MW 110.985), 5 HEPES (from Bowie, 2002). All ingredients were dissolved in milliQ H_2O and the solution was titrated to pH 7.3 with NaOH. The stock solution was filtered using a 0.2 µM Nylon filter (Corning Life Science, Amsterdam, Netherlands) and stored at 4°C. The 1 x Ringer solution was prepared freshly on the day of use (in milliQ H_2O). Before use, it was pre-warmed to 35°C, and degassed by vacuum-filtration through a 0.2 µm Nylon filter (Merck Millipore). This procedure largely removed particles and impurity, and eliminated bubble forming in the perfusion system during electrophysiological recordings.

Intracellular solution

In most experiments, the pipette solution contained (in mM; from Bowie, 2002): 115 NaCl, 10 NaF (MW: 41.99), 5 Na_4BAPTA (MW: 564.37; Life Technologies GmbH), 0.5 $CaCl_2$, 1 $MgCl_2$, 5 HEPES, 10 Na_2ATP (MW: 551.2; Calbiochem / Merck Millipore). After dissolving, the solution was titrated to pH 7.2 and filtered through a 0.2 µm Nylon filter (Merck Millipore). Aliquots were stored at –20°C.

100 µM polyamine intracellular solution

The polyamine internal solution included (in mM; from Bahring et al., 1997): 120 NaCl, 10 NaF, 5 Na_4BAPTA, 0.5 $CaCl_2$, 0.03 spermine (MW: 202.34; Ascent Scientific / Abcam Biochemicals®, Cambridge, UK), 5 HEPES. It was titrated to pH 7.2 and filtered through a 0.2 µm Nylon filter (Merck Millipore). Aliquots were stored at –20°C.

Glutamate solution

The glutamate stock solution contained (in M): 2 L-glutamic acid (kosher, MW: 147.13; SAFC®), 0.5 D (+) saccharose (MW: 342.3), and 1.5 NaOH. The ingredients were dissolved in 1 x Ringer solution, and titrated to pH 7.3 with NaOH. Glutamate stocks were stored at –20°C. The 10 mM glutamate solution was prepared freshly in 1 x Ringer solution on the day of use, with subsequent filtration through a 0.2 µm Nylon filter (Millipore).

Cyclothiazide (CTZ) solution

For a 50 mM stock solution, cyclothiazide (CTZ; Ascent Scientific, Weston-Super-Mare, UK) was dissolved in DMSO (MW 78.13). The CTZ stock aliquots were stored at –20°C. The 100 µM CTZ solution was prepared freshly in 1 x Ringer on the day of use.

2.3.2 Preparation of agar salt bridges

The ground electrode (Ag-AgCl Electrode Disc, 8 x 1 mm; Warner Instruments, Hamden, CT, USA) was physically isolated from the bath chamber. The electrical connection to the bath solution was provided by an agar salt bridge. The bath surrounding the ground electrode was filled with 3 M KCl and Agar bridges were prepared from a 3% agar solution in 3 M KCl (*w/v*). Glass capillaries (Borosilicate, thin wall with filament, Model No. G150TF-3; Warner Instruments) were bent into a square shape above a flame of a Bunson burner and filled with the pre-warmed agar solution, free from air bubbles. Agar bridges were dried at RT and stored in 3 M KCl to prevent drying-out. Before and after using, their outside was rinsed in milliQ H_2O.

2.3.3 Preparation of patch pipettes

Thin wall capillaries (Borosilicate; Warner Instruments) were pulled using the P-1000 Flaming / Brown puller system (Sutter Instrument, Novato, CA, USA). The capillaries were placed into the puller bar and melting was carried out by a box heating filament (Sutter Instrument). To ensure optimal heat settings, a ramp test was run initially, followed by setting up the pulling protocol. Patch pipettes were fire-polished using a microforge (CPM-2; Ala Scientific Instruments, Farmingdale, NY, USA) prior recordings. The open tip electrode resistance was usually 3-5 MΩ when dipping into the bath solution.

2.3.4 Preparation of perfusion tools

For rapid activation of AMPA receptors during electrophysiological recordings, outside-out patches were perfused using a four-barrel glass perfusion tool (the narrow tip of the tool is shown in **Figure 10**). To guarantee a fast solution exchange and a sharp interface between the

control (1 x Ringer) and the glutamate solution, the perfusion tools were prepared based on a standartized protocol from the lab. Square four-barrel glass tubings (Vitrocom, Mountain Lakes, NJ, USA) were cut into 10 cm pieces using a diamond pencil (Ted Pella, Inc., Redding, CA, USA). The glass capillaries were pulled apart in the middle (without breaking) in the P-1000 Flaming / Brown puller. A diamond cutter was used to make a sharp cut at the well-defined thin tip under the microscope. The tip was bent by ~30° by applying heat from a filament. The glass tubes were subsequently cut with a diamond pen ~0.5 cm from their short tip (~500 µm in length), which was incubated in hydrofluoric acid (48%) in order to etch the glass. Following rinsing steps with low concentrations of NaOH diluted in milliQ H_2O helped to remove the hydrofluoric acid. For assembly of the perfusion tool, 0.25 mm Silica tubes (Aligent Technologies GmbH, Waldbronn, Germany) were inserted into each barrel of the tool. The Silica tubes were fixed with a two-component glue (Araldite, epoxy resin) within the tool. In order to minimize the dead volume within the perfusion tool and to ensure a faster solution exchange, the four-barrel glass capillary was largely filled with glue, starting at the open end (where the cut was made), allowing the glue to flow inside, until proximity to the tip. After assembly, the perfusion tools were dried and stored at 42°C. Before use, freshly prepared perfusion tools were cleaned by sucking up milliQ water in order to prevent blocking of the tip. Subsequently, they were cleaned prior and after each experiment by pushing filtered water through the perfusion tools.

2.3.5 The experimental setup

The experimental setup, as used for outside-out patch-clamp recordings, is illustrated in **Figure 8**. The IX-71 inverted microscope (Olympus, Tokyo, Japan) with a 20 x LUCPLFLN Ph lens objective (Olympus) was mounted on a compressed air isolation table (TMC, Peabody, MA, USA). A Faraday cage (TMC) surrounded the setup to isolate it from electrical noise. For electrophysiological recordings, the cover slips were placed into a custom-made perfusion chamber, where they were constantly perfused with the 1 x Ringer solution with a flow rate of approximately 2 ml/min. The outflow was connected to a vacuum pump (Dymax 14; Charles Austen Pumps Ltd, Surrey, UK). A video camera (Model No. WAT-250D2; Watec, Inc., Newburgh, NY, USA) allowed to visualize the cells and the fast perfusion of patches on a

monitor. The perfusion tool was connected via Teflon tubing with valve-controlled 20 ml syringe vessels (BD Plastipak™, Hartenstein). It was mounted on a piezoelectric transducer (Physik Instrument, Palmbach, Germany) and was controlled via a Piezo amplifier (Physik Instrument) connected to the digitizer interface (Instrutech ITC-18; HEKA Instruments, Malsfeld, Germany). The patch pipettes were mounted onto a low noise holder (ISO-S-1.5G; G23 Instruments, London, UK) attached to a head stage. The volume of the external solution within the chamber was kept low, in order to minimize the noise. Movements of the patch pipette were controlled by a 3 D-PatchStar Micromanipulator (Scientifica). The resistance at the patch pipette tip was monitored by an oscilloscope (Tektronix; Beaverton, OR, USA). Currents (filtered at 5-10 kHz) were recorded using an Axopatch 200B amplifier and the Axograph software (AxoGraph X Scientific, Berkeley, CA, USA).

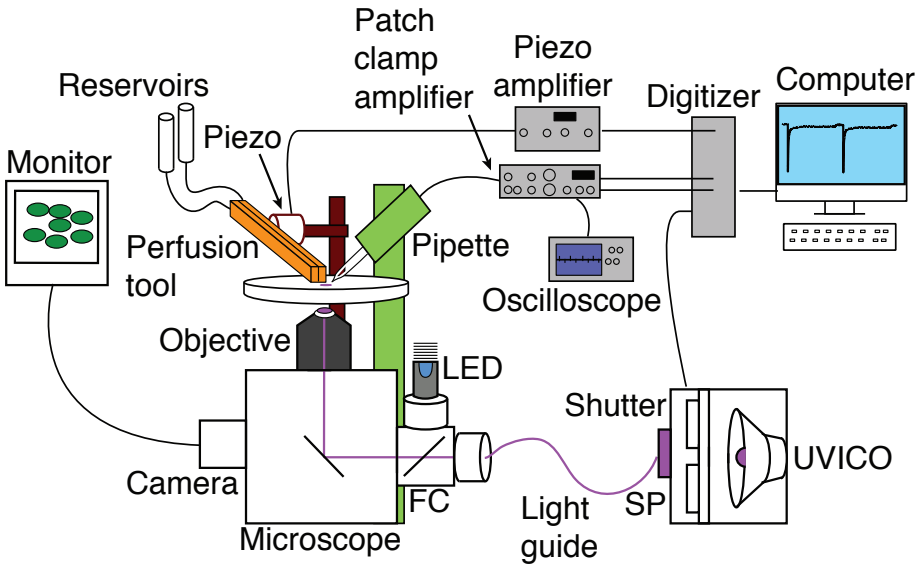

Figure 8 Schematic representation of the setup used for electrophysiology coupled to photoinactivation. Fluorescent cells were selected from cover slips within the bath using a video monitor. The fire-polished microelectrodes were mounted onto a pipette holder (*green*). The solutions were applied from a perfusion tool (*orange*). Rapid jumps into glutamate were made by switching a Piezo (*dark red*), which was controlled by a Piezo amplifier. UV pulses were applied through a 20 x objective and were provided by the UVICO lamp (see also Section 2.3.8). The path of UV light is indicated as a *violet* beam (*SP*, SP400 short path filter; *FC*, filter cube). AMPA receptor currents were measured with a patch-clamp amplifier and recorded with the AxoGraph X software (modified from Klippenstein et al., 2014).

2.3.6 Fast-perfusion outside-out patch-clamp recordings

To study ionic currents permeating through ion channels, the patch-clamp technique was used (Hamill et al., 1981; Sakmann & Neher, 1984). Electrophysiological fast-perfusion recordings were performed on excised outside-out patches. The *outside-out configuration* was obtained via several steps (**Figure 9**). Freshly-pulled and polished patch pipettes were back-filled with the electrolytic intracellular solution. Positive or negative pressure into the interior of the electrode holder was applied by mouth using a 1 ml syringe (BD Plastipak™, Hartenstein) connected to a Teflon tube. The resistance of the electrode was monitored on the oscilloscope by choosing the seal test mode. Initially, a test pulse of 5 mV and 10 ms in a frequency of 50 Hz was applied (**Figure 9 A**) and the patch pipette resistance was determined by Ohm´s law (R = V / I). The resistance of the open patch pipette was usually 3-5 MΩ. The liquid junction potential, which occured following dipping of the patch pipette into the bath solution, was corrected with the offset of the amplifier. Cells attached to adjacent cells and with a faint cytoplasmic fluorescence due to common eGFP expression or based on rescue of the Amber codon by an UAA in eGFP-Y40 (the dual Amber reporter was preferred; see **Results 3.2**), were selected. Application of positive pressure during simultaneous slow approach to the cell resulted in the *on-cell configuration* indicated by an increase in patch pipette resistance (**Figure 9 B**). To tightly seal the microelectrode onto the plasma membrane of the HEK-293 cell, negative pressure (slight sucking) was applied, until the seal resistance reached at least 1 GΩ, which is termed *gigaseal* (**Figure 9 B**). Brief suction through the patch pipette caused *break through*, which ruptured the plasma membrane. In this *whole-cell configuration*, the lumen of the patch pipette merged with the interior of the cell (**Figure 9 C**). To reach the *outside-out patch-clamp configuration*, with the extracellular part of the ion channel facing the bath solution, the microelectrode was slowly lifted (**Figure 9 D**). The excised patch was held at the interface between the control and test solution, in order to be activated by rapid jumps into 10 mM glutamate (**Figure 10**; Colquhoun et al., 1992). Currents of outside-out patches were clamped at –60 mV, except where noted.

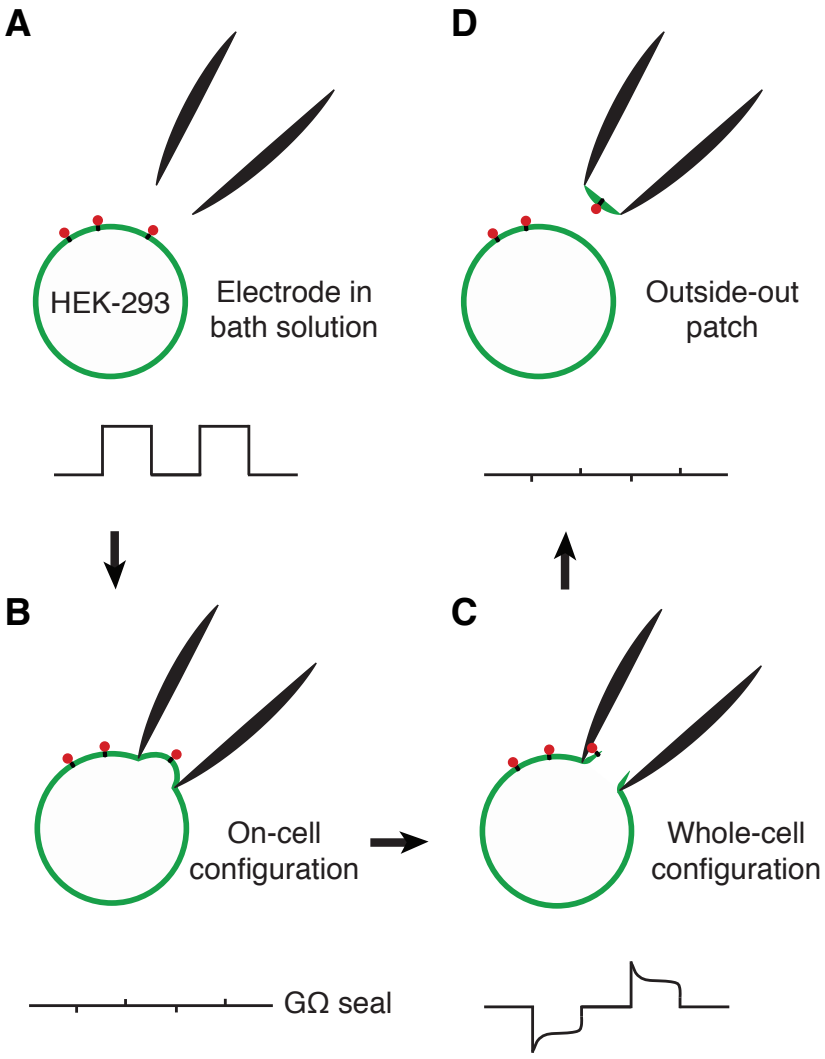

Figure 9 Obtaining the outside-out patch configuration. The schematic figure shows a cell (*green*) expressing plasma membrane located receptors (the extracellular domain is shown in *red*) and the tip of a patch pipette (*black*). Additionally, the characteristic patch pipette resistance for each configuration observed is shown below. (**A**) Dipping the electrode into the bath solution with simultaneous application of a test pulse. (**B**) Approaching of the microelectrode to the cell results in the *on-cell configuration*, indicated by an increase in resistance. Negative pressure induces the formation of a *gigaseal*. (**C**) To reach the *whole-cell configuration*, the plasma membrane has to be ruptured. This increases capacitive artefacts based on the cell capacitance. (**D**) Pulling a patch results in the *outside-out patch configuration* under maintenance of the *gigaseal*.

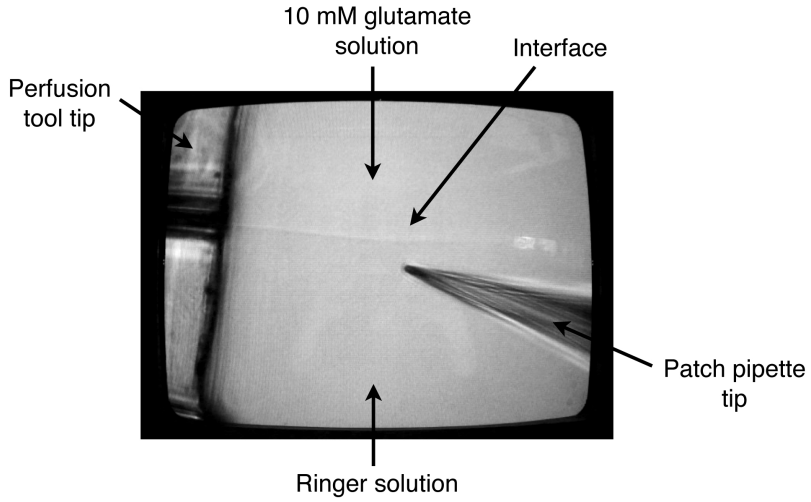

Figure 10 Rapid perfusion electrophysiology. Outside-out patches isolated from HEK-293 cells were held at the outflow of the Ringer solution, close to the interface between the control and test solution, and were activated by rapid jumps into a 10 mM Glu solution. Glutamate was applied for durations between 1 and 1000 ms. Fast solution exchange was ensured by a piezo-driven four-barrel glass-perfusion tool. The picture was taken during a recording from the monitor using the 20 x objective.

2.3.7 Open tip recordings as indicators of fast solution exchange

On every day of electrophysiological recordings, the solution exchange was first tested on an open microelectrode in the absence of the patch. Doing this before the actual patch-clamp recording provided information about the quality of the perfusion tool and the speed of the solution exchange. Hereby, the tip of the patch pipette was placed close to the interface between the 1 x Ringer and glutamate solution (see **Figure 10**). At least 30 jumps into 10 mM glutamate were recorded. In cases, where excised outside-out patches did not give any currents, the chosen position for the glutamate jumps could be tested. The patch was blown out by applying positive pressure, while the microelectrode was kept at the same position. As a rule, the solution exchange should be completed within 1 ms at most. Patches, in which the exchange of solutions was slower than 1 ms, were discarded. An example of an open tip recording is shown in **Figure 11**.

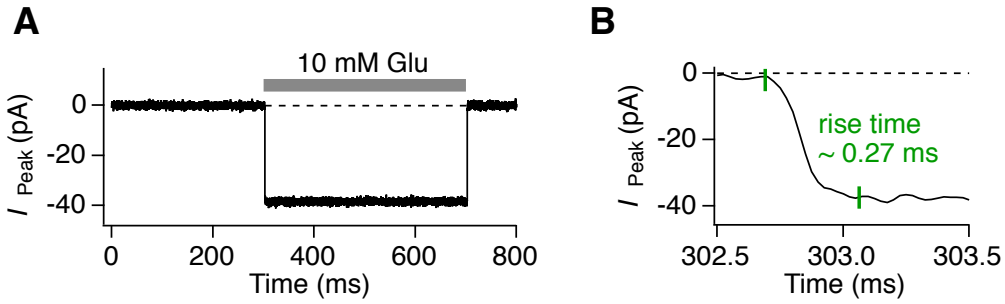

Figure 11 Example of a typical open tip recording. (**A**) An average of 30 episodes of glutamate applications for 400 ms is shown. For this example, the baseline was subtracted for clarity. (**B**) The solution exchange on a smaller timescale shows a rise time of ~0.27 ms.

2.3.8 Photoinactivation of AMPA receptors by UV

Following excision of the patch, the GFP filter at the microscope was switched to a UV filter. A shutter behind the UV filter allowed opening and closing of the UV pathway. By doing so, UV exposures could be stopped or started at any time throughout the recording. Different UV sources were tested in order to trap AMPA receptors harboring UAAs. The short-pulse UV lamp (SP-20) produced ~360 µs pulses of UV in a repetition frequency of 0.25 Hz and a pulse power of 200 kW. Longer UV pulses of 50-300 ms duration were applied by a 120 W metal halide bulb of the UVICO system with a repetition frequency of 0.5 Hz. The UV power at the focal plane was approximately 30 mW during full illumination (Gert Rapp, personal communication), or about 30 kW/m^2. The UV intensities could be roughly controlled manually, reaching from 0-100%. Both UV flash systems used were purchased from Rapp OptoElectronic (Wedel, Germany).

An integral mechanical shutter in front of the light guide under computer control (TTL pulse) generated UV pulses of defined durations, which were passed through a short-pass 400 nm (SP400) filter (see **Figure 8**). A liquid light guide coupled the excitation light to a FC70 filter cube (in which a 420 nm dichroic mirror combined a ~455 nm LED for visualizing GFP fluorescence) mounted on the epi-fluorescence port of the microscope.

UV could be applied in different conformational states (**Figure 12**) – either in the desensitized or active state (during applications of 10 mM glutamate), or in the resting state (prior activation by

glutamate). To isolate the active state, the allosteric modulator CTZ was applied. The pulse of UV during the desensitized or active state started ~100 ms after the peak of the current. In the absence of CTZ, at this point more than 90% of receptors were in the desensitized state. In order to trap the resting state, the pulses of UV ended ~100 ms prior jumping into glutamate.

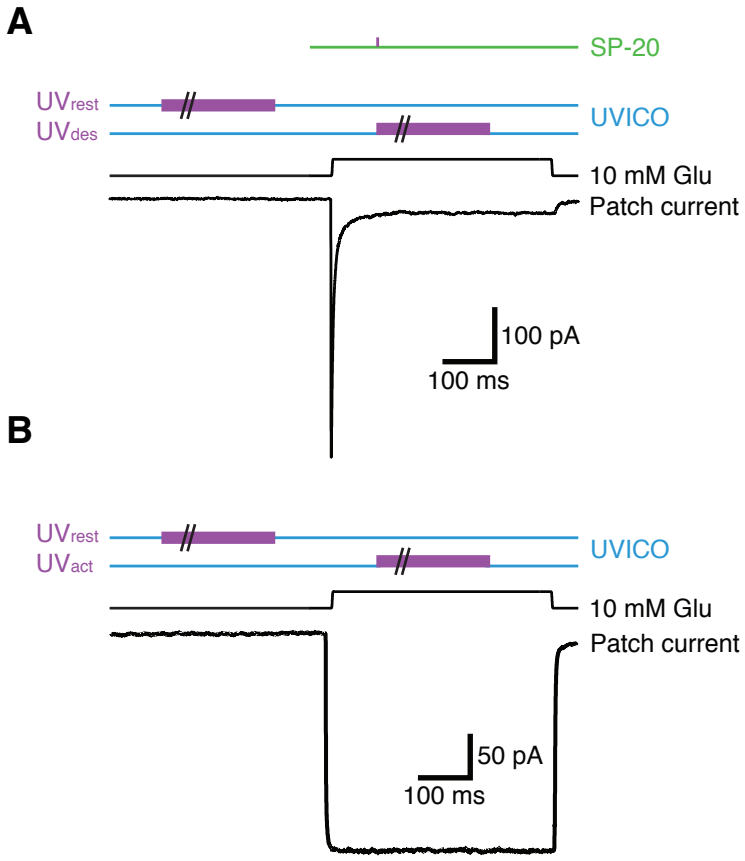

Figure 12 Electrophysiology coupled to photoinactivation. The traces indicate the response of outside-out patches to applications of 10 mM Glu in the absence (**A**) or presence (**B**) of CTZ, and the timing of exposure to UV (*violet*; the *strokes* indicate variable intervals of UV exposure) in different functional states during each episode. UV exposure times varied between 360 µs (using the SP-20 lamp; *green*) and 50-300 ms (using the UVICO system; *blue*). The intensity of UV illumination could be changed and was usually either 50 or 100%. (**A**) A typical AMPA receptor trace in the absence of CTZ. UV pulses of 50-300 ms duration (from the UVICO lamp) were applied in either the desensitized or resting state. An example for a further UV source (SP-20) that produced short pulses of ~360 µs is shown additionally. (**B**) A typical AMPA receptor trace in the presence of CTZ. CTZ was applied to outside-out patches in order to isolate the active state. Equivalent to panel *A*, receptors were exposed to UV for variable time periods during (within the active state) or prior (in the resting state) activation by 10 mM Glu.

2.4 Biochemistry

72 h after PEI transfection, HEK-293T cells expressing GluA2 receptors were exposed to UV (if required), collected, and lysed. All steps of sample preparation were carried out at 4°C, and all buffers and solutions used for biochemistry, if not differently indicated, were kept at 4°C, in order to prevent protein degradation. The final, optimized procedure involved GluA2 constructs lacking three native cysteines in order to reduce the tendency of the receptor to dimerize in basal conditions (Lau et al., 2013). To further reduce dimer fractions from adventitious disulfide formation, 20-40 mM N-ethyl-maleimide (NEM) was added to all buffers throughout the UV treatment of cells and protein purification. NEM is a membrane-permeable alkylating reagent, which forms stable, covalent thioether bonds with sulfhydryls (e.g. reduced cysteines) and thus quenches cysteines. Since the maleimide reaction is pH sensitive, with specificity for sulfhydryls at pH 6.5-7.5, all buffers including the UV flashing buffer (1 x PBS), the lysis buffer, and the elution buffer were adjusted to pH 7.1-7.2. All solutions including NEM were prepared freshly on the day of the experiment.

2.4.1 Buffers and solutions

Tris-buffered saline (TBS) solutions

The 10 x TBS stock solution contained (in M): 0.2 Trizma base, 1.5 NaCl. The pH was titrated to 7.4. The solution was diluted in milliQ H_2O to obtain a 1 x TBS solution. The 1 x TBS-T washing solution included 0.01% Tween®-20 (*v/v*).

4 x protein sample buffer

The 4 x protein loading buffer included: 250 mM Tris / HCl (pH 6.8; MW 157.6), 8% SDS (MW 288.38), 40% glycerol (MW 92.09), 6.6% DTT (MW 154.3), 0.4% bromphenol blue dye (MW 669.99). β-mercaptoethanol (β-ME; 20-500 mM) was added freshly on the day of use.

1% (*w/v*) dodecylmaltoside (DDM) cell lysis buffer

The 1% DDM lysis buffer included (in mM): 300 NaCl, 50 Tris-HCl (pH 8.0), 20-40 NEM (MW: 125.13; Thermo Fisher Scientific). Additionally, one tablet of a protease inhibitor cocktail

(cOmplete Mini EDTA-free; Roche Diadnostics GmbH, Mannheim, Germany) and 1% (*w/v*) DDM (Glycon Biochemicals GmbH, Luckenwalde, Germany) were added.

Elution buffer for FLAG-tagged proteins

The elution buffer contained 100 µg/µl of a FLAG® Peptide in 1% DDM cell lysis buffer.

1 x Towbins transfer buffer

The blotting buffer included (in mM): 192 glycine, 25 Trizma base. Additionally, 20% methanol were added.

Milk solutions

5% milk powder (*w/v;* Sucofin, tsi GmbH, Zeuen, Germany) was dissolved in milliQ H_2O. For the 2.5% milk solution, the 5% milk solution was mixed at a ratio of 1:1 with 1 x TBS-T (0.01%).

Ponceau S solution

0.2% Ponceau S (MW: 760.56) were added to a 3% acetic acid solution and stored at RT.

2.4.2 *In vivo* UV treatment of cultured cells

HEK-293T cells were washed with 1 x PBS. The UV treatment was carried out in 10 ml of 1 x PBS containing 20-40 mM NEM. Dishes with cells were placed on ice and exposed to UVA light in a ventilated chamber (Luzchem, LZC-1; Ottawa, Canada; **Figure 13**) for fixed time intervals (2-60 min). The UV intensities were measured on each experimental day using an integrated UV sensor and were usually between 330 and 440 mW/m^2. The power meter was calibrated at 350 nm by the manufacturer and had an accuracy of ~25%. The spectral band was wider than in electrophysiological experiments, since no short-path filter was integrated into the chamber, thus producing UVA light with a lower intensity. 10 cm dishes were covered with Pyrex glass (Duran) where indicated. Non-UV-treated HEK-293T cells were used as controls. These were washed with 1 x PBS and collected directly in 20-40 mM NEM in 1 x PBS. Glutamate or CTZ were included in a final concentration of 100 µM during the UV treatment, where indicated, in order

to analyze state-dependent trapping of GluA2 subunits biochemically. Control dishes were equally incubated with glutamate or CTZ (at 37°C), but were not exposed to UV.

Figure 13 Oven for the *in vivo* UV treatment (Luzchem, LZC-1). (**A**) Interior of the UV oven. The eight UV lamps were mounted at the top of the oven with a distance of ~19 cm from the bottom. After warming up the oven for ~15 min, the the UV intensity was monitored using an integrated UV sensor. (**B**) The monitor outside provided information about the UV intensity at the sensor´s location. Typically, UVA intensities were between 330 and 440 mW/m^2. (**C**) Usually, two dishes were exposed to UV simultaneously. The 10 cm dishes were put on crushed ice in order to prevent overheating, and covered with Pyrex lids, where indicated.

2.4.3 Collecting and lysis of transfected cells

Immediately after UVA exposure, HEK-293T cells were harvested in 1 ml 1 x PBS (including 20-40 mM NEM), and centrifuged for 5 min at 1000 x g and 4°C. The cell pellets were resuspended in 1% DDM lysis buffer and sonicated (UP200S sonicator; Hielscher Ultrasoncis GmbH, Teltow, Germany). The cells were lysed in a cold room (4°C) at 10 rpm for 60 min (end-to-end mixing). During centrifugation at 20000 x g for 20 min and 4°C, the cellular debris and DNA were pelleted. The supernatant was saved, since it solubilized crude membranes contained the (FLAG-tagged) GluA2 protein.

2.4.4 Bradford assay to determine protein concentrations

Protein concentrations in lysed samples were determined by Bradford analysis (Bradford, 1976). A calibration line using 1 mg/ml BSA (AppliChem GmbH, Darmstadt, Germany) in 1% DDM

lysis buffer was created by means of BSA standards. The Bradford reagent (Bio-Rad Protein Assay Dye Reagent Concentrate; Bio-Rad Laboratories GmbH, München, Germany) allowed to measure the protein concentrations at the wavelength of λ = 595 nm using a spectrophotometer (IMPLEN, Nano Photometer).

2.4.5 Purification of FLAG-tagged proteins

80 µl of M2-FLAG affinity beads (ANTI-FLAG® M2 Affinity Gel) were washed twice with 1% DDM cell lysis buffer. Clear protein lysates were applied to the beads and rotated for two h at 10 rpm in a cold room. Afterwards, the samples were centrifuged at 800 rpm for 3 min and loaded on purification columns (illustra™ MicroSpin™ Columns; GE Healthcare). The columns were washed three times with 800 µl lysis buffer and subsequently centrifuged for 30 s at 800 rpm. The first elution was collected by centrifugation for three min at 800 rpm. Prior the second elution, 20 µl of the elution buffer were applied on the columns, which were shaken for 15 min at 300 rpm in the cold room. The FLAG-tagged protein was eluted via centrifugation for three min at 800 rpm. Elution one routinely did not contain detectable amounts of FLAG-tagged protein. The second elution of material from the column was usually the one most enriched in GluA2 protein, and was therefore loaded on the gel. Collected sampled were stored at –20°C, if the SDS-PAGE was not performed on the same day.

2.4.6 SDS-PAGE and Western blot

2.4.6.1 SDS-PAGE

The protein samples were mixed with a reducing 4 x protein sample buffer containing 20-500 mM β-ME. Due to weaker expression of GluA2 Amber mutants compared to wild-type receptors, the whole volume of eluted Amber mutant protein (20 µl) was loaded for SDS-PAGEs. Unless otherwise stated, 1 µl of the eluted GluA2 wild-type protein sample was used, which was sufficient to achieve a comparable band signal. The samples were heated for five min at 80°C and subsequently loaded onto 4-12% NuPAGE® Novex SDS gels gels (Life Technologies GmbH). 7 µl of a High Molecular Weight Protein Standard (Precision Plus Protein™

WesternC™ Standard; BioRad) were used. Gel electrophoresis was performed on crushed ice in the cold room. The gels run in a SDS-containing 1 x MOPS buffer (NuPAGE®; Life Technologies GmbH) at 80 V for 10 min (in order to compress the proteins into thin layers) followed by an increase of the voltage to 180 V for 1 h, until full separation of the protein bands.

2.4.6.2 Western blot

Before use, PVDF membranes (0.2 µm; BioRad) were equilibrated for one min in 100% methanol and rinsed in milliQ H_2O. Membranes, filter paper sheets (thick Whatman paper; Hartenstein), and sponges were equilibrated in 1 x Towbins blotting buffer. The protein transfer was performed in XCell II™ Blot Modules (Life Technologies GmbH) as described by the manufacturer. The blotting module was covered by the Towbins tranfer buffer and the blot was performed on crushed ice in the cold room at 25 V for 2 h.

2.4.6.3 Antibody staining

Prior antibody staining, PVDF membranes were washed twice for 5 min in 1 x TBS-T and blocked for 15 min with 10 ml of the 5% milk solution at 120 rpm at RT. Afterwards, the membranes were washed twice for 5 min in 1 x TBS-T (0.01%) and incubated overnight at 4°C and 15 rpm with the primary antibody (1:1000 in 5% milk solution). Primary antibodies used were a monoclonal mouse *α*-FLAG® M2 antibody (Agilent Technologies, Böblingen, Germany), a polyclonal rabbit *α*-GluA2 antibody (C-terminal, clone 6C4; Merck Millipore), a monoclonal mouse *α*-GluA2 (N-terminal; Merck Millipore), and a polyclonal rabbit *α*-GFP antibody (Cell Signaling Technology, Inc., Cambridge, UK). Following three washing steps for 5 min in 1 x TBS-T, the membranes were incubated with the secondary antibody (1:5000 in 10 ml 2.5% milk solution) for 1 h at RT. These were either a goat *α*-mouse (IgG HRP; Cayman Chemical, Hamburg, Germany) or a goat *α*-rabbit antibody (IgG HRP; Cayman Chemical).

2.4.6.4 Membrane developing

Before developing, the antibody-stained membranes were washed three times for five min with 1 x TBS-T (0.01%). The ECL reagent (SuperSignal® West Pico Chemiluminescence Substrate; Thermo Fisher Scientific) was applied for five min at a ratio of 1:1 to the membrane (1.5 ml per membrane of solution A plus 1.5 ml of solution B). The protein bands very visualized using an imager (Peqlab Biotechnologie GmbH). The exposure time was variable, dependending on the antibody used. The best signal-to-noise was obtained with exposure times between five and 20 min.

2.5 Confocal microscopy

2.5.1 Solutions

3% Paraformaldehyde (PFA) solution

PFA was dissolved in 1 x PBS (*w/v*). For dissolving, the content was heated up to 60°C. The pH was adjusted to 7.2 with 1 N NaOH and filtered through a 0.2 µm Nylon filter (NALGENE™). Aliquots were stored in the dark at –20°C.

2.5.2 Mounting of cover slips and imaging

48 h after transfection, the cover slips were washed with 1 x PBS, covered with the 3% PFA solution, and incubated for 15 min at RT in the dark for fixation. Afterwards, they were washed twice with 1 x PBS, and mounted on object slides (Menzel glass; Thermo Fisher Scientific) using Fluoromount G (Southern Biotech, Birmingham, ALA, USA). Confocal micrographs were taken with a Zeiss LSM 510 META laser-scanning microscope (Carl Zeiss Microscopy GmbH, Berlin, Germany) using the ZEN software (Carl Zeiss Microscopy GmbH). The confocal micrographs presented in this study were taken with a 40 x (Plan-Apochromat, 1.40 Oil DIC M27) objective.

2.6 Data analysis

The decays of receptor deactivation and desensitization were fit with single exponential functions using the Chebyshev algorithm in the AxoGraph X software. The time constants were given in ms and calculated into s^{-1}. The rise time (in ms) was measured from 10 to 90% of the peak current. The recovery from desensitization was obtained using a two-pulse protocol. The ratio between the test pulse and the second pulse after a specific interval (rate of recovery, k) was fit with a Hodgkin-Huxley type function: $N = N_0 + (1 - N_0) * (1 - \exp(-k*t))^n$, where N represents the active fraction of receptors after the interval at a time t. N_0 is the active fraction at the end of the conditioning pulse. The slope (n) was usually 2 (Plested and Mayer, 2009). The relationship between the peak current and the extent of inhibition (in %) upon UV was fit with a linear function. The steady-state current (I_{ss}) was usually normalized to the peak current. To compare steady-state plateaus after exposures of UV between mutant and wild-type receptors, the I_{ss} after UV was normalized to the average I_{ss} obtained in the pre-UV condition.

Kymograms of peak current reductions were globally fit with monoexponential decay functions with a common steady-state level for individual patches (where appropriate) to compare the trapping rates obtained from different UV conditions. The time constant was analyzed in episodes, if not differently stated. The function was as follows: $Y = -y_0 - A * \exp(-(x - x_0) / \tau)$. Hereby, *tau* ($\tau$) represents the exponential peak current reduction constant. The coefficients y_0 (the peak current at the steady-state level following receptor inactivation), A (the inactivating component of the current), x_0 (the span in episodes to reach the plateau), and τ were specified by initial guesses. Any discrepancy in terminal peak currents due to the potentiation of responses by CTZ was ignored.

The counting of fluorescent cells was performed 24 h, 48 h, and 72 h after transfection from an entire field of view using a 20 x objective lens. Usually, two confluent regions on the cover slip were chosen and the obtained number of fluorescent cells was averaged. Every fluorescent cells was included into counting. The numbers obtained for the different conditions were normalized to the amount of fluorescent cells 24 h after transfection and with all components included.

The rectification ratio (RR) of current-voltage (IV) relationships was calculated as the ratio between the current at –60 mV and the current at +40 mV. The IV curves were normalized to the peak current at –60 mV prior UV application.

Desensitizing fractions of receptors with blocked desensitization (due to CTZ or aromatic amino acids at position L483 in GluA2) were obtained from the ratio between the peak current at the end and the peak at the beginning of the glutamate pulse.

For biochemistry, data analysis was performed applying densitometric analyses using the ImageJ software (National Institutes of Health, Bethesda, MD, USA). The dimer fraction was calculated as the fraction of the dimer band intensity divided by the sum of the dimer and monomer band intensities.

The statistical significance was assessed with Student`s t-test, using either pairwise comparisons for different values from a single patch recording, or unpaired tests for comparisons between mutants or different cells. For multiple comparisons, such as to assess the statistical significance of any differences between the kinetic properties of the Amber mutants tested and GluA2 S729Y (seven groups in all, with wild-type GluA2 as the control group), or the time constants of current reduction in crosslinking experiments, One-way ANOVA with Dunnett's post-hoc test was performed using the KaleidaGraph software (Synergy Software, Reading, PA, USA).

Statistical results are presented as the average ± standard deviation (STDEV). Statistical significance was assumed at $^{*}p < 0.05$ and high significance at $^{*}p \leq 0.001$.

All graphs presenting the results were created using the IgorPro software (WaveMetrics, Inc, Lake Oswego, OR, USA). Adobe Illustrator CC (Adobe Systems, Inc.) was used for creating schematic representations or cartoons. For graphical representation, AMPA receptor structures were adapted in MacPyMOL.

3 RESULTS

3.1 The GluA2 S729 and G725 Amber mutants for initial characterization of receptor photoinactivation

For initial functional characterization of glutamate receptors with Amber stop codons genetically suppressed by the photoactive UAAs AzF and BzF, sites within the lower lobes (D2) of the LBD were chosen (S729, G725; **Figure 14**). These interfacial sites have been previously shown to form intermolecular disulfide crosslinks that inhibit the receptor (Armstrong et al., 2006; Plested & Mayer, 2009) and were expected to produce dimerization of subunits following UV-driven activation of the photoactive side chains of the introduced UAA groups.

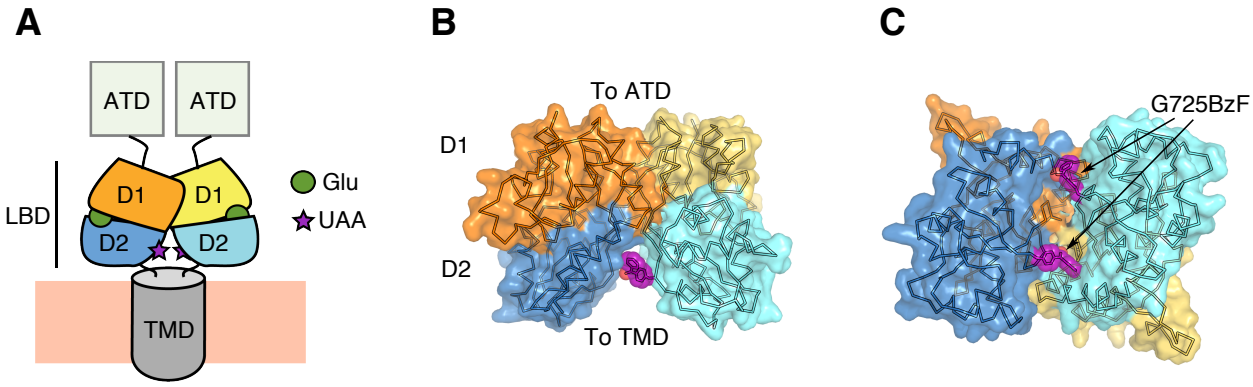

Figure 14 Sites of UAA incorporation within the lower LBDs (D2) of GluA2. (**A**) Diagram of a glutamate-bound (*green spheres)* AMPA receptor dimer, including its LBDs, ATDs, and the TMD. The UAAs (AzF or BzF; *purple asterisks*) were incorporated into the D2 lobes of the LBD. (**B**) Side view of the glutamate-bound LBD dimer of GluA2 (PDB: 1FTJ, chains A and C; Armstrong & Gouaux, 2000) with the same colour coding as in panel *A*. Only one of the BzF side chains is shown for clarity. BzF was taken from the crystal structure of a BzF-synthetase (PDB: 2HGZ; Liu et al., 2007) and was inserted at position 725 instead of glycine. (**C**) View of the same dimer as in *B* from below. Both BzF side chains at position G725 are shown within the dimer (modified from Klippenstein et al., 2014).

3.2 The dual Amber construct as a reporter of TAG codon suppression

Bicistronic vectors containing genes for a GluA2 Amber mutant and eGFP, separated by an IRES site, were initially used for electrophysiological recordings. The eGFP expression marked transfected cells. A graphical representation of the vector with the Amber codon site at position S729 in GluA2 for suppression by BzF is shown as an example (**Figure 15 A**). Typically, outside-out patches pulled from HEK-293 cells transfected with this construct together with the orthogonal tRNA / tRNA-synthetase pair and inclusion of either AzF or BzF did not give any detectable glutamate-activated currents (n = 17 for suppression by AzF, n = 13 for BzF; **Figure 15 C**). The experimental procedure, which involved a co-transfection of three different plasmids (the GluA2 Amber mutant, the tRNA, and the tRNA-synthetase) required a higher selective screening method in order to identify cells that received the whole set of components required for TAG codon suppression. To overcome the issue of low selectivity, a second Amber stop codon was introduced into eGFP, at position Y40 (**Figure 15 B**). This position is equivalent to the Y37TAG site, which has been used in various studies to characterize *in vivo* rescue of eGFP by different tRNA / tRNA-synthetase pairs (Liu et al., 2007; Takimoto et al., 2009). Using the dual Amber reporter, cells that showed green fluorescence contained eGFP rescued by an UAA, and therefore also a functional tRNA-synthetase / tRNA pair. Almost all outside-out patches pulled from these cells gave large responses to 10 mM glutamate, with a decrease in the ratio of blank to non-blank patches to ~5% with AzF, and to ~3% with BzF at the GluA2 S729 Amber codon site (n = 20 for S729AzF, n = 32 for S729BzF; **Figure 15 C**). These values are akin to GluA2 wild-type recordings, for which only 2-3% of outside-out patches do not respond to glutamate activation (*not shown*).

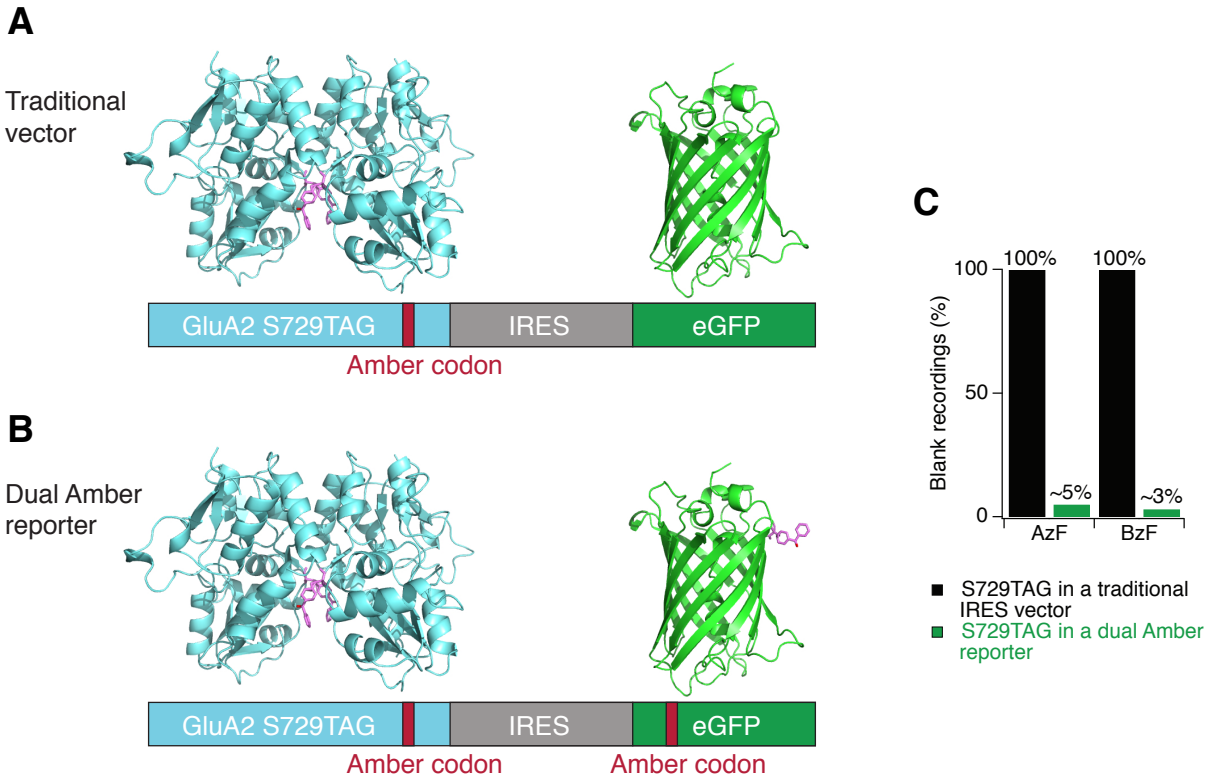

Figure 15 The bicistronic dual Amber reporter as a marker of Amber codon suppression in GluA2 receptors. (**A**) The common bicistronic vector encoded genes for GluA2 and eGFP, which were separated by an IRES motif. This construct contained one Amber codon site only (in this example at position S729). BzF modelled at position S729 into GluA2 (PDB: 1FTJ; Armstrong & Gouaux, 2000) is shown. The GFP structure was taken from Yang et al. (1996; PDB: 1GFL). (**B**) The dual Amber construct with an additional Amber stop codon at position Y40 in eGFP, which acted as a reporter for cells containing the whole plasmid set required for TAG codon suppression by UAAs. (**C**) Without Y40TAG within eGFP, all outside-out patches transfected with GluA2 S729TAG and the tRNA / tRNA-synthetase pair were blanks (n = 17 for AzF, n = 13 for BzF). The rate of blank recordings was immensely decreased after insertion of Y40TAG into eGFP – to ~5% after AzF incorporation (n = 20) and to ~3% after inclusion of BzF (n = 32).

An example of the rescue of fluorescence by suppression of the Y40 Amber codon within eGFP is shown in **Figure 16**. HEK-293 cells, co-transfected with the wild-type dual Amber reporter, the tRNA, the tRNA-synthetase, and incubated in a cell culture medium containing 0.5 mM AzF showed strong cytoplasmic fluorescence, due to suppression of the Amber stop codon within eGFP. A plasmid encoding mCherry was used to mark transfected cells. Cells, equally transfected with the same constructs, but not incubated in a medium supplemented with AzF, showed very faint fluorescence in only a small number of cells (**Figure 16 B**), which probably derived from an unspecific Amber stop codon suppression by endogenous amino acids. Similar eGFP fluorescence was observed for BzF (*not shown*). The degree of unspecific rescue of fluorescence under different conditions will be further presented in **Section 3.6.1**.

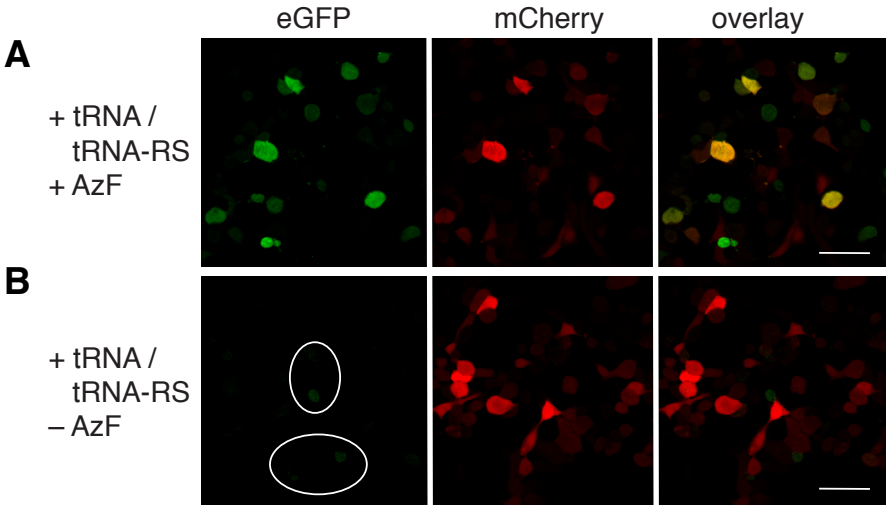

Figure 16 Rescue of fluorescence by AzF incorporated at position Y40 within eGFP from the dual Amber reporter. Confocal micrographs of HEK-293 cells were taken 48 h after PEI transfection. A plasmid encoding mCherry was used to mark transfected cells. The scale bars represent 50 µm. (**A**) Cells expressing the dual Amber reporter construct carrying genes for wild-type GluA2 and eGFP-Y40TAG showed rescued fluorescence with inclusion of the tRNA / tRNA-synthetase pair and 0.5 mM AzF in the cell culture medium. (**B**) A few very faint fluorescent cells per 10 mm cover slip were detected 48 h after transfection in the absence of AzF (*white circles*), suggesting that unspecific readthrough was manageable.

3.3 Functional properties of AMPA receptors incorporating AzF and BzF at the D2 sites S729 and G725

Cells were transfected with the cocktail of tRNA, tRNA-synthetase and GluA2_IRES_eGFP-Y40TAG plasmids (with GluA2 harboring the S729TAG or G725TAG mutation), and were incubated in the presence of 1 mM BzF or 0.5 mM AzF. Outside-out patches were pulled 48-72 h after PEI transfection, from cells expressing rescued eGFP. Responses to 10 mM glutamate were invariably large, with average peak currents in outside-out patches of –470 ± 50 pA (at –60 mV; n = 50) for GluA2 S729BzF and –620 ± 90 pA for GluA2 G725BzF (n = 43), compared to –750 ± 158 pA (n = 33) for GluA2 wild-type channels. Along with other biophysical readouts for specific UAA incorporation that are presented in the following sections, it is strongly assumed that these currents arose from receptors in which the Amber stop codon was rescued.

Patch-clamp electrophysiology coupled to rapid perfusion demonstrated that BzF-rescued GluRs had kinetic properties akin to wild-type GluRs. Rates of desensitization for the GluA2 mutants S729BzF (k_{des} = 186 ± 9 s^{-1}, n = 20) and G725BzF (k_{des} = 197 ± 8 s^{-1}, n = 22) were modestly increased (~1.5-fold) compared to wild-type GluA2 expressed on the background of BzF and the tRNA / tRNA-synthetase pair (k_{des} = 121± 6 s^{-1}, n = 22; **Figure 17 A & B**). One-Way ANOVA gave p = 0.25 for S729BzF and p = 0.11 for G725BzF (with wild-type as the control group). Surprisingly, suppressing the Amber stop codon with AzF at position S729 produced receptors with about ~8-fold faster desensitization kinetics (k_{des} = 930 ± 80 s^{-1}, n = 15) compared with wild-type GluA2 (p < 0.0001). This effect was not observed with incorporation of AzF at position G725 (k_{des} = 171 ± 15 s^{-1}, n = 9, p = 0.75). The similar natural substitution of tyrosine (S729Y) produced a receptor with a 4-fold faster desensitization (k_{des} = 420 ± 40 s^{-1}; n = 5, p < 0.0001). Deactivation following a brief pulse (~1 ms) of 10 mM glutamate gave rates for BzF mutants (S729BzF k_{deact} = 1500 ± 120 s^{-1}, n = 22; G725BzF k_{deact} = 1400 ± 200 s^{-1}, n = 15) indistinguishable from those of wild-type receptors (WT k_{deact} = 1600 ± 150 s^{-1} , n = 13, p = 0.98 for S729BzF and p = 0.86 for G725BzF; **Figure 17 C & D**). Rates of recovery from desensitization for S729BzF (k_{rec} = 36 ± 3 s^{-1}, n = 12, p = 0.89) and G725BzF (k_{rec} = 23 ± 4 s^{-1}, n = 5, p = 0.03) were also similar to that of wild-type receptors (k_{rec} = 40 ± 3 s^{-1}, n = 10; **Figure 17 E & F**), suggesting that the substitutions had little effect on glutamate affinity (Robert et al.,

2005; Weston et al., 2006a).

It is possible that the distinct kinetics of the AzF- and BzF-rescued mutants at S729 arise from different random mixtures of endogenous and UAAs that are incorporated at these sites by the specific synthetases. However, the subsequent photocrosslinking experiments, the highly efficient rescue as assessed by biochemistry, and the weak effects of other natural amino acids introduced at this site, strongly argue that the genetic method of incorporation is specific. Thus, it is presumed that the intended UAAs were incorporated, rather than a random selection. The strong divergence of S729AzF kinetics from those of wild-type receptors, the known limitations of azide groups as photocrosslinkers (see **Section 1.2.4.2 & Discussion**), and the potential of BzF substitutions to be functionally silent in native receptors, were crucial factors to concentrate exclusively on BzF rescue for subsequent experiments.

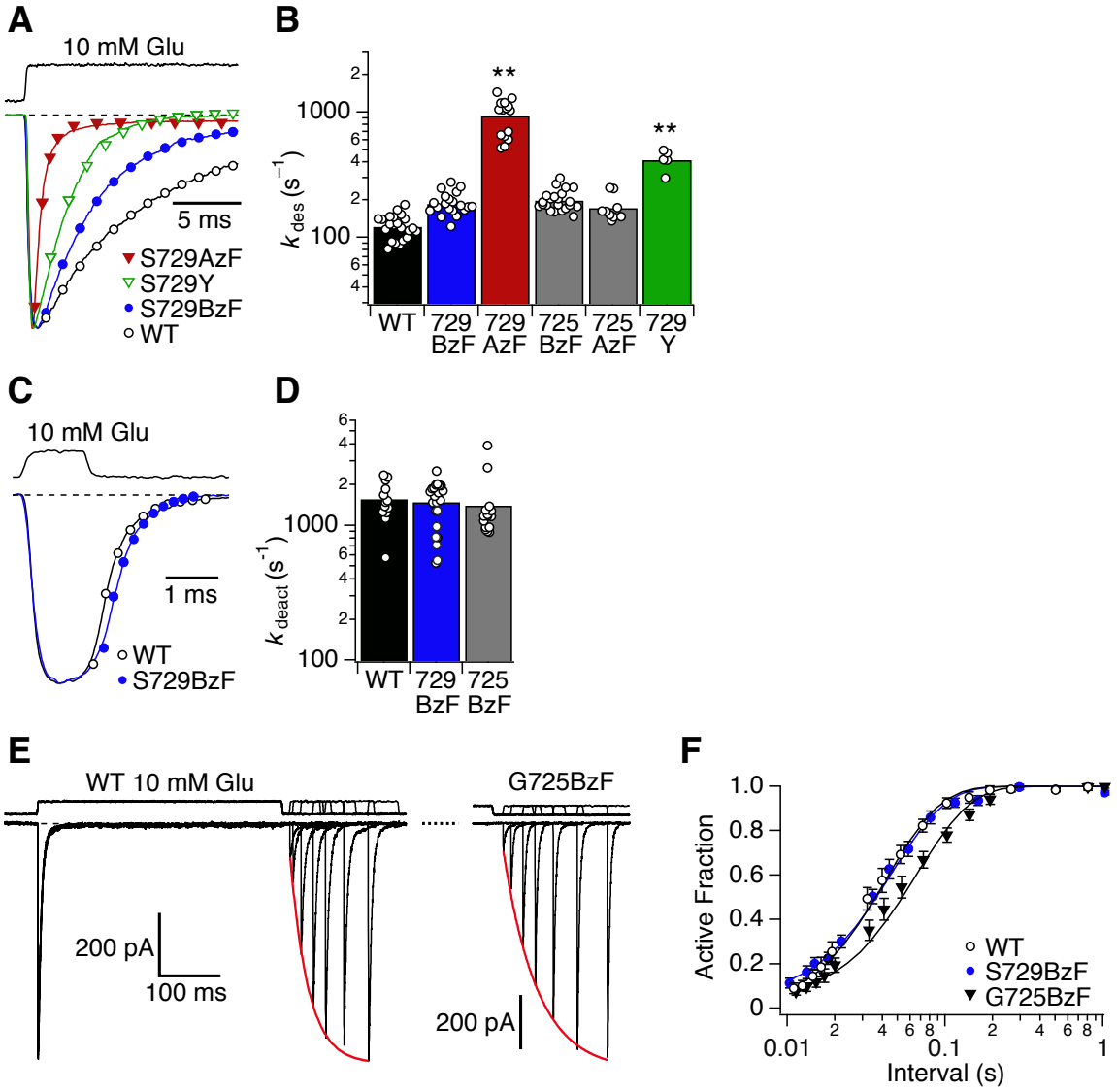

Figure 17 Kinetic properties of GluA2 receptors harboring UAAs. (**A**) The rate of desensitization for GluA2 S729BzF (*blue trace*, here, k_{des} = 252 s^{-1}) was similar to WT GluA2 (*black,* k_{des} = 135 s^{-1} in this example). Incorporation of AzF at position S729 resulted in 8-fold faster (*red,* here, k_{des} = 1470 s^{-1}), and the S729Y mutant in 4-fold faster (*green,* k_{des} = 435 s^{-1}) desensitization kinetics compared to WT. (**B**) Summary of desensitization rates of WT receptors, the two Amber mutants S729 and G725 carrying BzF or AzF, and a natural substitution mutant (S729Y). The averaged rates are given in the text. $p < 0.0001$** (**C**) Deactivation rates for GluA2 S729BzF and G725BzF mutants were similar to WT GluA2 (here, k_{deact} = 1910 s^{-1} for WT, *black*, and k_{deact} = 1730 s^{-1} for S729BzF, *blue*). (**D**) Summary of deactivation rates with BzF at positions S729 or G725. The averaged values are given in the text. (**E**) Seven overlaid traces show that recovery from desensitization for G725BzF (k_{rec} = 46 s^{-1}) was similar to WT GluA2 (k_{rec} = 43 s^{-1}). (**F**) Summary of recovery rates of WT (*opaque circles*) and the BzF mutants G725 (*black triangles*) and S729 (*blue circles*). The exact values are given in the text (modified from Klippenstein et al., 2014).

3.4 UV-induced photoinactivation of homomeric GluA2 receptors with BzF at the lower lobes of the LBDs

3.4.1 UV applied in the desensitized state resulted in a monoexponential reduction of peak current

Outside-out patches from HEK-293 cells expressing GluA2 with BzF substitutions at positions S729 and G725 were exposed to pulses of UV light during applications of 10 mM glutamate (see **Figure 12**). Previous studies showed that receptor inhibition by means of disulfide crosslinking at equivalent sites was most pronounced during the desensitized state (Armstrong et al., 2006; Plested & Mayer, 2009). Therefore, UV pulses were initially given ~100 ms after the peak of the current, by which point more than 90% of receptors were in the desensitized state. After 50-200 ms exposures with a repetition frequency of 0.5 Hz, a remarkably consistent peak current reduction was detected for both Amber mutants tested, GluA2 S729BzF (**Figure 18 C & D**) and GluA2 G725BzF (**Figure 18 E & F**). The rate of current reduction depended on UV intensity and exposure time, with longer applications and higher intensities resulting in faster receptor trapping rates (**Figure 18 C & E**). Pausing the UV exposures also stopped the peak current reduction, with subsequent responses having stable amplitudes over many episodes. This excluded non-specific run down of the peak current as a cause of the inhibition. The time course of reduction in peak current was invariably well fit with a single exponential, independent of the length of the UV interval or the intensity of the illumination (**Figure 18 C & E**). This suggests that a single rate-limiting step (for example, the trapping of one LBD dimer in an inactive conformation by a single crosslink) produced the inhibition (see **Discussion**).

Wild-type channels expressed on the background of tRNA, the BzF tRNA-synthetase, and BzF were comparatively unaffected by similar UV exposures (**Figure 18 A & B**). Extended UV exposures of up to 20 s were accompanied by peak current reduction of only 13 ± 3% (n = 4), which was not related to intensity or cumulative UV exposure, and was more likely to be a result of peak current rundown during these long-lasting recordings (see also **Figure 36**).

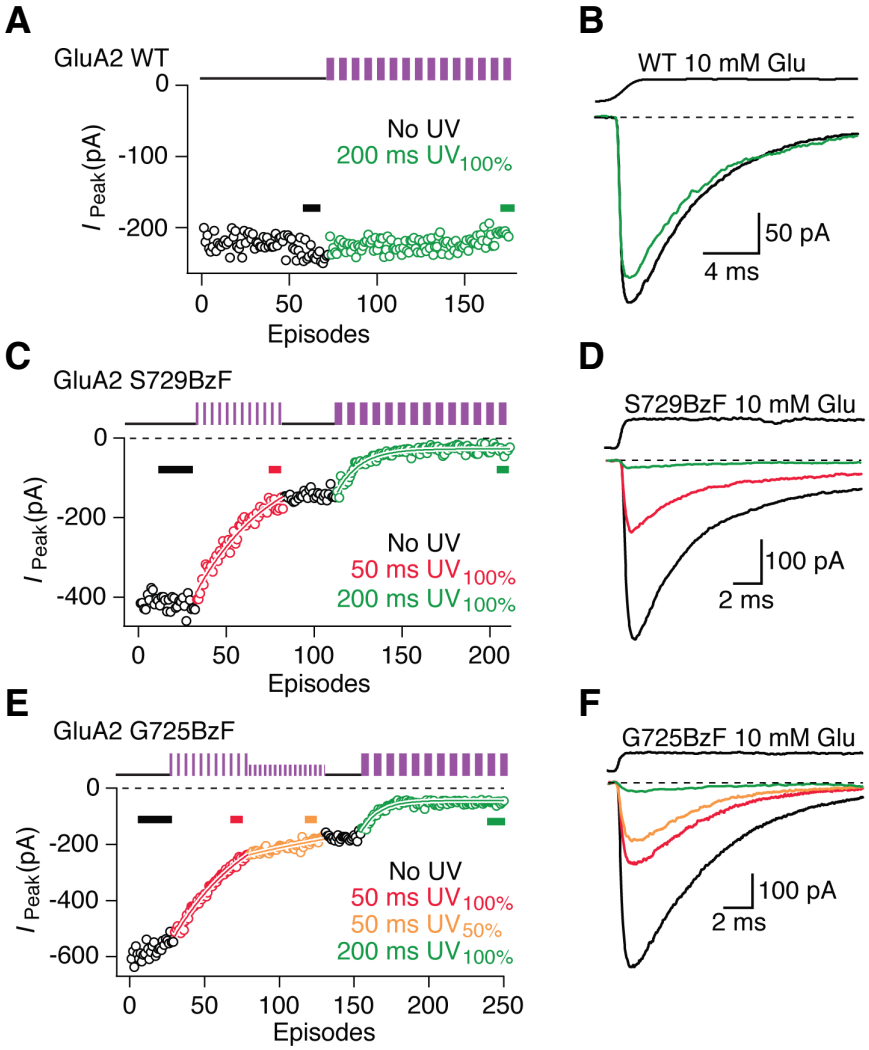

Figure 18 UV-induced reduction in peak current. UV pulses (50 or 200 ms per episode) are indicated by *violet pulse trains* (not representative of the actual number of exposures). The circles represent the peak current activated by 10 mM Glu in each episode. (**A**) Example of peak current responses of WT receptors before (*black*) and after (*green*) exposure to UV (200 ms per episode). WT receptors were not inactivated by a cumulative UV of 20 s and full intensity. (**B**) Example pre- and post-UV traces for WT receptors, averaged of 5-20 responses to 10 mM Glu from the stretches indicated with bars in *A*, are overlaid. (**C**) Example for GluA2 S729BzF (full UV illumination). Periods of serial UV exposure promoted receptor inactivation. The trapping rate was monoexponential (*white outlined fits*), and ~3-fold faster when 200 ms pulses were applied (*tau* = 13 episodes, *green*) compared to pulses of 50 ms (*tau* = 45, *red*). Currents amplitudes did not change during brief pauses of UV exposure (*black*). (**D**) Example traces for GluA2 S729BzF show the peak current reduction induced by UV. Averaged stretches are indicated in panel *C*. (**E**) The time course of trapping for GluA2 G725BzF ($tau_{50\ ms}$ = 53 episodes, *red*; $tau_{200\ ms}$ = 14, *green*). An additional series of exposures at 50% intensity was applied ($tau_{50\ ms}$ = 144, *orange*). (**F**) Equivalent to panel *D*, example average traces for GluA2 G725BzF during photoinactivation (from Klippenstein et al., 2014).

3.4.2 Photoinactivation of GluA2 receptors depended on UV intensity and exposure times

As shown in **Figure 18**, the rate of photoinactivation was related to the UV conditions used. Longer UV exposures times and full intensities invariably resulted in faster trapping rates compared to shorter UV intervals or pulses with a decreased illumination power. The averaged rates (in episodes) of GluA2 S729 and G725 receptor inactivation are shown in **Figure 19 A.** GluA2 S729BzF was inactivated with: $tau_{50ms\ 50\%} = 160 \pm 27$ ($n = 9$); $tau_{50ms} = 65 \pm 8$ ($n = 19$); $tau_{100ms} = 36 \pm 6$ ($n = 10$); $tau_{200ms} = 22 \pm 2$ ($n = 9$). One-way ANOVA gave $p_{50\ ms\ 50\%} = 0.001$; $p_{100\ ms} = 0.21$; $p_{200\ ms} = 0.04$ (with 50 ms exposure intervals at 100% intensity as the control group). GluA2 G725 produced the following trapping rates: $tau_{50ms} = 56 \pm 6$ ($n = 9$); $tau_{200ms} = 22 \pm 4$ ($n = 9$, $p = 0.0002$ as revealed by Student's t test). Photoinactivation of mutant receptors occurred with the time constant of 3.3 ± 0.4 s with cumulative UV exposure for GluA2 S729BzF if UV pulse trains of 50 ms were used and with a constant of 4.4 ± 0.4 s for 200 ms pulses (probability of no difference = 0.49). The trapping half times for GluA2 G725BzF were 2.8 ± 0.3 s for short pulses of 50 ms and 4.4 ± 0.8 s for 200 ms pulses ($p = 0.96$). The trapping half-times (in episodes) for the different UV exposure times, although significant, were on average variable between different patches (as shown in **Figure 19 A**) and thus did not represent the ratios within individual recordings. These variations might arise from variable optical properties due to different patch sizes, non-identical distances between the patch and the UV light source, or the arrangement of the patch at the pipette tip. To compare the trapping rates within individual patches, a reference value (the inactivation half-time in episodes during UV exposures of 50 ms) was chosen, which was obtained from every outside-out patch to be compared with trapping rates during longer pulses of UV or variations in UV intensity. The trapping rates (in episodes) were normalized to the inactivation half-times obtained with 50 ms pulses (**Figure 19 B**). The normalized average time constants obtained for GluA2 S729BzF were: $tau_{50ms\ 50\%} = 2.5 \pm 0.4$ ($n = 8$, $p = 0.007$ compared to the control inactivation rate); $tau_{100ms} = 0.5 \pm 0.07$ ($n = 5$, $p = 0.003$); $tau_{200ms} = 0.3 \pm 0.02$, ($n = 6$, $p < 0.0001$). GluA2 G725 revealed: $tau_{200ms} = 0.4 \pm 0.05$ ($n = 6$, $p < 0.0001$ as revealed by Student's t test).

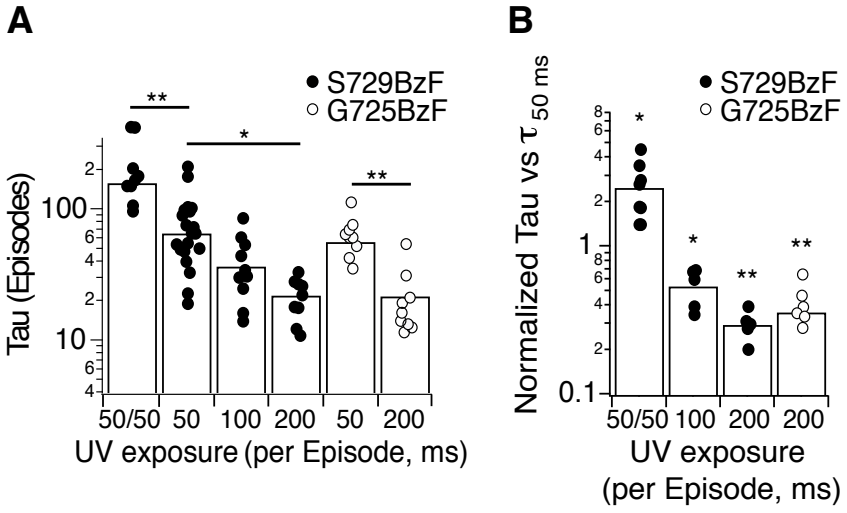

Figure 19 Trapping rates produced by different UV exposure times for the GluA2 S729BzF and G725BzF mutants. (**A**) Summary of the exponential half-times (in episodes) of S729BzF (*solid markers*) and G725BzF (*opaque markers*) mutant inactivation, plotted against the UV exposure periods per episode in ms. The intensity of UV illumination was 100%, unless otherwise noted. The detailed values are given in the text. $p < 0.05$*; $p \leq 0.001$** (**B**) Summary of normalized exponential half-times obtained for the different UV exposure intervals, with the inactivation rate during 50 ms pulses as the reference value. $p < 0.01$*; $p < 0.0001$** (modified from Klippenstein et al., 2014).

3.4.3 The extent of trapping did not correlate with the initial peak current amplitude

Activation of BzF groups at the positions S729 and G725 by UV at 365 nm resulted in photoinactivation of receptors by ~90%, which was achieved with about 10 s of cumulative exposure to UV. Further applications of UV pulses did not change the plateau of trapped receptors. No correlation was observed between the extent of trapping and the initial current amplitude of the GluA2 mutants. Cumulative UV exposures of 12 s during the desensitized state gave the following correlation coefficients: $R^2_{S729BzF} = 0.001$ ($n = 8$); $R^2_{G725BzF} = 0.18$ ($n = 9$; **Figure 20**), indicating that unspecific readthrough did not dominate at low current densities, which would produce a population of untrappable receptors.

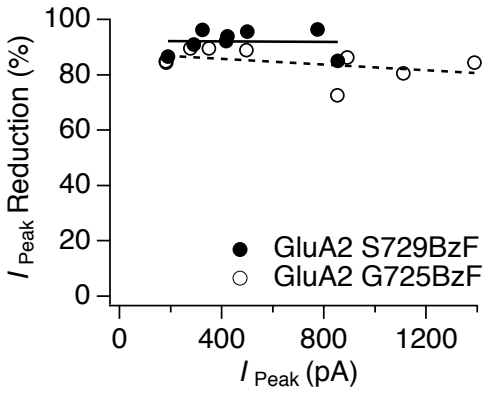

Figure 20 Relationship between the peak current at the start of the experiment and the degree of inhibition (in %). 12 s of cumulative UV applied in the desensitized state inhibited the peak current by 92 ± 4% (n = 8) in GluA2 S729BzF (*solid markers*), and by 88 ± 3% (n = 9) in GluA2 G725BzF (*opaque markers*) receptors. The individual values were fitted with linear functions (*solid line* for S729BzF; *dashed line* for G725BzF). There was no correlation between inhibition and the initial peak current. The correlation coefficients were as follows: $R^2_{S729BzF}$ = 0.001 and $R^2_{G725BzF}$ = 0.18.

3.4.4 UV exposures in the desensitized state did not affect kinetics of wild-type and Amber mutant receptors

Notably, despite the large reduction in the peak current amplitude following trapping, the kinetics of homomeric GluA2 receptors with BzF-groups at D2 sites were not affected by exposures of UV. Rates of desensitization for the S729BzF and G725BzF mutants following 14 s of UV in the desensitized state were equal to those in the pre-UV condition (**Figure 21 A**). For GluA2 wild-type, the desensitization rate was 124 ± 18 s^{-1} after 14 s of cumulative UV, compared to 117 ± 15 s^{-1} before UV (p = 0.78), as obtained from the same patch (n = 5). The GluA2 mutant S729BzF gave rates of 163 ± 19 s^{-1} after UV exposures and 143 ± 13 s^{-1} (n = 4; p = 0.45) before. GluA2 G725BzF was also similar with 228 ± 21 s^{-1} prior UV and 235 ± 23 s^{-1} after 14 s of cumulative UV exposure (n = 9; p = 0.83). Activation rise times (in ms) were also identical after 14 s (or longer) of cumulative UV applied in the desensitized state (**Figure 21 B**). GluA2 S729BzF was activated within 0.43 ± 0.04 ms (n = 7; p = 0.72 compared to wild-type GluA2) before and within 0.47 ± 0.04 ms (n = 4; p = 0.98) after 16 s of cumulative UV in the

desensitized state. G725BzF gave a rise time of 0.35 ± 0.03 ms (n = 7; p = 0.46 compared to wild-type GluA2) before UV application, compared to 0.4 ± 0.04 ms (n = 6; p = 0.71) after 16 s UV.

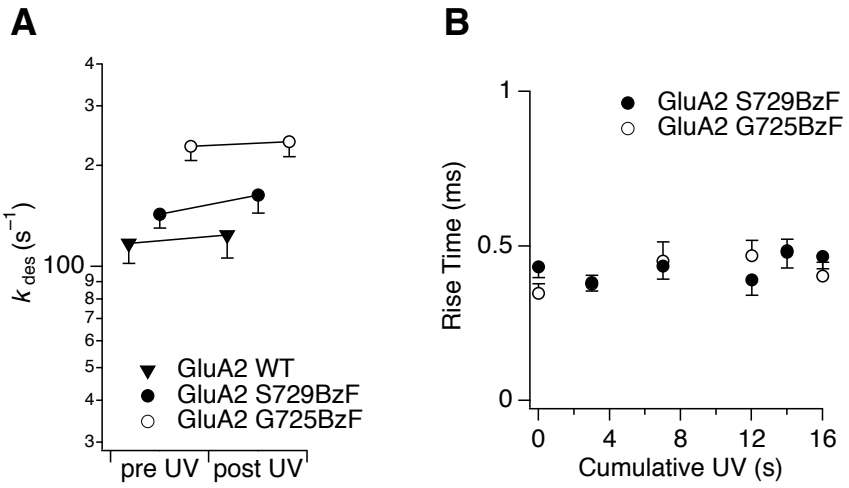

Figure 21 UV exposures in the desensitized state did not change kinetics of GluA2 S729BzF and G725BzF receptors. (**A**) Rates of desensitization of GluA2 WT (shown as *triangles*), S729BzF (*solid round markers*), and G725BzF (*opaque markers*) receptors were not affected following 14 s of cumulative UV. The averaged rates are given in the text. (**B**) Long UV exposures of up to 16 s did not have any impact on the rise time (n = 4-7 patches for each point). The exact values are given in the text.

3.4.5 A substantial steady-state current appeared upon application of UV in GluA2 S729BzF receptors

Photoinactivation of GluA2 S729 and G725 Amber mutants was characterized by effective peak current reduction, without changing their kinetic properties. Extensive UV exposures, however, resulted in a remarkable increase (~6.5-fold) of the the steady-state current (I_{ss}) in the GluA2 S729BzF mutant (**Figure 22 A & D**), indicating trapping of receptors in weakly active, non-inactivating states. In contrast, for the G725BzF mutant, a weaker UV-driven development of the I_{ss} was seen (~3.5-fold; **Figure 22 B & D**). This effect suggests that the position of photoactivatable BzF groups within the D2 lobes might be relevant. BzF at the G725 site is more

distal to the clamshell hinge within the interface (**Figure 22 E**), which might produce a more pronounced UV-driven inhibition due to the bigger movement of the D2 domains involved in crosslinking. To test whether different positions within D2 promote trapping of different geometries, BzF was additionally incorporated at position M721, a site even further away from the LBD dimer hinge and with a distance of 22.5 Å between the two C_αs of BzF in the desensitized dimer structure, compared to 6 Å for S729BzF or 7 Å for G725 (**Figure 22 E**). As predicted, UV exposures during the desensitized state resulted in equally strong reduction of the current amplitude for GluA2 M721BzF receptors (see **Figure 39**), however, no changes in I_{ss} were seen. This indicates that activation of BzF groups further away from the hinge results in trapping that is more inhibitory (**Figure 22 D**). Since steady-state currents prior exposures to UV slightly differed for the individual mutants, the I_{ss} obtained following UV application was normalized to the average I_{ss} before UV to allow comparison. Normalization of I_{ss} gave: for wild-type receptors (n = 10): $I_{ss\ pre\ UV}$ = 1 ± 0.1; $I_{ss\ 7s\ UV}$ = 0.97 ± 0.1 (probability of no difference compared to $I_{ss\ pre\ UV}$ was p = 0.98); $I_{ss\ 14s\ UV}$ = 1.07 ± 0.1 (p = 0.92). For S729BzF (n = 6): $I_{ss\ pre\ UV}$ = 1 ± 0.2; $I_{ss\ 7s\ UV}$ = 3.4 ± 0.6 (p = 0.15); $I_{ss\ 14s\ UV}$ = 6.4 ± 1.5 (p = 0.002). For G725BzF (n = 11): $I_{ss\ pre\ UV}$ = 1 ± 0.4; $I_{ss\ 7s\ UV}$ = 2.5 ± 0.9 (p = 0.37); $I_{ss\ 14s\ UV}$ = 3.7 ± 1 (p = 0.06). For M721BzF (n = 7): $I_{ss\ pre\ UV}$ = 1 ± 0.2; $I_{ss\ 7s\ UV}$ = 1.3 ± 0.2 (p = 0.56); $I_{ss\ 14s\ UV}$ = 1.3 ± 0.2 (p = 0.4).

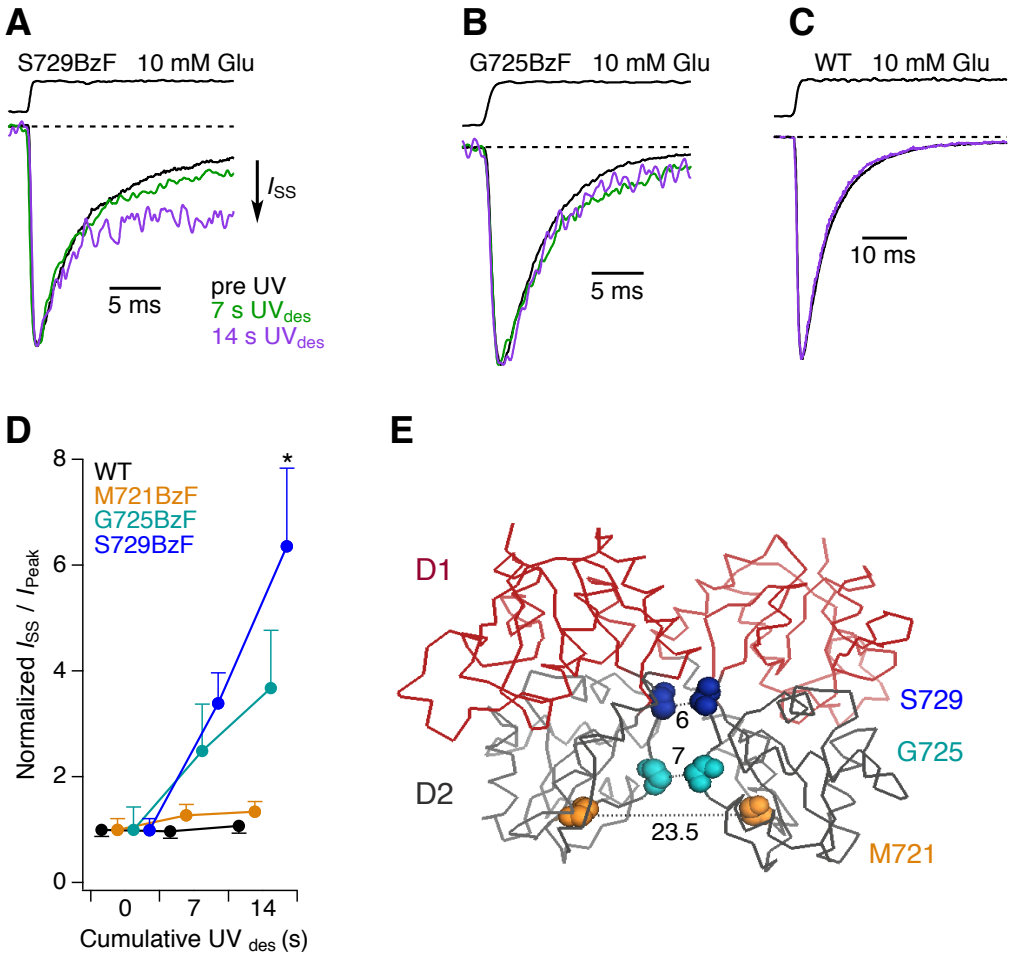

Figure 22 Extensive UV exposures generated a site-specific increase in I_{ss}. (**A**) Normalized traces show the development of the steady-state current. For this example, the I_{Peak} was –410 pA and the I_{ss} was 0.06 (*black trace*). 7 s of UV in the desensitized state gave: I_{Peak} = –48 pAs and an I_{ss} of 0.22 (*green*). 14 s of cumulative UV resulted in I_{Peak} = –17 pAs and an I_{ss} of 0.31 (*purple*). With prolonged UV exposures, the I_{ss} was dramatically increased in the GluA2 S729BzF mutant. (**B**) For GluA2 G725BzF, the increase in steady-state current was less pronounced than for S729. The color scheme is equivalent to panel *A*. Here, GluA2 G725BzF following inactivation gave: $I_{Peak\ pre\ UV}$ = –180 pA, $I_{ss\ pre\ UV}$ = 0.01; $I_{Peak\ 7s\ UV}$ = –28 pA, $I_{ss\ 7s\ UV}$ = 0.04; $I_{Peak\ 14s\ UV}$ = –17 pA, $I_{ss\ 14s\ UV}$ = 0.07. (**C**) GluA2 WT gave: $I_{Peak\ pre\ UV}$ = –630 pA, $I_{ss\ pre\ UV}$ = 0.02; $I_{Peak\ 14s\ UV}$ = –540 pA, $I_{ss\ 14s\ UV}$ = 0.02. For clarity, only two traces are overlaid (pre-UV and after 14 s UV). (**D**) Normalization of steady-state currents gave on average a ~6.5-fold increase for GluA2 S729BzF and a ~3.5-fold increase in steady-state level for the G725BzF mutant. UV application on WT and M721BzF mutant channels did not lead to a development of the I_{ss}. The exact averaged values are given in the text. $^{*}p < 0.01$ (**E**) The three positions of BzF incorporation within a desensitized LBD dimer (PDB: 2I3W; Armstrong et al., 2006). D1 is shown in *red*, D2 in *grey*. Dashed lines indicate the distance (in Å) between the Cαs of the BzF groups for the M721, G725, and S729 sites.

3.4.6 AzF groups at the GluA2 S729 site did not induce receptor photoinactivation upon UV

Placing AzF at the S729 site within GluA2 resulted in a pronounced increase of the desensitization rate (see **Figure 17 A & B**). The resting activity of AzF in the absence of UV illumination (see **Discussion**) disqualified it for the usage as a photocrosslinker in this study. To confirm the limitations of AzF, receptors carrying this UAA at position S729 were exposed to UV during the desensitized state, analogously to the experiment presented in **Figure 18**. All outside-out patches tested (n = 3) showed a pronounced increase in the peak current amplitude upon long exposures of UV (an example is shown in **Figure 23 A & B**), which ranged between 34 and 84%. This effect was accompanied by a strong increment of the steady-state current (**Figure 23 B & C**) along with a slowing down of the desensitization rate (**Figure 23 B & D**). Normalizing the steady-state level after 12 s of cumulative UV in the desensitized state to I_{ss} in the pre-UV condition, gave a ~9-fold increase of I_{ss} / I_{Peak} (n = 3; p = 0.02; **Figure 23 C**). The rate of desensitization was slowed from $k_{des\ pre\ UV}$ = 1300 ± 200 s^{-1} to $k_{des\ 12s\ UV}$ = 250 ± 30 s^{-1} (n = 3; p = 0.008; **Figure 23 D**).

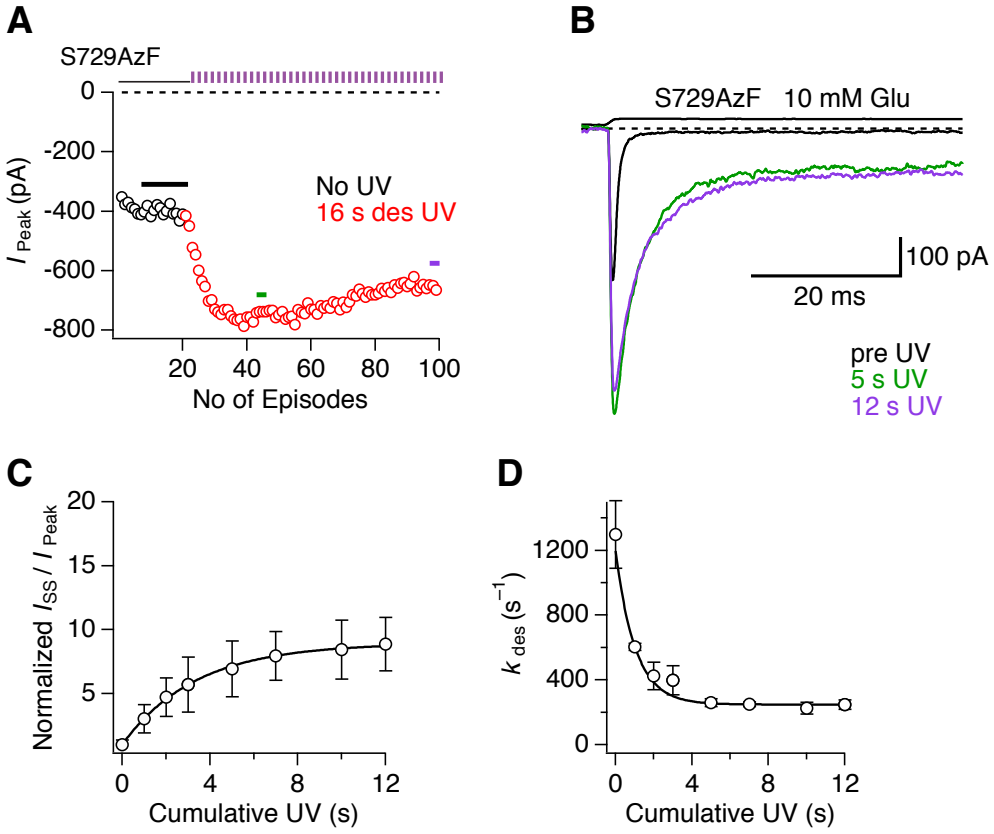

Figure 23 UV-induced recovery of basal kinetics in the GluA2 S729AzF mutant. (**A**) Example of peak current responses of S729AzF receptors before (*black markers*) and after (*red*) exposure to UV. UV pulses (200 ms per episode) are indicated by pulse trains (*violet;* not representative of the actual number of exposures). The circles represent the peak current activated by 10 mM Glu in each episode. GluA2 S729AzF receptors were not inactivated by a cumulative UV of 16 s and full intensity, but rather returned to kinetics comparable to WT receptors. (**B**) Example pre- and post-UV traces for S729AzF receptors. Averages of 3-15 responses to 10 mM Glu from the stretches indicated with bars in *A* are overlaid. 16 s of cumulative UV resulted in an increase in current by ~84% and a ~6-fold increase in I_{ss}. The desensitization rate prior to UV was 1400 s^{-1} and 200 s^{-1} following 16 s UV. (**C**) Normalized steady-state levels show a ~9-fold increase of the steady-state current. The developing I_{ss} was fit with a mono-exponential function and gave a tau of 3.4 ± 1.9 s. The exact values are given in the text. (**D**) Cumulative UV in the desensitised state returned AzF-driven effects on the desensitization rate to `normal` desensitizing behavior. The decay was fit with a mono-exponential function and gave a *tau* of 1 ± 0.2 s.

3.4.7 Very short UV pulses were not efficacious in promoting trapping

Prior to establishing UV pulses in the range of hundreds of milliseconds, as produced by the UVICO system, other UV sources were tested in order to achieve trapping between GluA2 receptors subunits harboring BzF at the S729 site – the SP-20 lamp (which gives ~360 µs UV pulses), and the UV LED (365 nm, Thorlabs). The intensity of the UV LED was too low to promote strong trapping on the timescale of our experiments (*not shown*). The short-pulse UV lamp (SP-20) produced UV pulses of ~360 µs with a repetition frequency of 0.25 Hz. Applying serial UV pulses of short intervals to outside-out patches expressing GluA2 with BzF at position S729 resulted in no evident changes in the peak current (**Figure 24**), in contrast to the longer pulses produced by the UVICO lamp (**Figure 18**). In due consideration of the BzF photochemical pathway, it was concluded that the produced pulses were too short to promote efficacious trapping (see **Discussion**).

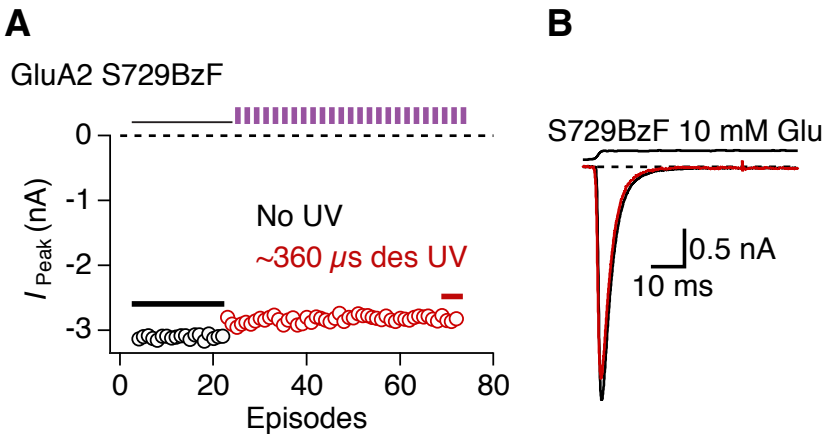

Figure 24 Very short UV pulses were insufficient to initiate photocrosslinking in GluA2 S729BzF receptors. (**A**) Example of the time course of full UV illumination of a whole-cell expressing GluA2 S729BzF. Periods during which the patch was serially exposed to UV exposures (~360 µs), are indicated schematically by pulse trains (*violet*, not representative of the actual number of exposures). The circles represent the peak current activated by 10 mM glutamate in each episode. A total of 55 pulses of UV did not induce changes in the peak current amplitude. (**B**) Example traces for GluA2 S729BzF illustrate the lack of peak current reduction upon short UV exposures. The averages of 5-20 responses to 10 mM Glu from the stretches indicated with bars in panel *A* are overlaid.

3.5 Biochemical detection of trapped subunits

3.5.1 Establishment of the Western blot protocol for detection of GluA2 monomers and crosslinked dimers

In order to confirm the assumption that receptor inhibition originates from physically linking adjacent GluA2 subunits rather than intrasubunit BzF crosslinking, Western blots were performed following *in vivo* treatment with UV.

Initially, dual Amber reporter constructs with Amber mutations at positions S729 and A665 were used for Western blots. The mutant A665C was shown to form an interdimer crosslink in partially activated GluA2 receptors in a previous study (Lau et al., 2013). Cells expressing the wild-type or Amber mutant ion channels in the presence or absence of the orthogonal tRNA / synthetase pair were incubated in a cell culture medium either supplemented with 0.5 mM AzF or without the UAA. After lysis in a 0.1% DDM-containing buffer, cleared lysates with a total amount of 50 µg protein per lane were run under reducing conditions (20 mM β-ME) on SDS-PAGEs. Antibodies binding at the C- or N-terminus of GluA2 were tested (**Figure 25 A & B**). The C-terminal antibody (**Figure 25 A**) was expected to detect monomeric bands of wild-type and rescued Amber mutant subunits by AzF. Staining with the N-terminal antibody meant to detect truncated proteins due to termination of translation at the inserted stop codon site, for comparison with rescued full-length subunit products (**Figure 25 B**). An antibody against GFP was additionally used to show suppression of the TAG stop codon at position Y40 within eGFP (**Figure 25 A**).

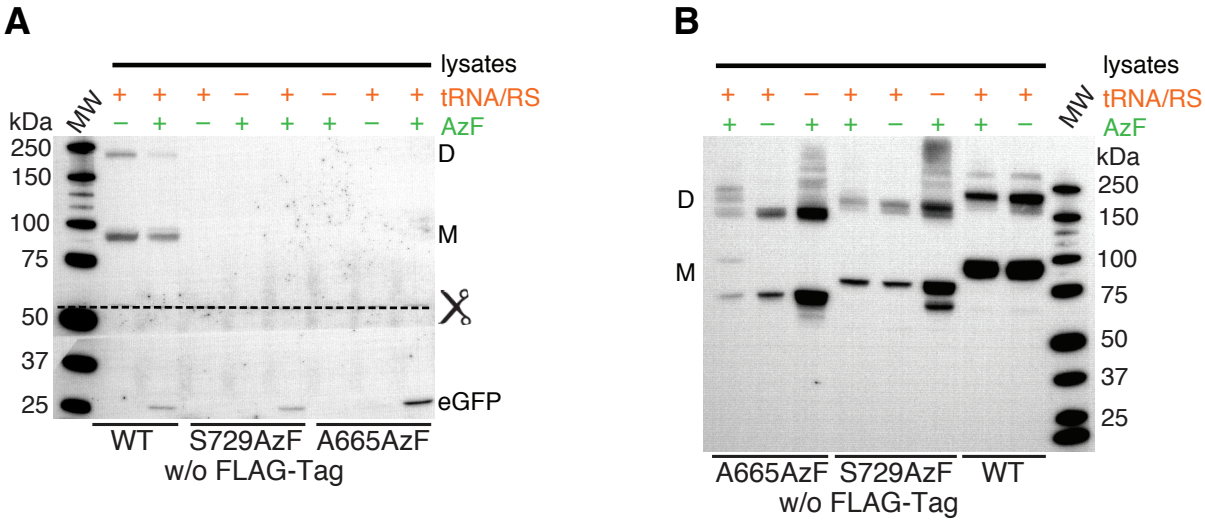

Figure 25 Rescue of GluA2 Amber mutant subunits could not be detected by the C- or N-terminal *α*-GluA2 antibodies. (**A**) Cleared lysates of the GluA2 Amber mutants S729 and A665 along with the GluA2 WT were stained against the C-terminus of GluA2 (rabbit *α*-GluA2, 1:1000) and GFP (rabbit *α*-GFP, 1:1000). For this purpose, PVDF membranes were cut at ~50 kDa prior antibody incubation. No monomeric bands (M) of rescued GluA2 Amber mutant subunits at ~90 kDa were detected using the C-terminal antibody, independently of the presence or absence of the tRNA / tRNA-synthetase pair (*red*) or AzF (*green*). Monomeric signals were only obtained for GluA2 WT channels. Dimeric bands, probably due to disulfide formations between the GluA2 WT subunits were seen at ~240 kDa (D). Amber codons within eGFP were effectively suppressed by AzF in both WT and Amber mutant mRNAs, represented by GFP signals at ~25 kDa. In the absence of the exogenous tRNA / sythetase pair or AzF, no GFP-bands were detected. (**B**) Samples from the same transfection as in panel *A* were stained against the N-terminus of GluA2 (mouse *α*-GluA2, 1:1000). Monomeric bands at ~90 kDa were detected for GluA2 WT. Bands at this MW, which represent full-length GluA2 subunits, were absent for the Amber mutants A665 and S729. Strong signals at lower MWs were seen representing truncated products of expressed Amber mutants. Their size was in accordance with the Amber position within GluA2. Transfection of all constructs resulted in additional high MW signals, which might be products of multimeric formations of WT or truncated subunits.

Both GluA2 Amber mutants, S729 and A665, gave glutamate activated currents in electrophysiological recordings, with larger responses of ~170 ± 40 pA (n = 19) for GluA2 S729AzF compared to ~40 ± 14 pA for A665AzF (n = 5). These currents probably resulted from AzF-rescued subunits. Rescued full-length monomeric subunits by AzF, however, were not detected with the antibodies used. A low sensitivity of the biochemical approach was hypothesized and in order to boost detection of rescued GluA2 subunits by UAAs, genes encoding the GluA2 S729 Amber mutant or wild-type subunits were decorated with a C-terminal FLAG-tag for purification. Cleared lysates (50 µg) of FLAG-tagged GluA2 ion channels were loaded along with the second elution product after FLAG-tag purification for comparison, and stained with a FLAG-tag antibody (**Figure 26 A**). The BzF-synthetase also contained a FLAG-tag (Ye et al., 2008) that was detected at ~45 kDa, and thus served as a control for transfection and gel-loading. The GluA2 S729 Amber mutant was expressed in HEK-293T cells in the presence or absence of the UAA. Since S729BzF mutants were inactivated upon UV illumination, as shown in electrophysiological recordings, the cells were accordingly incubated in 1 mM BzF. Wild-type channels were not expressed on the tRNA / tRNA-synthetase background for this example. All protein samples were lysed in 0.1% DDM and run under reducing conditions containing 20 mM β-ME in the gel loading buffer. Loading the second elution of FLAG-tag purified GluA2 S729 proteins resulted in a clear signal at ~100 kDa (slightly higher that staining with the C- or N-terminal antibody) when cells were incubated in a BzF-containing medium, representing rescue of the S729 Amber codon by the UAA. These bands were not detected in the absence of BzF or in lanes where cleared lysates were loaded, confirming higher protein abundance due to FLAG-tag purification. Still, dimer bands, probably due to basal formations of disulfide bonds following denaturation, were detected at around ~240 kDa, which were particularly strong with higher expressions of proteins as for wild-type GluA2. Since detection of dimers, covalently trapped at the lower LBDs upon UV, was infeasible under these conditions, three native cysteine residues within GluA2 were deleted to minimize spontaneous disulfide bond formation (Lau et al., 2013). Additionally, the concentration of β-ME within the protein loading buffer was increased to 200 mM in order to provide stronger reducing conditions (**Figure 26 B**).

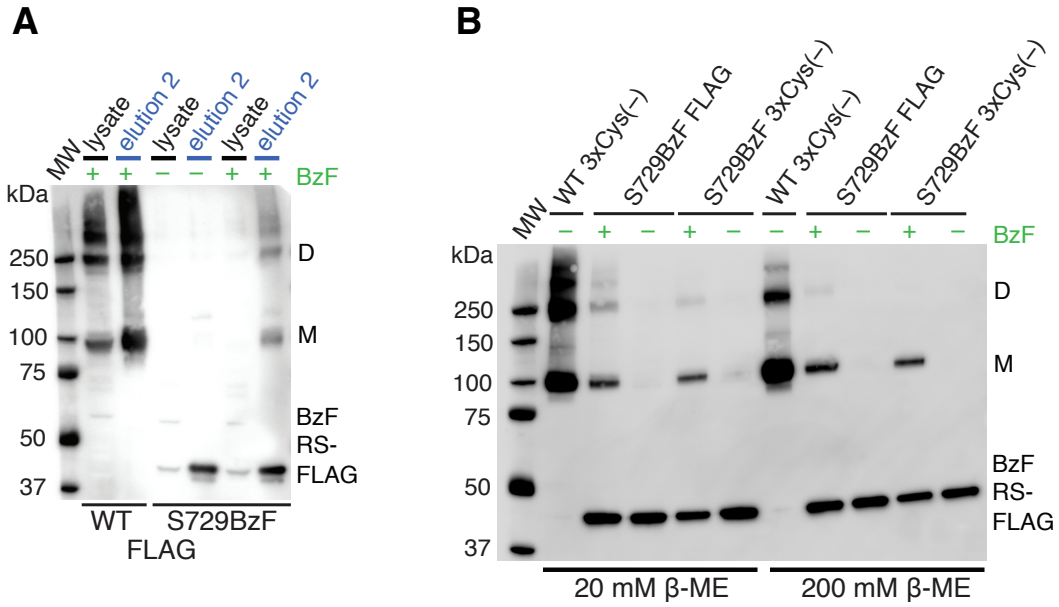

Figure 26 Strategies to improve detection of GluA2 Amber mutant monomers rescued by BzF. (**A**) Detection by the mouse *α*-FLAG antibody (1:1000) gave signals for monomeric GluA2 subunits (M) suppressed by BzF at position S729 (M, ~100 kDa) after FLAG-tag purification (elution 2; *blue*). No bands were detected for elutions in the absence of BzF, or when cleared lysates were loaded (*black*). As expected, purification of GluA2 subunits resulted in greater abundance of rescued protein. In all lanes, which gave signals of monomeric bands, strong higher MW bands (D and above) were detected, probably due to basal oligomerization properties of GluA2 subunits from disulfide formation. The BzF-synthetase also contained a FLAG-tag and was detected at ~45 kDa. (**B**) All proteins loaded were FLAG-tag purified. Rescued monomeric bands (M) for GluA2 S729 were only detected in the presence of BzF, the unspecific readthrough in the absence of the UAA was minor. Deletion of three cysteines (3 x Cys (–)) resulted in less pronounced dimeric products. For GluA2 S729, dimer bands vanished almost completely, especially under higher reducing conditions when gels were run in 200 mM β-ME. For WT, dimers still formed under these conditions, as previously reported (Lau et al., 2013). The band corresponding to the co-expressed FLAG-tagged tRNA-synthetase was, however, readily detected at ~45 kDa, indicating similar loading across S729 lanes.

Under consideration of the previously established conditions for effective detection of rescued GluA2 S729 Amber mutant subunits (three cysteine deletions and highly reducing SDS PAGEs), and the precedent inhibition through functional disulfide (Plested & Mayer, 2009; Armstrong et al., 2006) or BzF crosslinking (Klippenstein et al., 2014) at D2 sites, the propensity of BzF to physically crosslink receptor subunits was tested biochemically. HEK-293T cells expressing GluA2 wild-type or the S729 mutant were exposed *in vivo* to UV for intervals between one and 60 minutes (**Figure 27**). To minimize protein damage by short-wavelength UV light, dishes were covered with Pyrex glass lids. Pyrex is an effective long pass UV filter, passing only light >320 nm and thus removing damaging light (Farrell et al., 2005). The FLAG-tag purified protein samples were run under reducing conditions in 200 mM β-ME. A band corresponding to a dimer of subunits (~240 kDa) appeared in a time-dependent manner, with longer UV exposures resulting in a higher dimer fraction (**Figure 27**). UV-driven development of dimer fractions for the GluA2 S729TAG mutant could, however, not be effectively compared to wild-type lanes. These showed strong dimeric bands at the same MW (~240 kDa) even under high reducing conditions, three cysteine deletions, and in the absence of UV. To distinguish between specific UV-induced dimer formations and unspecific disulfide dimerization, further cysteine residues within GluA2 wild-type and S729 Amber mutant subunits were deleted resulting in 7 x Cys (–) constructs. The seven cysteine deleted background has previously been shown to result in an essentially monomeric background (Lau et al., 2013). In accordance to this study, GluA2 constructs with increased cysteine deletions gave a cleaner monomeric background. However, receptor expression strongly suffered and dimer fractions upon treatment of UV up to 60 min could not be detected with either the Pico or Femto chemiluminiscence detection system (*not shown*). Thus, constructs with seven cysteine deletions were dismissed as an appropriate background for UV-induced photocrosslinking.

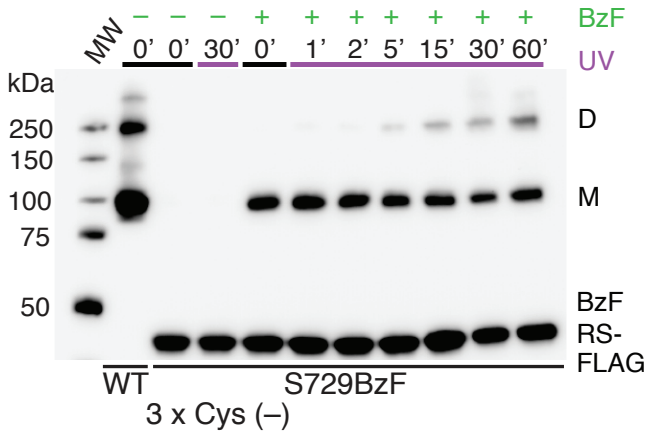

Figure 27 *In vivo* crosslinking of GluA2 S729BzF 3 x Cys (–) subunits. (**A**) Cells exposed to UV for intervals between one and 60 min showed an UV-dependent increase in the dimer fraction (D, ~240 kDa), as detected with a mouse *α*-FLAG antibody (1:1000). WT receptors run under the same conditions did not give an appropriate control for the UV-driven dimerization effect due to overloading of the lane and strong background signal at the same MW (~240 kDa) even in the absence of UV. Dishes, which were exposed to UVA, were covered by Pyrex glass lids during the exposure.

To further reduce the naturally occuring wild-type dimer fraction due to disulfide bonds, the concentration of β-ME in the loading buffer was increased. Purified GluA2 wild-type samples were run in either 200 mM (the previously used concentration) or 500 mM β-ME (**Figure 28 A**). To prevent overloading of the SDS-PAGE lanes, different volumes of the second elution containing GluA2 wild-type monomers ranging from 0.5 to 2 µl were loaded. UV-unspecific dimer fractions were less pronounced under higher reducing conditions (500 mM β-ME) and their degree was dependent on the volume loaded, with more protein applied to the lanes resulting in higher dimer fractions. Based on this result, 1 µl of the second elution containing wild-type subunits was loaded for all following experiments. To decrease unspecific dimerization, the cysteine quencher NEM (**Figure 28 B**) was further included into all protein buffers throughout the UV treatment, cell lysis, and protein purification. GluA2 wild-type subunits with a three cysteine-deleted background were compared in the presence and absence of NEM and run under highly reducing conditions (500 mM, as in panel *A*) on SDS-gels. Additionally, the effect of the Pyrex glass lid during the UV treatment was examined (**Figure 28**

B). Wild-type receptors treated with UV for exposure intervals between two and 30 minutes did not show any increase in dimer fraction when NEM was present, indicating resistance to background dimerization. Without NEM, however, increasing UV exposure times produced bands at ~240 kDa (and higher), probably due to photodamage. No differences were observed between wild-type subunits deriving from HEK-293T cells covered with Pyrex glass lids during UV application compared to those flashed in open dishes, indicating that UV-induced cell damage (upon 30 min) was not detectable.

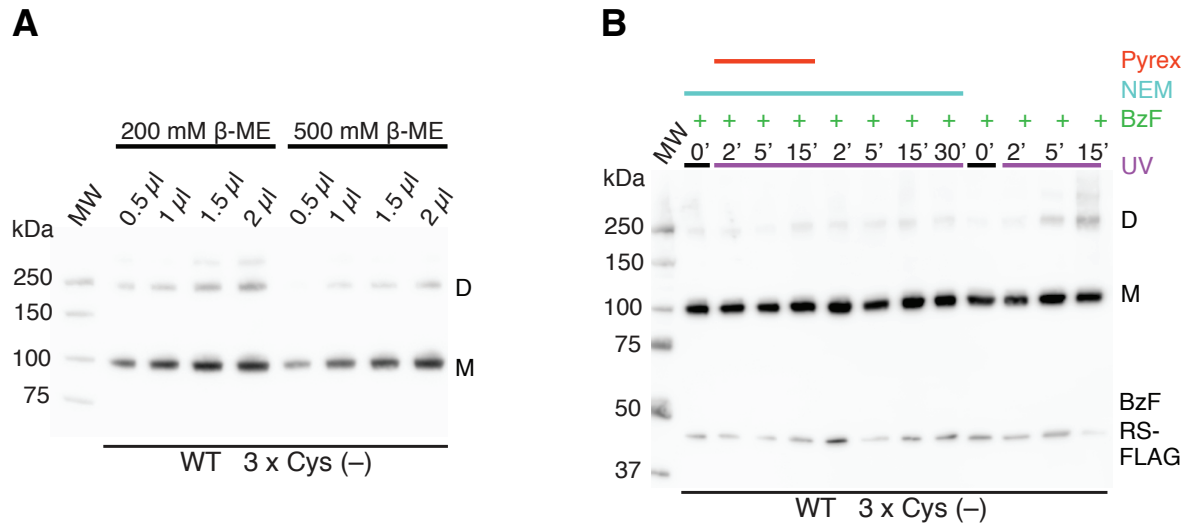

Figure 28 High reducing conditions and quenching by NEM ensured stable monomeric signals. (**A**) Different volumes of the second elution for WT GluA2 ranging from 0.5 to 2 µl were loaded. The gel run at reducing conditions with either 200 or 500 mM β-ME in the gel loading buffer, and proteins were stained with a mouse *α*-FLAG antibody (1:1000). Higher concentrations of β-ME and smaller volumes of the elution product loaded resulted in less pronounced unspecific disulfide formations. (**B**) GluA2 WT with three cysteine deletions was treated with UV in the presence and absence of 20 mM NEM (*blue*) and in the presence or absence of the Pyrex lid (*red*). With longer intervals of UV, an unspecific increase in dimer fraction was observed in the absence NEM, which was less pronounced with including NEM to every buffer during the sample preparation. The presence of the Pyrex lid did not have any impact on the expression pattern of monomeric GluA2 subunits or unspecific dimeric formations.

3.5.2 UV-driven crosslinking of subunits with BzF at lower LBD sites (S729, G725)

Having established proper experimental conditions for detection of UV-driven dimerization of BzF-containing GluA2 subunits (including FLAG-tag purification, the deletion of three native cysteines, NEM-supplementation, and high reducing conditions), the GluA2 Amber mutants S729 and G725 carrying BzF were exposed to UVA for intervals between two and 30 min in the Luzchem chamber. Amber mutant subunits rescued by BzF could be detected after FLAG-tag purification from whole-cell lysates as a characteristic ~100 kDa band (**Figure 29 A & B**). Upon UV exposure (2-30 min), a band corresponding to a dimer of subunits (at ~240 kDa) appeared in a time-dependent manner, with longer UV exposures resulting in a higher dimer fraction (*DF*; **Figure 29 B & C**). The formation of dimer in the absence of UV was limited ($DF_{\text{S729BzF pre UV}}$ = 1.6 ± 0.5 %; $DF_{\text{S729BzF post UV}}$=15 ± 3 %, n = 9; p = 0.002). Purified subunits from cells expressing wild-type receptors on the background of the tRNA and tRNA-synthetase and co-incubated with BzF did not yield an appreciable dimer band after 30 min of UV exposure ($DF_{\text{WT pre UV}}$ = 3 ± 1%, $DF_{\text{WT post UV}}$ = 5.4 ± 1.8 %, n = 11, p = 0.166; **Figure 29 C**). Lysates of cells transfected in the same way that were not pre-incubated in BzF-containing medium expressed a very weak band at 100 kDa, which had an average intensity of 4.5 ± 3% (n = 4) compared with the monomeric BzF-containing subunit (**Figure 29 A**), showing that rescue by BzF is ~20-fold more efficient than readthrough, at the level of individual subunits. In these lanes, no band corresponding to dimer molecular weight appeared after 30 min of UV exposure. An equal biochemical experiment was performed for the GluA2 G725 mutant (**Figure 29 D**). Similarly to GluA2 S729, the average intensity in the absence of BzF in the cell culture medium was minor. Increasing intervals of UV, however, did not result in dimerization, probably due to low expression efficiency.

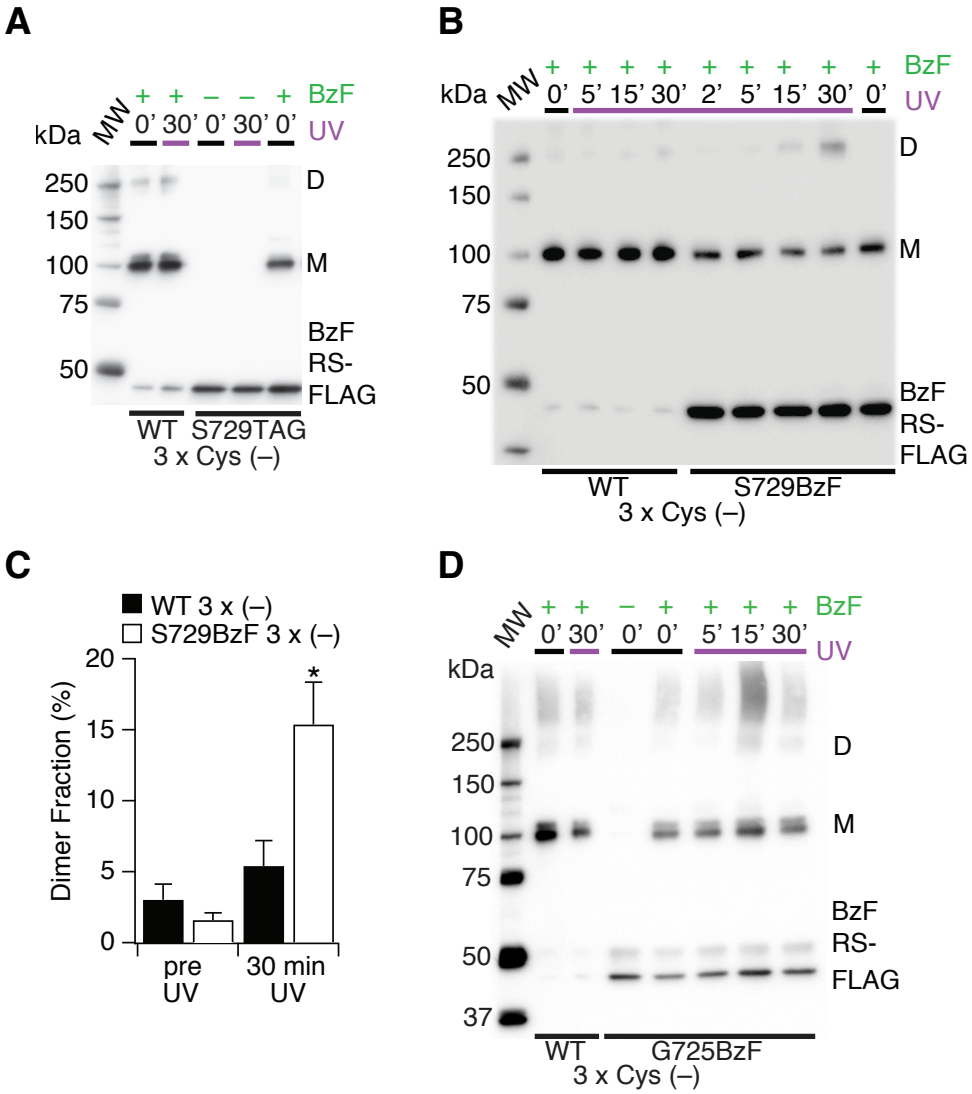

Figure 29 *In vivo* crosslinking produced a UV-dependent dimerization of GluA2 S729BzF subunits. (**A**) Western blot of GluA2 WT and S729BzF 3 x Cys (–) receptors. Monomeric GluA2 bands (M) were detected at ~100 kDa and only in the presence of BzF. Neither monomer nor dimer (D) bands were detected by the mouse α-FLAG antibody (1:1000) in the absence of BzF for S729TAG mutants. (**B**) HEK-293T cells were exposed to UV for time intervals between 2 and 30 min, resulting in an increasing dimerization (D) of GluA2 S729BzF, but not for WT subunits. Because WT subunits were expressed to a greater extent, for the WT lanes, 1/20th of the elution was loaded, explaining the lower intensity of the synthetase bands. (**C**) Summary of the *DF* detected after 30 min of continuous UV exposure. The *DF* did not differ between pre-UV and post-UV for WT 3 x Cys (–). For S729BzF 3 x Cys (–), UV exposure caused a significantly higher *DF*. The exact values are given in the text. $^{*}p < 0.01$. (**D**) Monomeric bands (M) for GluA2 G725 in the presence of BzF could be detected, however, no increase of *DF* was observed for this mutant (modified from Klippenstein et al., 2014).

To check that the crosslinking observed in three cysteine-deleted Amber mutants corresponds to receptors that can be photoinactivated, electrophysiological recordings were performed. Consistent with the GluA2 S729BzF mutant without any cysteine deletions, the 3 x Cys (–) variant could be trapped with a monoexponential time course. In contrast, wild-type 3 x Cys (–) was essentially insensitive to UV in electrophysiological recordings (**Figure 30 A & B**). The rates of the monoexponential inhibition of S729BzF 3 x Cys (–) upon serial exposures to UV illumination were on average similar to receptors containing the native cysteines (time constant for cumulative exposure: 5 ± 0.3 s, n = 4; **Figure 30 C**). GluA2 S729TAG 3 x Cys (–) receptors, rescued by co-expression of tRNA, tRNA-synthetase, and co-incubation with BzF, displayed fast activation and desensitization (k_{des} = 300 ± 40 s^{-1}, n = 9), indistinguishable from wild-type GluA2 on the 3 x Cys (–) background (k_{des} = 230 ± 13 s^{-1}, n = 9; **Figure 30 D**). The biochemical analysis along with the functionality of the 3 x Cys (–) Amber mutant variants confirms that UV illumination can drive dimerization of GluA2 subunits equipped with BzF in the lower lobes of the LBDs.

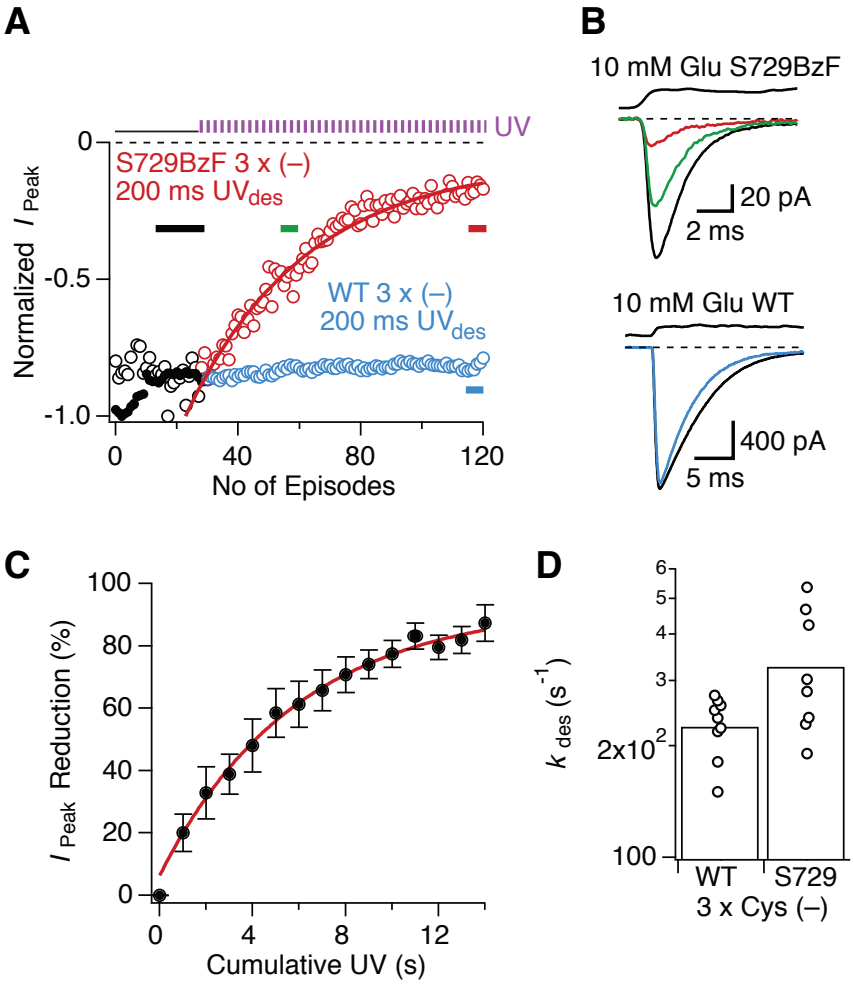

Figure 30 GluA2 receptors with three cysteine deletions were functional and UV-sensitive when BzF was incorporated. (**A**) Peak current kymogram for WT and S729BzF 3 x Cys (–) GluA2 receptors. UV exposures in the desensitized state (200 ms pulses) are shown schematically as a pulse train (*violet*). On the 3 x Cys (–) background, S729BzF receptors were trapped with an exponential time course (*red markers*), equally to receptors containing the native cysteines (see **Figure 18**). WT 3 x Cys (–) receptors were insensitive to an equivalent UV treatment (*blue*). The example time courses shown here were normalized to their maximal peak currents. (**B**) Example traces for GluA2 WT and S729BzF on the 3 x Cys (–) background from the averages of 20 (*black*) or five traces (*green*, *red*, and *blue*) from the stretches indicated with color-coded bars in the kymogram in *A*. (**C**) Averaged rates of monoexponential inhibition of GluA2 S729BzF 3 x Cys (–) were 5 ± 0.3 s (n = 4). (**D**) Deletion of three cysteines did not dramatically change the rates of desensitization of WT and GluA2 S729BzF compared to receptors harbouring these three cysteines (see **Figure 17**).

3.6 Biophysical readouts of specific BzF incorporation at GluA2 Amber codon sites

3.6.1 Unspecific Amber codon suppression within eGFP-Y40TAG by endogenous amino acids depended on the presence of the UAA and the orthogonal tRNA-synthetase

With eGFP fluorescence as a reporter of Amber codon suppression in the bicistronic dual Amber vector, a certain degree of rescue of fluorescence in the absence of the UAA (AzF or BzF) for all mutants tested was observed. The fluorescence intensity was usually quite faint (see example in **Figure 16**). To investigate the degree of unspecific incorporation of endogenous amino acids and its development over time, HEK-293 cells were transfected with the GluA2 wild-type dual Amber reporter and fluorescent cells were counted 24 h, 48 h, and 72 h after PEI transfection on a confluent region on the cover slip (see **Data analysis** for details). To identify the `leaky` components, transfection and cultivation of cells expressing wild-type receptors were performed under different conditions – in the presence or absence of the BzF-tRNA, with or without the tRNA-synthetase, and incubated in a cell culture medium with or without BzF (**Figure 31**). The number of fluorescent cells, including those that showed only a very faint fluorescence, was determined from an entire field of view using a 20 x objective lens. The obtained number was normalized to the amount of fluorescent cells 24 h after transfection with all components required for Amber codon suppression included (this condition is labelled with a circle in **Figure 31**). Background fluorescence from unspecifically rescued eGFP was not detectable in the absence of one of the transfection components 24 h post transfection. The number of fluorescent cells (when the whole suppression set was included) gradually increased with time to ~2-fold 48 h and to ~6-fold 72 h after transfection, both times when most of the electrophysiological and biochemical experiments were performed. In the absence of BzF in the cell culture medium, a background fluorescence of ~20-30% was observed for incubation times of 48-72 h, which is equivalent to other studies employing BzF (Wang et al., 2007; see also **Discussion**). Surprisingly, a similar background was seen in the absence of the BzF tRNA-synthetase, which was independent of the presence of BzF. This observation strongly indicates that specificity is prevalently provided by the tRNA-synthetase, but that the presence of all Amber suppressor components including the tRNA, the synthetase, and the UAA, ensures specific incorporation of BzF. Further experiments, which are presented in the following sections, support the idea of

specific BzF-insertion at Amber codon sites and indicate that endogenous amino acids do not effectively compete with UAAs, when the whole transfection cocktail is introduced to HEK-293 cells.

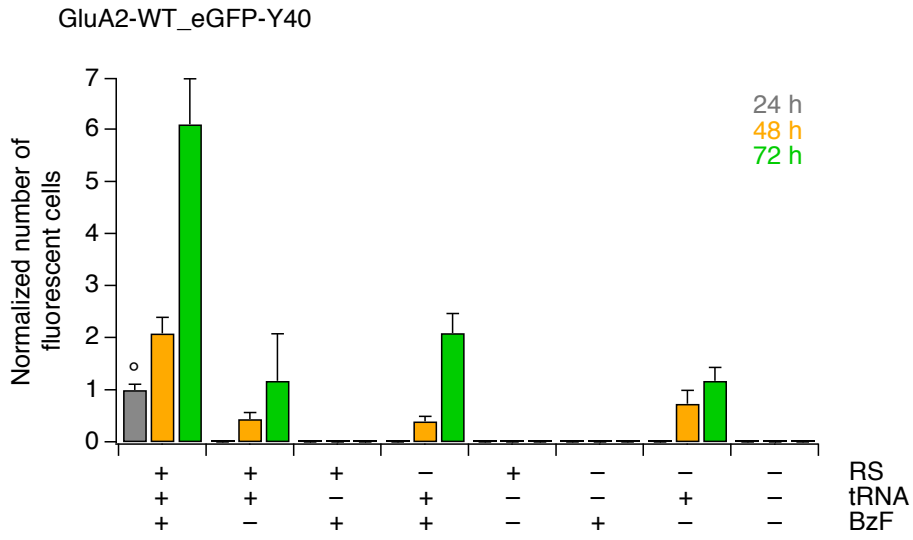

Figure 31 Quantitation of specific and non-specific rescue of fluorescence in eGFP-Y40TAG. The WT dual Amber reporter was transfected in the presence or absence of the different components of the Amber codon suppression set. The number of fluorescent cells from a confluent field of view was counted 24 h (*grey*), 48 h (*orange*), and 72 h (*green*) post transfection (n = 3-4 cover slips from different transfections for each column). For comparison, the obtained number of fluorescent cells was normalized to the cell number obtained 24 h after transfection of the dual Amber reporter in the presence of the RS, tRNA, and BzF (labelled with a *circle*).

3.6.2 GluA2 receptors carrying endogenous amino acids at introduced Amber codon sites were insensitive to UV

With the assumption that the faint fluorescent in the absence of one of the components required for BzF incorporation is based on unspecific incorporation of endogenous amino acids, the unspecific expression level of GluA2 Amber mutants was investigated electrophysiologically. Following extended culture intervals (2-7 days), outside-out patches from fluorescent cells, which were transfected with GluA2 S729TAG or G725TAG along with the tRNA / tRNA-

synthetase pair, but incubated in the absence of BzF, yielded glutamate activated currents (**Figure 32**). The unspecific readthrough peak current for GluA2 S729BzF was –20 ± 9 pA (n = 7), equivalent to ~4% of the average current amplitude obtained in the presence of BzF (–470 ± 50 pA, n = 50). GluA2 G725BzF gave larger background currents (–320 ± 100 pA, n = 17, ~52%) compared to BzF-containing receptors (–620 ± 90 pA, n = 43), indicating site-selectivity of unspecific Amber codon suppression by endogenous amino acids. Wild-type receptors expressed on the the background of the tRNA / tRNA-synthetase pair and BzF gave peak currents amplitudes of 750 ± 158 pA (n = 33). The rates of desensitization of receptors carrying unspecific endogenous amino acids at positions S729 or G725 did not significantly differ from those after BzF incorporation with k_{des} = 204 ± 53 s^{-1} (n = 4; p = 0.76 compared to S729BzF) for GluA2 S729 (–BzF) and k_{des} = 170 ± 10 s^{-1} (n = 13; p = 0.04 compared to G725BzF) for G725 (–BzF; **Figure 32 B**). Critically, in contrast to the BzF-containing GluA2 G725 Amber mutant, these glutamate activated currents were unaffected by long-lasting UV exposures, similarly to GluA2 wild-type channels expressed on the BzF-synthetase and tRNA background (**Figure 32 C**). Currents obtained from the G725 mutant in the absence of BzF were usually not stable for many episodes. In patches that lasted, cumulative UV exposures of 12 s in the desensitized state resulted in a peak current reduction of 29 ± 6% (n = 6), which was never monoexponential, as seen for photoinactivation after Amber codon suppression by the UAA BzF at the same site. Crucially, the reduction in peak current of the GluA2 S729BzF and G725BzF mutants was invariably mono-exponential, demonstrating that the presence of BzF in the cell culture medium does not underlie any competitive behaviour between endogenous and UAAs. Lastly, expression of TAG mutant GluA2 subunits alone (with the eGFP Amber reporter) yielded no green cells (see **Figure 31**) and no currents (*not shown*), confirming that TAG stop codons do effectively block translation in HEK-293 cells.

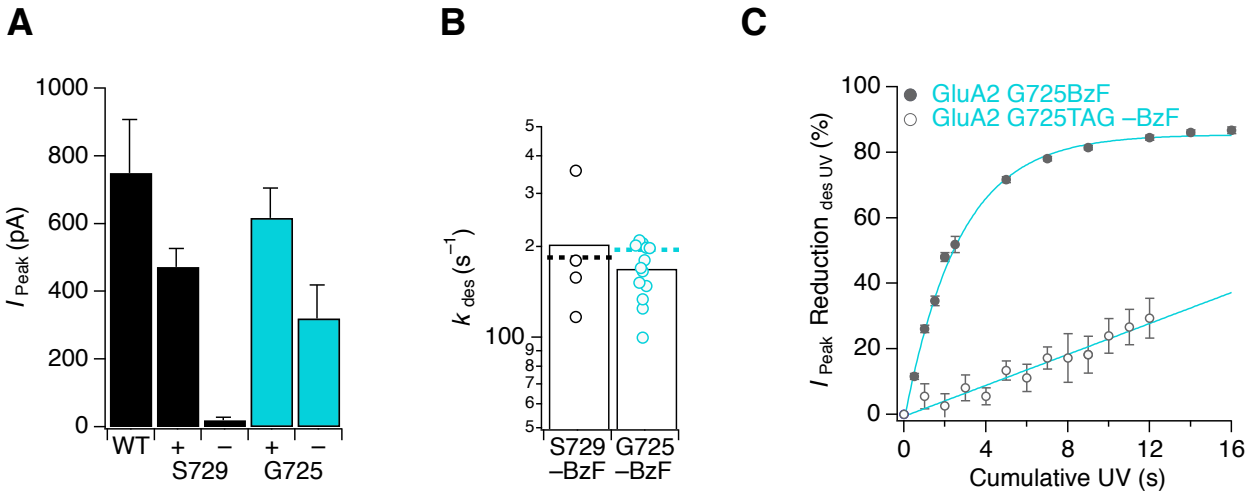

Figure 32 Unspecific Amber codon suppression at the GluA2 S729 and G725 sites. (**A**) The average peak current amplitudes for WT, on the background of the tRNA / tRNA-synthetase pair, and for the two GluA2 Amber mutants S729 (*black columns*) and G725 (*blue*) incubated in the presence (+) or absence (–) of BzF. The unspecific readthrough for GluA2 G725TAG was ~52% higher compared to ~4% for GluA2 S729TAG. The exact values are given in the text. (**B**) The rates of desensitization were not significantly different in the presence (*dotted line*) or absence (*columns with individual values*) of BzF for both Amber mutants S729 (*black*) and G725 (*blue*). The exact values are given in the text. (**C**) Pooled and normalized current reduction curves for the G725 Amber mutant in the presence or absence of BzF upon UV application in the desensitized state. Receptors containing BzF at position G725 were effectively photoinactivated by ~85% upon 16 s of UV (*solid circles; n* = 4-8 patches for each point). The photoinactivation rate was 3 ± 0.1 s. In the absence of BzF, receptors were not inactivated, 12 s of cumulative UV exposure resulted in a peak current reduction of ~29% with a rate of 53.2 ± 0.002 s, when fitted monoexponentially (*opaque circles; n* = 3-6 patches for each point).

3.6.3 Biophysical readout of specific UAA incorporation at position L483

Introducing aromatic amino acids as tyrosine (Y) or phenylalanine (F) at position L483, a site at the interface between the upper lobes of the LBD (D1), has been shown to block desensitization in GluA2 receptors (Sun et al., 2002). The degree of block depended on the amino acid introduced, with 90% reduced desensitization for L483Y, and 60% for L483F. Assuming that the aromatic UAAs (AzF and BzF) used in this study should produce receptors with similar blocked desensitization properties as the natural substitution mutants L483Y or L483F, the GluA2 L483 Amber mutant was suppressed by AzF or BzF to compare their ability to inhibit desensitization. As expected, L483 Amber mutants harboring one of these UAA groups showed a block of desensitization similar to that seen for L483Y and L483F (**Figure 33**). Outside-out patches expressing GluA2 L483AzF or L483BzF receptors were activated by 10 mM glutamate for either 400 or 1000 ms. The desensitizing fractions obtained did not depend on the time the patch was exposed to glutamate. However, the UAAs incorporated gave different desensitizing fractions with 40 ± 5% (equivalent to ~60% of desensitization block; n = 7) for L483AzF and 24 ± 2% (equivalent to ~76% of desensitization block; n = 18) for L483BzF (p = 0.02 compared to the AzF counterpart). As in previous studies, the leucine residue was also replaced by either tyrosine or phenylalanine. In agreement with Sun et al. (2002), both aromatic substitutions resulted in a distinctive block of desensitization, comparable to wild-type channels in the presence of the allosteric modulator CTZ (desensitizing fraction of 9 ± 4%, n = 7). However, in contrast to the previous study, the difference in the degree of block between these two mutants was smaller. Both natural substitutions at position L483 produced receptors with nearly full block of desensitization (**Figure 33**). The desensitizing fractions were 2 ± 3% for L483Y (n = 4) and 12 ± 3% for L483F (n = 8). Notably, cells expressing GluA2 receptors with natural substitutions have shown to have a lower cell viability compared to cells producing GluA2 receptors carrying UAAs on the day of recordings (48-72 h after PEI transfection). Introduction of AzF or BzF at position L483 resulted in GluA2 receptors that were less challenging to patch and which gave more robust ionic currents compared to the L483Y or L483F mutants.

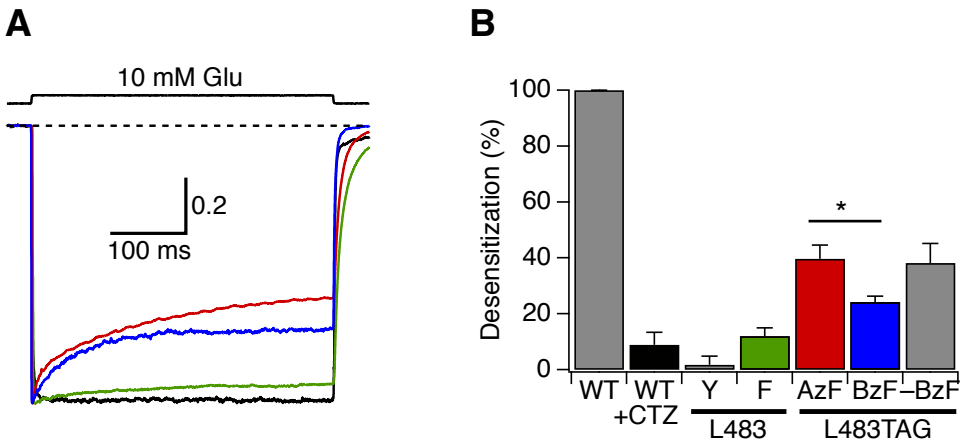

Figure 33 AzF or BzF groups at the GluA2 L483 site blocked receptor desensitization. (**A**) Example traces of outside-out patch recordings for GluA2 WT (in the presence of CTZ; *black*), L483F (*green*), L483BzF (*blue*), and L483AzF (*red*) activated by 10 mM Glu. The degree of desensitization block noticeably differed depending on the aromatic amino acid group placed at the sensitive position at the D1 interface. (**B**) Non-mutant receptors desensitized completely, when no allosteric modulators were applied. Both the allosteric modulator CTZ and natural and unnatural aromatic substitutions at the GluA2 position L483 resulted in a block of desensitization. The average desensitizing fractions are given in the text. $^{*}p < 0.05$.

3.6.4 Investigating the nature of endogenous amino acids non-specifically incorporated at Amber codon sites of GluA2

Given the fact that the tRNA / tRNA-synthetase pair specific for BzF used in this study was evolved from a pair that was specific for the incorporation of tyrosine (see **Methods and Materials 2.2.1**), it was assumed that the absence of BzF might drive unspecific insertion of tyrosine. To test this possibility, a GluA2 L483 Amber mutant was used. Equally to the previously described block of desensitization by tyrosine at this site (Sun et al., 2002), a similar block of desensitization was expected in the absence of BzF driven by the orthogonal BzF-pair. HEK-293 cells were transfected with the GluA2 L483 Amber mutant and the BzF-specific tRNA / tRNA-synthetase pair. Cells, which were incubated in 1 mM BzF, gave average peak currents of –690 ± 140 pA (n = 18) and showed a remarkable block of desensitization, due to the aromatic side chain of BzF (see previous section). The peak current amplitudes in the absence of BzF were –250 ± 150 pA (n = 6) 48 h after PEI transfection, which correlates to ~35% compared

to receptors with BzF at the same site (**Figure 34 A**). All patches showed a similar block of desensitization (**Figure 34 B**), which was, however, smaller compared to receptors carrying BzF at position L483 (desensitizing fraction of 38 ± 7%, n = 6). This result strongly suggests, that endogenous amino acids with aromatic side chains might preferentially be incorporated unspecifically, but suppression of random amino acids cannot be excluded, given the less pronounced block of desensitization.

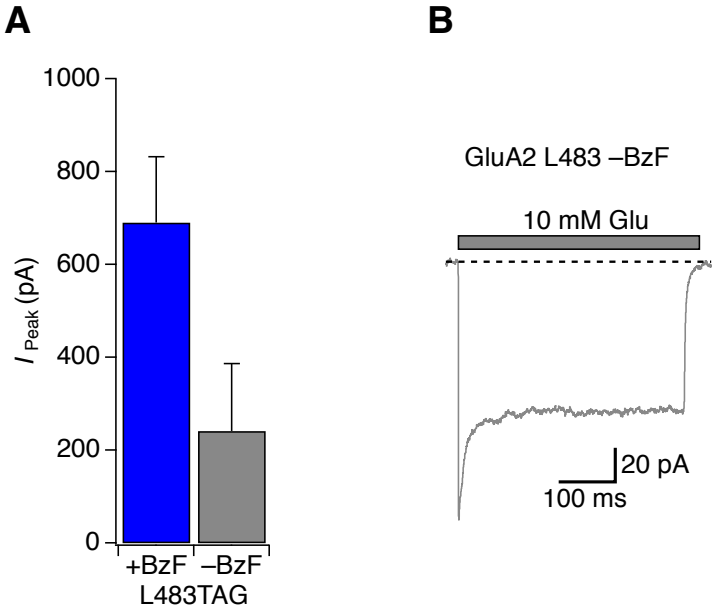

Figure 34 Suppression of the GluA2 L483 Amber codon by endogenous amino acids. (**A**) The average peak current amplitudes for the L483 Amber mutant on the background of the tRNA / tRNA-synthetase, in the presence (*blue*) or absence (*grey*) of BzF. See text for average peak current amplitudes. (**B**) Example current trace (*grey*) for the GluA2 L483TAG mutant in the absence of the UAA BzF. All outside-out patches (n = 6) obtained gave square currents upon activation by 10 mM Glu. For this example, the fraction of desensitisation was ~34%.

3.7 Photoinactivation at the G725 and S729 sites was state-independent

Previous experiments on cysteine mutants at the S729 and G725 sites indicated preferential trapping in the desensitized state (Plested & Mayer, 2009). The faster time resolution of UV exposures allowed to access different states of the receptor simply by opening the shutter at different points during the recording. Patches were exposed to UV either before the glutamate pulse (resting state) or during the glutamate application (desensitized or active state, depending on the presence or absence of CTZ; see **Methods and Materials 2.3.8**), and the rate of peak current reduction upon UV exposures was measured. When comparing active and desensitized states (**Figure 35**), there was little difference in the time constants of current reduction for the S729BzF mutant (*tau* = 5.6 ± 0.2 s for the active state, *n* = 5-9; *tau* = 3.2 ± 0.1 s for the desensitized state, *n* = 3-10; *p* = 0.35, **Figure 35 A**) or for G725BzF (active: *tau* = 4.2 ± 0.3 s, *n* = 3-6, and desensitized: *tau* = 3 ± 0.1 s, *n* = 4-8; *p* = 0.04, **Figure 35 B**). These small differences in mean trapping time constants were similar to the differences seen between individual recordings. Similarly, receptor inactivation remained striking, and with similar time constants, when patches were exposed to UV in the resting state. GluA2 receptor inactivation with BzF at the S729 occurred with *tau* = 1.8 ± 0.07 s (*n* = 2-14; **Figure 36 A**) in the resting state. G725 gave *tau* = 2.2 ± 0.07 s (*n* = 3-18; **Figure 36 B**). The trapping rates in the resting state were independent of the presence or absence of CTZ for both Amber mutants, and thus these rates were pooled. Wild-type GluA2 receptors were not affected by UV exposures for all states tested. Pooled peak current reductions for all states gave only a reduction of 13 ± 3% (*n* = 4-22) upon 20 s of cumulative exposure of UV (**Figure 36 A**).

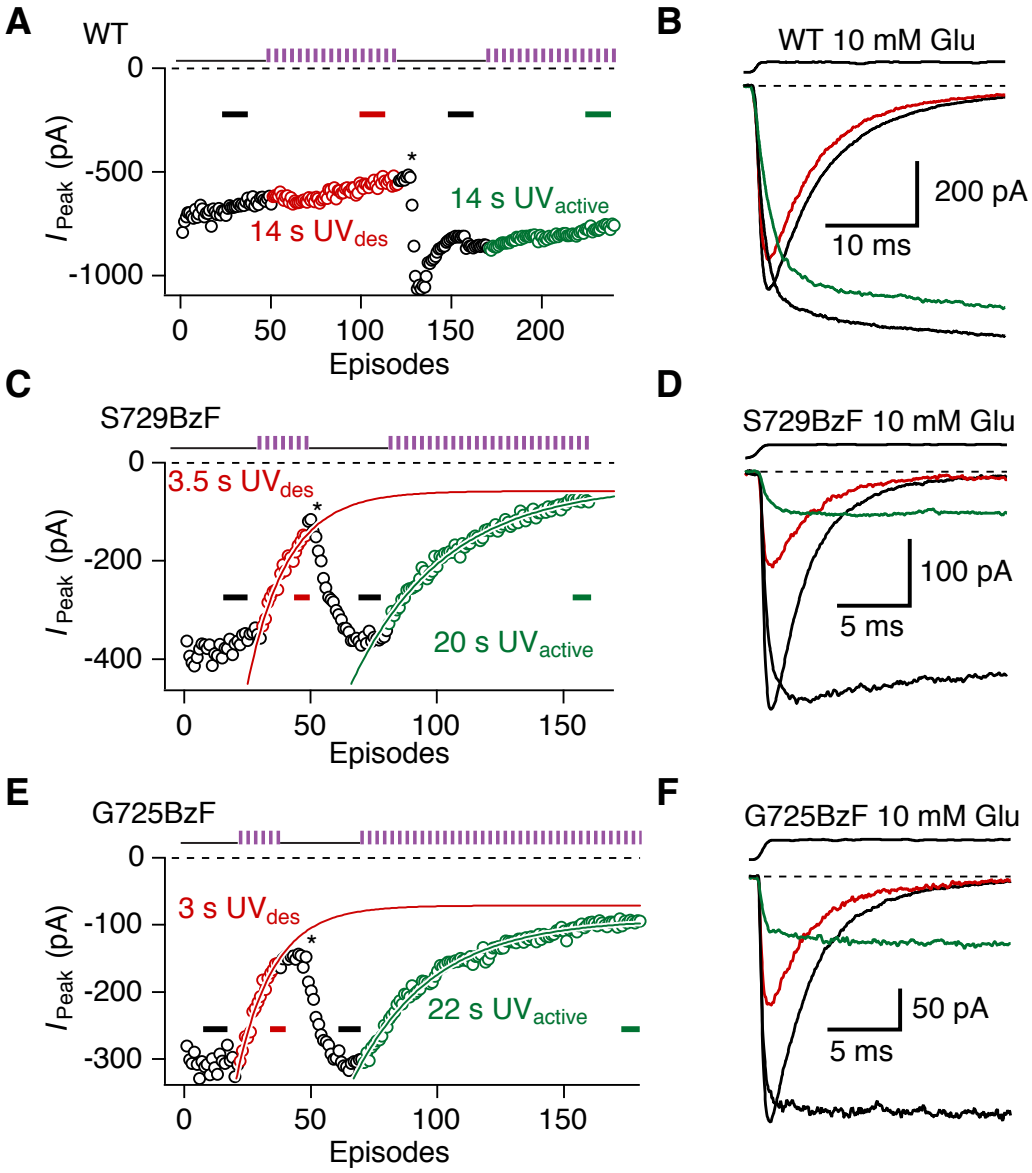

Figure 35 Limited state dependence for GluA2 S729BzF and G725BzF. The peak current kymograms show UV exposures (200 ms per episode, indicated as a pulse train; *violet*) in the desensitized (*red*) and active (*green*) state. The asterisk indicates the start of 100 µM CTZ application. (**A**) Cumulative UV exposures of 14 s did not cause any current reduction in WT receptors in either the desensitized or active state. (**B**) Responses to 10 mM Glu for WT GluA2, averaged over ~20 traces from stretches indicated by color-coded bars in *A*. (**C**) Peak current reduction kymogram for the S729BzF mutant. White outlined fits to the current reduction in response to 3.5 s cumulative UV exposure in the desensitized (*tau* = 18 episodes) and 20 s exposure in the active state (*tau* = 42 episodes) were monoexponential. (**D**) As in *B* for the S729BzF mutant. Averages of 5–20 traces were taken. (**E**) Kymogram, as in *C*, for the G725BzF mutant. The exponential half-times of peak current reduction were 14 episodes for the desensitized and 37 episodes for the active state. (**F**) Averages over groups of traces from stretches indicated by bars in *E* (from Klippenstein et al., 2014).

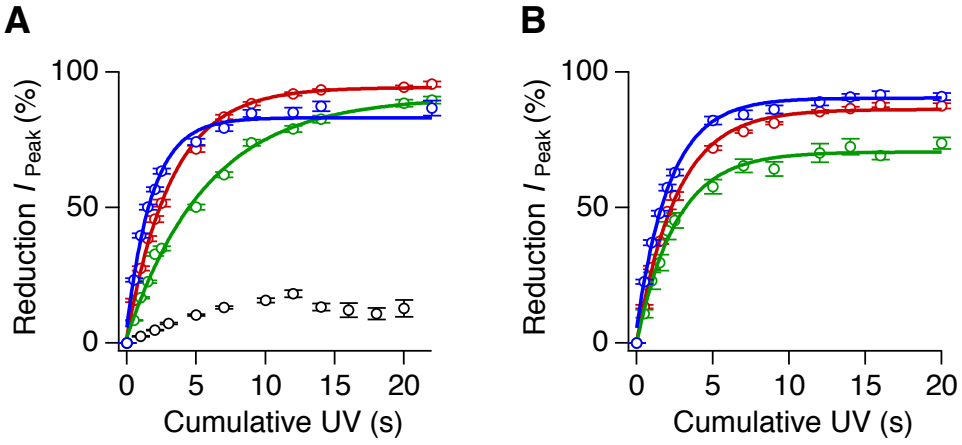

Figure 36 Summary of UV-induced peak current reduction rates for GluA2 S729BzF, G725BzF, and WT receptors, obtained during different functional states. (**A**) Pooled, normalized peak current reduction curves for the desensitized (*red*), active (*green*), and resting (*blue*) states for the S729BzF mutant. The decays were fit single-exponentially. The current reduction of WT receptors was pooled for all states and was 13 ± 3% after cumulative UV exposure times of 20 s (*black*). The exact values are given in the text. (**B**) As for *A*, for the G725BzF exponential fits to pooled peak current reduction curves. The color-coding is equivalent to panel *A*. The exact values are given in the text (modified from Klippenstein et al., 2014).

3.8 State dependence of crosslinking at the sites M721 and Y768

Knowing that a different chemistry underlies the crosslinking of disulfide bonds and BzF groups (see **Discussion**), state dependence with BzF was expected to be more likely at sites that move to greater extents. Following the logic that state dependence should be obtained at more distant sites, BzF was introduced at position M721 (the position within the LBD dimer is shown in **Figures 22 & 37**). When modelled in place of M721 in the active dimer (Armstrong & Gouaux, 2000), the BzF side chain cannot span the separation of the lower lobes (**Figure 37 A**). In the candidate inactive dimer (Armstrong et al., 2006), the lower lobes of the LBDs approach, but the oxygen radical remains 14 Å from the nearest backbone in the opposed subunit (**Figure 37 B**). In the full-length antagonist-bound structure, although this distance is reduced to 8 Å (*not shown*), the ketone remains far too distant for crosslinking. Thus, crosslinking with M721BzF would imply either intrasubunit crosslinking, or a substantial conformational change upon

desensitization (Schauder et al., 2013). BzF was further inserted in place of Y768, a site important for receptor gating at the end of Helix K (Carbone & Plested, 2012). In the full-length, antagonist-bound crystal structure of GluA2, the 768BzF side-chain in subunit A can be oriented to allow its ketone to approach within 6 Å of the electron-rich Cβ of Val666 in subunit D. Crosslinking at this site is likely to result in inhibition (Lau et al., 2013). However, the bond coplanarity required for H-atom abstraction may be difficult to achieve, and the distance is long compared to the preferred 2.5 to 3.1 Å range (Dormán & Prestwich, 1994). BzF is even further from a neighboring subunit in the active dimer (**Figure 38 C**). However, modeling the BzF side chain in place of Y768 in the candidate inactive dimer suggests that an intersubunit crosslink might be possible in this state (**Figure 37 D**).

The GluA2 M721BzF and Y768BzF mutants had similar rates of desensitization to wild-type channels ($k_{\text{des M721BzF}}$ = 101 ± 6 s^{-1}, n = 16, p = 0.99; $k_{\text{des Y768BzF}}$ = 183 ± 8 s^{-1}, n = 19, p = 0.31; **Figure 38 A & B**), but Y768BzF had a slower deactivation decay ($k_{\text{deact M721BzF}}$ = 1400 ± 160 s^{-1}, n = 7, p = 0.89; $k_{\text{deact Y768BzF}}$ = 700 ± 60 s^{-1}, n = 11, p = 0.0008; **Figure 38 C & D**). The recovery from desensitization of the M721BzF mutant was noticeably faster than wild-type ($k_{\text{rec M721BzF}}$ = 67 ± 9 s^{-1}, n = 8, p = 0.0004; **Figure 38 E & F**), whereas Y768BzF was slower ($k_{\text{rec Y768BzF}}$ = 28 ± 3 s^{-1}, n = 4, p = 0.3), consistent with the kinetic changes caused by related mutations in this region (Carbone & Plested, 2012). In addition to the Amber mutants at the LBD interface, the GluA2 Y768TAG mutant was electrophysiologically tested in the absence of BzF. On average, the peak current amplitudes were –102 ± 58 pA (n = 5), equivalent to ~18% of the BzF-containing counterpart (–570 ± 134 pA, n = 35; *not shown*).

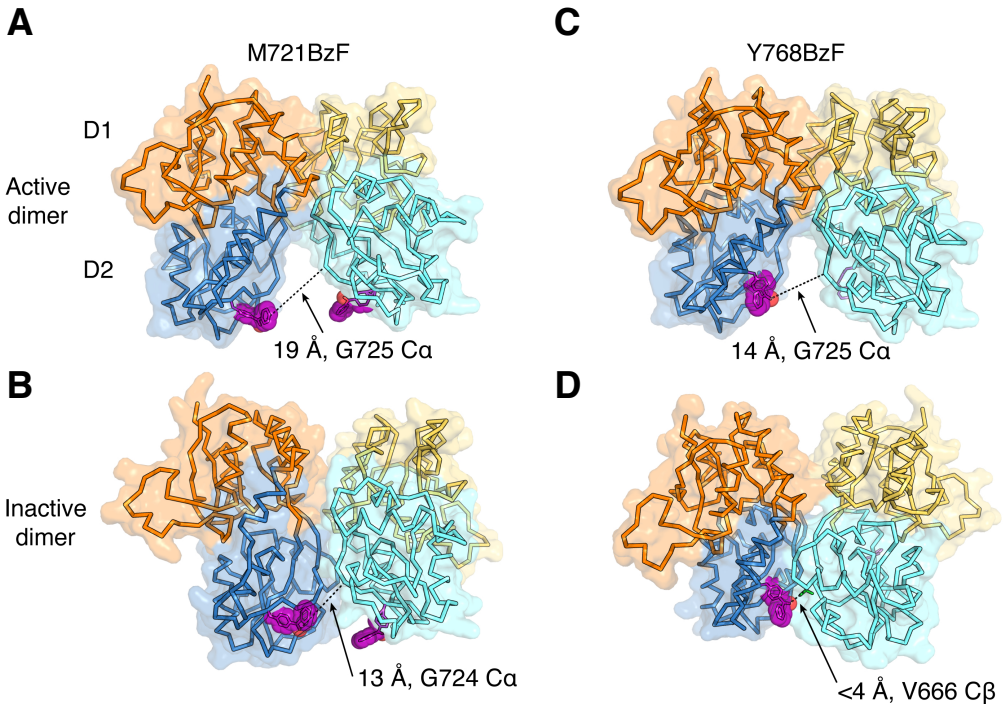

Figure 37 BzF modeled into the M721 and Y768 positions within the LBDs. (**A**) The M721BzF mutation modeled into the active LBD dimer of GluA2 (PDB ID: 1FTJ, chains A and C). Same color scheme as in Figure 14 with BzF indicated in *violet*. Dashed line indicates the distance to the nearest C–H bond in the opposite subunit. (**B**) The M721BzF mutation modeled into the candidate desensitized dimer (PDB ID: 2I3W). (**C**) The Y768BzF mutation modeled into active LBD dimer of GluA2. (**D**) The Y768BzF mutation modeled into the candidate desensitized dimer (from Klippenstein et al., 2014).

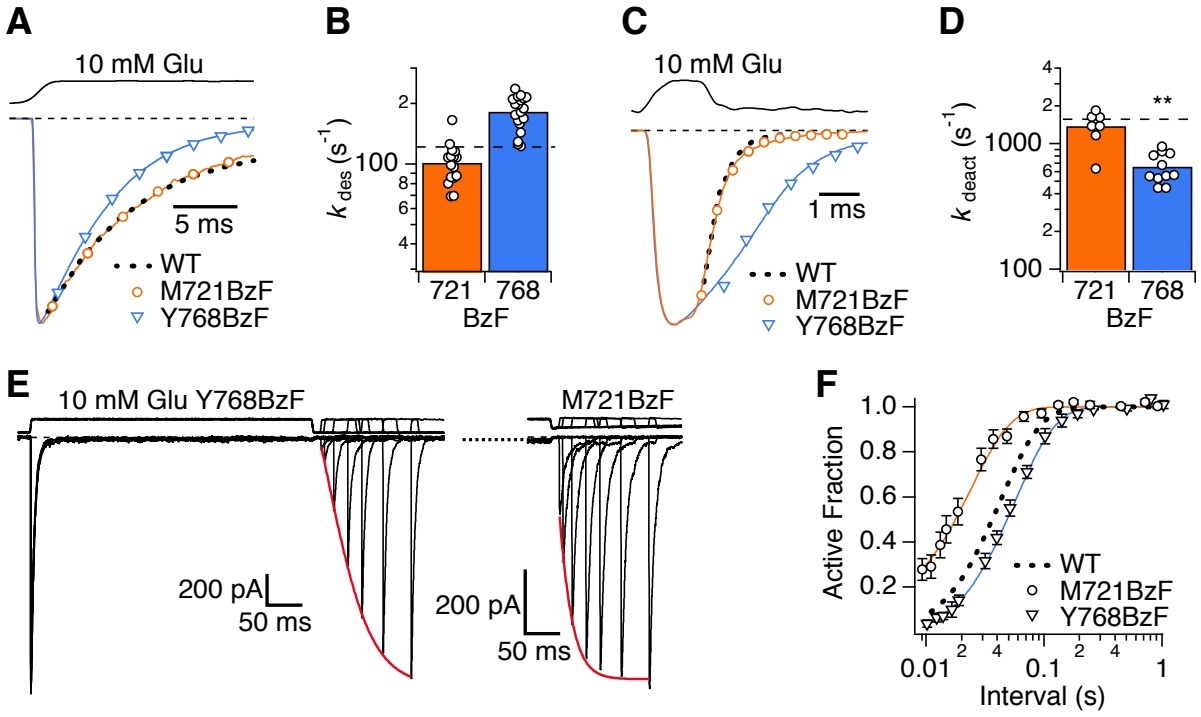

Figure 38 Kinetic properties of the M721BzF and Y768BzF mutants. (**A**) Normalized responses to 400 ms pulses of 10 mM Glu for M721BzF and Y768BzF mutants. The desensitization rates in the examples shown were k_{des} = 134 s^{-1} for M721BzF (*orange*) and k_{des} =185 s^{-1} for Y768BzF (*blue*). An equivalent decay from a WT patch is drawn as a *dashed line*. (**B**) Summary of desensitization rates of receptors with BzF at positions M721 and Y768. Dashed line indicates the WT rate. The average values are given in the text. (**C**) Normalized responses to 1 ms pulses of 10 mM Glu for the M721BzF and Y768BzF mutants. The deactivation rates for the examples plotted here were k_{deact} = 1961 s^{-1} for M721BzF (*orange*) and k_{deact} = 617 s^{-1} for Y768BzF (*blue*). A WT trace is shown as a *dotted line* for comparison. (**D**) Summary of deactivation rates of M721BzF mutant and the Y768BzF mutant. The dashed line indicates the WT rate. The average values are given in the text. $^{**}p < 0.001$ (**E**) Example time courses of recovery from desensitization for Y768BzF (here, k_{rec} = 32 s^{-1}) and M721BzF (here, k_{rec} = 64 s^{-1}) mutants (7 overlaid traces for each panel). (**F**) Pooled recovery data for M721BzF and Y768BzF. WT GluA2 recovery is shown as a *dotted line*. The average values are given in the text (modified from Klippenstein et al., 2014).

In contrast to BzF substitutions at positions S729 and G725, the M721BzF mutation exhibited state-dependent reduction of peak current by UV. Consistent with a conformational change that promotes crosslinking upon desensitization, current reduction in the active state (*tau* = 140 ± 40 episodes, 200 ms UV per episode; *n* = 5) was on average about 3.5-fold slower than that in the desensitized state (*tau* = 40 ± 8 episodes, 200 ms UV per episode, *n* = 7, *p* = 0.04; **Figure 39 A & D**). State-dependent current reduction was even more pronounced for the Y768BzF mutant than for the M721BzF mutant (**Figure 39 B & E**). The state dependence was inverted, indicating that current reduction is highly sensitive to geometry of BzF photoinactivation in the lower (D2) lobes of the LBD. The peak current was preferentially reduced when UV was applied to receptors in the open, fully active state (*tau* 49 ± 6 episodes, *n* = 14 patches, 200-300 ms UV per episode; **Figure 39 B & E**), or in the resting state with CTZ present (*tau* = 26 ± 5 episodes, *n* = 4; **Figure 39 C & E**). Surprisingly, given the expectation from the candidate inactivated dimer of intersubunit crosslinking between lower lobes, the 768BzF mutant was almost unaffected by UV in desensitized states, being trapped at least an order of magnitude more slowly (*tau* = 400 ± 90 episodes, *n* = 8; *p* = 0.006 vs active state, *p* = 0.005 vs resting state). The time constant of trapping (and thus state dependence) is probably underestimated in this case, due to the inability to hold patches stable for the requisite amount of time (> 10 min) to accurately measure such slow modification. State dependence did not depend on the order in which the states were assessed, with strong current reduction by UV either if exposures were first made in the desensitized state, or if this step was omitted.

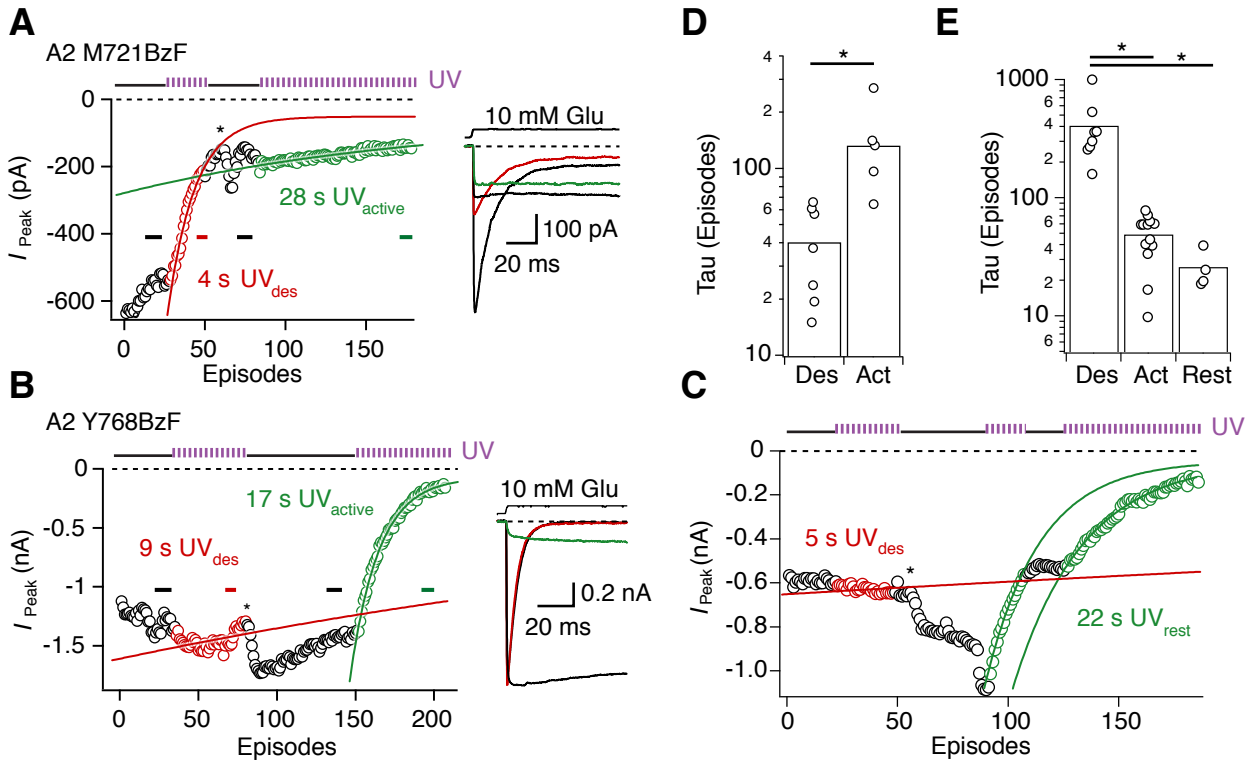

Figure 39 The M721BzF and Y768BzF mutants were trapped state-dependently. Peak current reduction kymograms for M721BzF and Y768BzF for the desensitized state (*red*) and the active state (*green)*. Monoexponential fits to the current reduction were fixed to a common minimum. UV exposures are shown schematically as a pulse train (*violet;* 200 or 300 ms per episode). Asterisk indicates the point of 100 µM CTZ application. (**A**) For this example, the peak current reduction for M721BzF gave tau_{des} = 20 episodes (ep) and tau_{active} = 270. Cumulative exposure of UV was 4 s in the desensitized and 28 s in the active state. Representative average currents activated by 10 mM Glu are shown, color-coded according to the bars in the kymogram. (**B**) Current reduction kymogram for Y768BzF gave tau_{des} = 535 ep and tau_{active} = 17 (for this example). Cumulative UV exposure was 9 s in the desensitized and 17 s in the active state. Representative average currents are shown, color-coded according to the bars in the kymogram. (**C**) Current reduction kymogram for Y768BzF with tau_{des} = 1000 ep and tau_{active} = 25 ep. Cumulative UV exposure was 5 s in the desensitized and 22 s in the active state. There is a brief interval in the resting state trapping when no UV exposures were made (*black*). (**D**) Summary of time constants for peak current reduction (in ep) for the M721BzF mutant with UV exposures of 200 ms for active and desensitized states. The exact values are given in the text (*$p < 0.05$). (**E**) Summary of time constants for peak current reduction for the Y768BzF mutant for desensitized and resting states. For the active state, no difference in the trapping time constant for 200 or 300 ms UV exposures per episode was seen, and these were pooled. The exact values are given in the text (*$p < 0.01$; modified from Klippenstein et al., 2014).

To further investigate whether the reductions in current observed for the Y768BzF and M721BzF mutants was due to intersubunit covalent bonds, biochemical experiments were performed. For GluA2 Y768BzF, no UV-driven dimerization even after 30 min exposure was detected (*DF* before UV: 3.5 ± 1.2%, *DF* after UV: 3.3 ± 0.7% n = 3 blots; **Figure 40 A**). Also, isolation of specific states during the treatment with UVA, did not lead to an increase of detectable trapped subunits. For GluA2 M721BzF, biochemical detection of rescued subunits remained challenging, probably due to low expression levels. A Western blot following UV treatment for 30 min is shown in **Figure 40 B**. Equally to Y768BzF, no UV-induced dimerization of subunits could be detected. This suggests that either any crosslinking between subunits was limited or the amount of dimer fractions upon UV was too low to be detected biochemically (equally to GluA2 G725BzF).

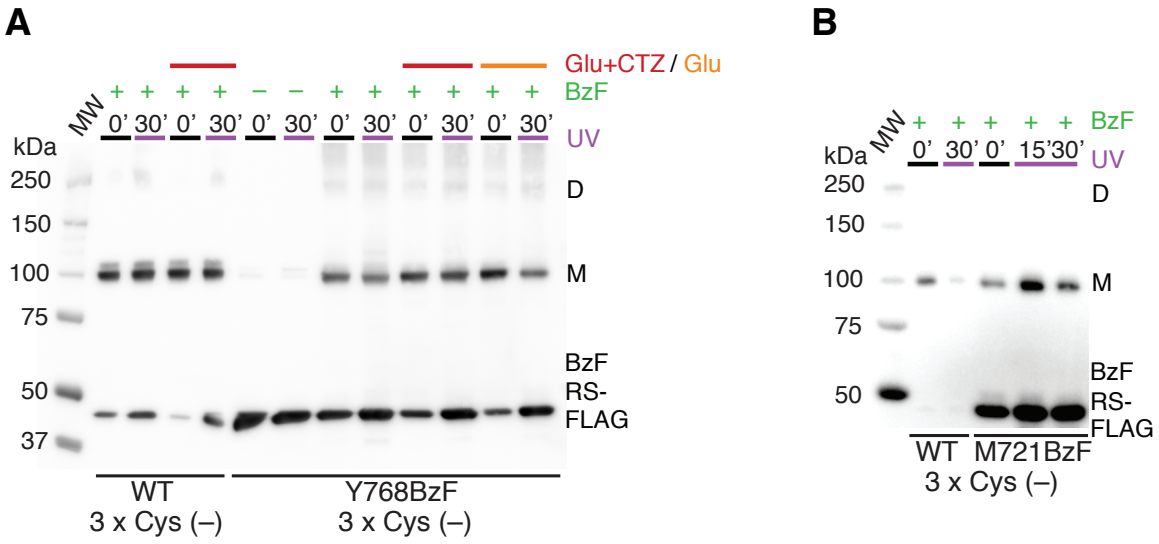

Figure 40 *In vivo* trapping of the GluA2 Y768BzF and M721BzF mutants. (**A**) Western blot of GluA2 WT and Y768BzF 3 x Cys (–) receptors before and after 30 min of UV exposure (stained with a mouse α-FLAG antibody, 1:1000). No UV driven dimerization was detected both WT and the Y768BzF mutant. Additionally, UV was applied on cells with 100 µM Glu or in the presence of 100 µM Glu / 100 µM CTZ in the illumination medium. Equally, UV exposures of 30 min did not induce dimerization of subunits. (**B**) Similar to the experiment shown in panel *A*, UV of 30 min was applied to GluA2 receptors with BzF at position M721. No UV-driven dimer formation could be detected.

3.9 Photoinactivation of heteromeric AMPA receptors

Since a single trapping event per complex was reasoned to be sufficient to abolish ~95% of the current response of homomeric GluA2 receptors, the inclusion of at least one subunit harboring a photoactive crosslinker was expected to effectively inactivate heteromeric complexes containing naive subunits. To investigate this possibility, wild-type GluA1 (Q) subunits were co-transfected with GluA2 (R) S729 or G725 Amber mutant subunits, and tRNA and tRNA synthetase vectors. For the GluA2 (R) subunit, an IRES_eGFP-Y40TAG mutant vector was used, whereas the GluA1 vector did not encode any fluorescent reporter. Patches were clamped at +40 mV during fast perfusion electrophysiology, in order to block homomeric GluA1 Q-containing channels with 30 μM spermine. In these conditions, green cells that gave currents after incubation in BzF were likely to express A1:A2 heteromeric receptors with BzF substitutions only on the GluA2 subunit. Responses at positive voltages were compared with those of the potentially mixed population at –60 mV. Neither homomeric wild-type GluA1 controls (n = 4), nor heteromeric wild-type receptors containing A1 (Q) and A2_IRES_eGFP-Y40TAG (R) subunits (n = 4), exhibited a UV-dependent reduction in current (**Figure 41 A & B**). However, consistent with crosslinking of homomeric receptors, UV exposure in the desensitized state caused a monoexponential loss of the peak current at positive potentials for heteromeric receptors with either BzF mutant, A1:A2 S729BzF (**Figure 41 C & D**) or A1:A2 G725BzF (**Figure 41 E & F**). The time constants for current reduction of 4.9 ± 0.8 s of cumulative UV exposure for A1:A2 G725BzF (n = 6) and 4.7 ± 0.4 s for A1:A2 S729BzF (n = 6; **Figure 42 A**) did not significantly differ between the mutants (p = 0.84), and were similar to the time constants obtained for homomeric receptors under similar UV conditions. The maximum extent of current reduction was less than that for homomeric mutant receptors. After 10 s of cumulative UV exposure, A1:A2 G725BzF receptor peak currents were reduced by 58 ± 3% (p < 0.00001 compared to the reduction of homomeric receptors following 12 s of UV, n = 11; see also **Figure 20**) and for S729BzF, the reduction was 56 ± 3% (p < 0.00001 vs. homomeric; n = 11). As for the homomeric counterparts, these extents were not significantly different from each other (p = 0.71). Heteromeric complexes with a BzF substitution at the M721 site were only weakly inhibited. 10 s of UV in the desensitized state promoted a peak current amplitude reduction of 29 ± 3% (n = 4; **Figure 42 C**). As for homomeric GluA2 receptors, the reduction of the peak current

upon 10 s cumulative UV exposures was not related to the initial current amplitude ($R^2_{S729BzF}$ = 0.27, n = 11; $R^2_{G725BzF}$ = 0.25, n = 11; $R^2_{M721BzF}$ = 0.22, n = 4; **Figure 42 B**). Contamination with homomeric channels was limited, because for most patches, the IV relation was almost linear, with rectification ratios (RR) of 1.7 ± 0.04 for A1:A2 S729BzF (n = 12; **Figure 41 D**) and 1.5 ± 0.1 for A1:A2 G725BzF (n = 13; **Figure 41 F**). These rectification ratios did not evolve with continuing application (~20 s) of UV for A1:A2 G725BzF ($RR_{post\ UV}$ = 1.4 ± 0.2, n = 7, p = 0.5 vs. before UV) or A1:A2 S729BzF ($RR_{post\ UV}$ = 1.7 ± 0.1, n = 8, p = 0.72). In some patches, higher initial rectification ratios were obtained, consistent with a largely homomeric A1 receptor population (RR > 2). In this case, a substantial proportion of the receptors were homomeric GluA1, and selective inactivation of heteromers by UV light led to an increasingly rectifying IV relation, as expected (increase in RR for S729BzF was 30 ± 6%; range of initial rectification ratios was 2.7–5.8, n = 4; *not shown*). The current reduction at +40 mV, after 20 s UV exposure, was independent of the rectification ratio (linear regression gave R^2 =0.04 for A1:A2 S729BzF; range of RR values 1.5–5.8), consistent with effective isolation of BzF-containing heteromers by spermine.

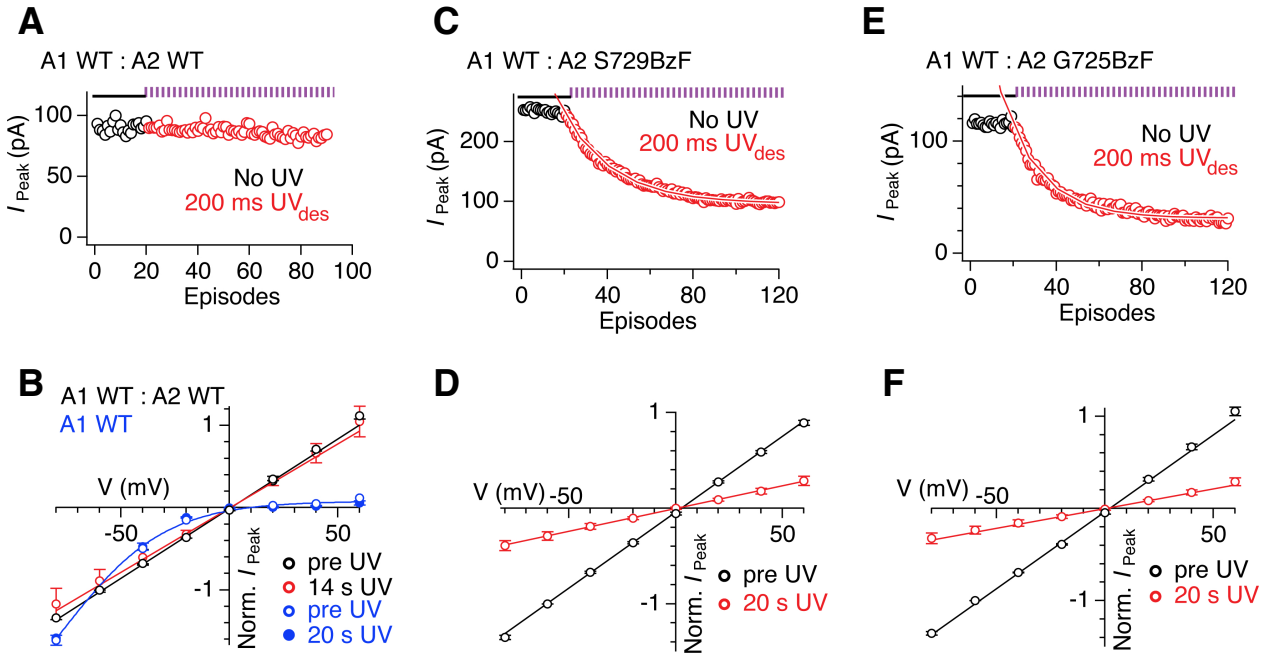

Figure 41 Heteromeric receptors could be photoinactivated. The example kymograms show the peak current responses before (*black markers*) and upon 200 ms UV pulses (*red)* in the desensitized state (indicated schematically as a pulse train; *violet*). (**A**) Example kymogram for WT GluA1:GluA2 heteromers. Cumulative exposure of UV for this example was 14 s. (**B**) IV relations for GluA1 WT (*blue*) and WT GluA2:GluA1 heteromeric receptors (*black* for pre-UV; *red* for post-UV) in the presence of 30 µM spermine. 20 s of cumulative UV did not induce any reduction in peak current for either condition (n = 4 for each IV relation). (**C**) Example kymogram for the same experimental procedure as in *A* on A2 S729BzF:A1 receptors. The time course of trapping was monoexponential (*white outlined fits*), and the time constant for peak current reduction in this example was 24 episodes (4.8 s UV). The extent of trapping after a cumulative UV exposure of 20 s was 61%. (**D**) IV relation before and after UV-induced photoinactivation for A2 S729BzF:A1. The linear IV relation (*black*) before UV exposure indicates a predominately heteromeric population of receptors. UV exposures of 20 s did not induce rectification (*red*). The exact values are given in the text. (**E**) As in *A*, an example kymogram for A2 G725BzF:A1 receptors exposed cumulatively to 20 s UV. The time course of trapping was monoexponential (*white outlined fits*) and the time constant of the current reduction for this example was 18 episodes (3.6 s UV), resulting in inhibition of the peak current by 74%. (**F**) IV relation before and after UV-induced photoinactivation for A2 G725BzF:A1. The IV relation was linear before (*black*) and after UV exposure (20 s; *red*). The exact values are given in the text.

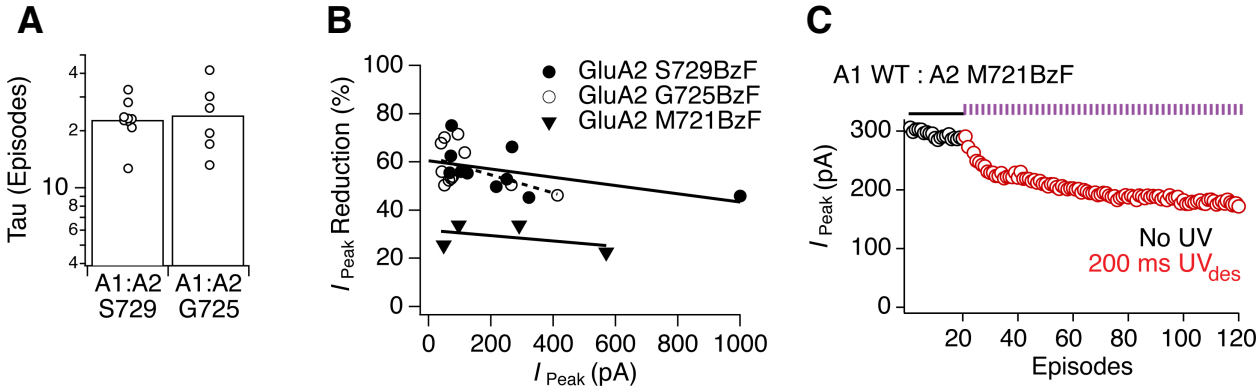

Figure 42 Characteristics of heteromeric receptor photoinactivation. (**A**) Summary of the exponential half-times (in episodes) for both BzF-containing heteromeric receptors GluA1/GluA2 S729BzF and GluA1/GluA2 G725BzF. The average *taus* are given in the text. (**B**) No correlation between the peak current at the start of the experiment and the degree of their inhibition upon 10 s of UV was observed. The exact values are given in the text. (**C**) Example kymogram for the same experimental procedure as in Figure 41 on A2 M721BzF:A1 receptors. The extent of trapping after a cumulative UV exposure of 20 s was 40% for this example.

4 DISCUSSION

4.1 Effective rescue of Amber mutant receptors by photoactivatable UAAs

In the framework of this study, two different unnatural amino acids, AzF and BzF, were site-specifically incorporated into GluA2 receptors by means of genetically encoded mutagenesis. Four different amino acids within the D2 lobes of the GluA2 LBDs – M721, G725, S729 (all at the lower D2 lobes; Armstrong et al., 2006; Plested & Mayer, 2009), and Y768 (in helix K; Carbone & Plested, 2012) were replaced by Amber codons for UAA incorporation and subsequent photoinactivation. Two further Amber codon mutations as the L483 (at the interface between the D1 lobes; Sun et al., 2002) and A665 site (helix G; at the interface between LBD the dimers; Lau et al., 2013) also contributed to the establishment and understanding of Amber codon suppression in AMPA receptors.

As assessed by a range of biophysical readouts, it is strongly favoured that the introduced Amber codons within the D2 lobes (**Figure 14**) were specifically rescued by the photoactivatable UAAs, AzF and BzF. This includes the following major considerations: (*i*) the fluorescence of eGFP expressed from the dual wild-type Amber reporter was effectively rescued by the inclusion of AzF or BzF, as shown on confocal micrographs (**Figure 16**), and corroborated by determination of the number of fluorescent cells transfected and cultured under different conditions (**Figure 31**); (*ii*) the rates of desensitization upon AzF and BzF incorporation at the GluA2 S729 site dramatically differed depending on the UAA group introduced (**Figure 17**); (*iii*) the presence of AzF and BzF produced receptors that were optically active – with remarkable opposite effects following UV exposure at position S729 (**Figures 18, 19, 23**); (*iv*) BzF at the same site promoted a physical crosslink between two subunits upon exposures of UV, as confirmed biochemically (**Figure 29**); (*v*) in the absence of BzF, unspecific readthrough by endogenous amino acids at Amber codon sites within GluA2, produced receptors that could not be inactivated with UV (**Figure 32**); (*vi*) the block of desensitization differed significantly after incorporation of AzF and BzF at the GluA2 L483 Amber codon site (**Figure 33**). These points of evidence will be discussed in detail in the following sections.

4.2 Specific suppression of the Y40 Amber codon resulted in rescue of eGFP fluorescence

The introduction of a TAG stop codon within eGFP (at the Y40 site) turned out to be a convenient strategy in order to screen for cells with UAA-suppressed Amber codons. Rescue of fluorescence within eGFP guaranteed also a rescue of GluA2 subunits, as shown exemplarily for for the S729 Amber codon site (**Figure 15**). 95-97% of all outside-out patches obtained gave large responses to fast applications of 10 mM glutamate (see also **Section 3.3**), probably arising from rescued receptors in which the TAG stop codon was suppressed by AzF or BzF. Subunits truncated within the S2 segment are unlikely to form functional receptors. In general, cell viability did not suffer in the presence of 0.5 mM AzF or 1 mM BzF within the cell culture medium. This observation is fortunate, knowing that 23% of all stop codons belong to the Amber-type (Liu et al., 2007) suggesting that Amber codon suppression at true stop codons is limited. The concept of rescuing fluorescence in eGFP was introduced in previous studies by Peter Schultz and Lei Wang, who utilized a construct encoding an eGFP Amber mutant (at the Y37 site). The small protein of ~27 kD facilitated the evolution of various engineered *Ec*Tyr-tRNA-synthetase / *Bst* Amber suppressor tRNA pairs (Liu et al., 2007; Wang et al., 2007; Takimoto et al., 2009). In accordance with the published work, specific expression of the fluorescent full-length eGFP was strongly dependent on the presence of the orthogonal tRNA / tRNA-synthetase pair and also the presence of the UAA group, for both AzF and BzF (**Figures 16 & 31**). With the introduction of the whole Amber codon suppression set, strong cytoplasmic GFP-fluorescence was detected. In the absence of the orthogonal suppressor tRNA and its cognate synthetase, or with excluding the UAA in the cell culture medium, only a minor fraction of cells showed a faint eGFP-fluorescence. (**Figures 16 B & 31**). These results strongly suggest that the tRNA-synthetase used selectively charges the tRNA with its appropriate UAA, followed by Amber codon suppression at the Y40 site.

Quantification of fluorescent cells from rescued eGFP by UAAs within the dual Amber reporter and of the background fluorescence in the absence of one of the Amber codon suppressor components at time points when electrophysiological or biochemical experiments were performed, gave a more detailed picture of the Amber codon suppression functionality (**Figure 31**). Unsurprisingly, specific and unspecific (in the absence of one of the components) fluorescence signals strongly developed with the cell incubation time, and depended on the

presence of the UAA (here BzF), and on the presence of the tRNA-synthetase. In the absence of BzF in the cell culture medium, expression of the wild-type GluA2 dual Amber reporter along with a BzF-tRNA / tRNA-synthetase pair revealed an unspecific fluorescence background of ~20% following two days of cell incubation. This fluorescence was very faint (as shown in **Figure 16 B**). The unspecific background observed agrees with a previously reported FACS study, with the same transfection condition (transfection of genes encoding eGFP, the tRNA, and the tRNA-synthetase) and an equal incubation time of 48 h resulting in a comparable quantitative eGFP-fluorescence background (Wang et al., 2007). Also, the non-specific background of the eGFP-derived fluorescence in the absence of the UAA or the tRNA-synthetase was marginal at the level of individual cells compared to the total fluorescence intensity, as shown in the mentioned publication and supporting the results presented here. Interestingly, specific aminoacylation of the tRNA with its cognate UAA group was strictly accompanied by the presence of the UAA-specific tRNA-synthetase. Cells not transfected with a gene encoding the tRNA-synthetase invariably expressed eGFP from the 37TAG construct unspecifically, which was independent of the inclusion of the UAA to the cell culture medium. This effect was also seen in another study on NMDA-type glutamate receptors, employing a tRNA / tRNA-synthetase pair of the same origin (Ye et al., 2013). This work showed that tRNA charging by endogenous synthetases was also pronounced in the absence of the UAA-synthetase, resulting in readthrough of Amber codons introduced to NMDA subunits. Considering the origin of the *Bst*RNA being capable of charging both AzF and BzF (Ye et al., 2008; 2009; see also **Section 2.2.1**), *Bst*RNA-aminoacylation by endogenous mammalian TyrRSs cannot be excluded.

The results presented in this study show, that introducing the whole set required for Amber codon suppression generally works for proteins of diverse size and habitat – small proteins like eGFP, resulting in a rescue of fluorescence (Liu et al., 2007; Wang et al., 2007; Takimoto et al., 2009), or glutamate receptors with a ~120 kDa size of each subunit (Ye et al., 2013; Klippenstein et al., 2014) – to name just two examples. Employing orthogonal pairs of *Bst*RNAs / *Ec*RSs to reduce proteins in mammalian cells requires care, since unspecific readthrough, probably due to suppression by endogenous amino acids, cannot be excluded at a given condition. The absence of the UAA or the tRNA-synthetase did not hinder expression of eGFP, identifying the tRNA as the „leaky“ component of the system. Electrophysiological recordings exploring the nature of the

endogenous amino acids unspecifically incorporated at Amber codon sites within the GluA2 receptor, will be discussed more detailed in **Section 4.8**.

4.3 AzF at the GluA2 S729 Amber codon site produced receptors with faster desensitization properties

The introduction of different photoactive groups (AzF and BzF) at the GluA2 S729 Amber codon site was accompanied by distinct kinetics of homomeric GluA2 receptors, arguing for specific UAA incorporation. The rate of desensitization was greatly faster when AzF was incorporated in place of S729 (~8-fold faster compared to wild-type channels), but only slightly faster following BzF introduction (~1.5-fold faster compared to wild-type channels; **Figure 17**). The effect of AzF on receptor desensitization was site-specific and not pronounced at the GluA2 G725 Amber codon site. Small increases in the desensitization rate, as observed for both mutants S729BzF and G725BzF, were also seen for cysteine mutants at these positions in a comparable range (Plested & Mayer, 2009). To verify, that the different side chains of AzF and BzF (shown in **Figures 5 & 6**) induce this kinetic effect, the most similar natural aromatic amino acid to AzF, tyrosine, was introduced at position S729 within GluA2. Given the fact, that the natural substitution produced receptors with a ~4-fold faster desensitization rate compared to wild-type channels, it is likely that the changed kinetic properties towards faster desensitizing receptors were caused by the single phenyl ring that probably resilted in different hydrophobic interactions compared to BzF. The adjacent GluA2 subunit offers a lysine residue (position K763) in a good context for a hydrophobic cation-π interaction with AzF (~6 Å distance between the ring of AzF and the amino group of lysine in 1FTJ; Gallivan & Dougherty, 1999).

The reaction pathways of AzF and BzF were introduced in detail in **Section 1.2.4**. In contrast to BzF, the use of AzF is accompanied by some major disadvantages. With its multiple reaction possibilities upon UV illumination including specific insertion into hydrogens of C–H and N–H bonds or phenyl ring expansion with following non-specific insertions into nucleophiles in the absence of eligible acute crosslinking partners, the photochemistry of AzF is less predictable. Activation of AzF is also irreversible, thus eliminating functional and reactive AzF groups for effective photocrosslinking with prolonged exposures of UV (Knowles, 1972). Another disadvantage of AzF as a photocrosslinker is its high photosensitivity, even to ambient daylight

(Grunbeck et al., 2011). Considering these limitations of using AzF, the observed effect on the kinetics of desensitization after introduction at the GluA2 S729 site is not surprising. The experimental process including the preparation of the medium and the electrophysiological recordings were not performed in complete darkness. It is likely, that ambient daylight triggered unspecific phenyl ring expansion followed by insertion into nucleophiles upon ambient daylight, a pathway, which is known to be the dominant one (Thermo Fisher Scientific, Handbook, 2009). It seems unlikely that the fast desensitizing GluA2 S729AzF mutants are a result of an actual crosslink produced by ambient daylight. The turn-on function upon UV exposures gained in this mutant speaks strongly against this idea (see **Section 4.7**). A previous study suggested to perform experiments involving AzF groups strictly under a red photographic light in order to avoid photolysis of the aryl-azide group, an experimental condition to consider when working with AzF (Chin et al., 2002b).

The strong divergence of GluA2 S729AzF kinetics, the known limitations of azide groups as photocrosslinkers, and the potential of BzF substitutions to be functionally silent, were crucial factors to concentrate exclusively on BzF for GluA2 receptor photoinactivation.

4.4 The degree of desensitization block at the GluA2 L483 site depended on the aromatic amino acid introduced

AMPA receptors are characterized by rapid and nearly-complete desensitization (Mayer & Vyklicky, 1989; Koike at al., 2000). This property can be easily modified by the introduction of aromatic residues at the GluA2 L483 site or by allosteric modulators such as CTZ (Sun et al., 2002). The block of desensitization develops hereby as a result of the D1–D1 interface stabilization within the LBD dimers. Since amino acids such as tyrosine or phenylalanine at the L483 site promote a distinctive block of desensitization, the introduction of aromatic UAAs such as AzF and BzF was expected to induce a similar effect. As expected, suppression of the L483 Amber codon by AzF and BzF within GluA2 resulted in a pronounced block of desensitization (**Figure 33**), verifying that the two UAAs induce comparable hydrophobic interactions with neighboring subunits to tyrosine or phenylalanine. The degree of block was hereby dependent on the UAA introduced, with BzF producing a larger block of desensitization (~76%) compared to AzF (~60%). In contrast to the two standard amino acids tyrosine and phenylalanine at the same

site, the block of desensitization was never complete. These results strongly argue for a specific incorporation of UAAs at the L483 Amber codon site and confirm that different aromatic side chains induce variable degrees of desensitization block, in relation to the strength of the produced cation-π-interactions, and in accordance to Sun et al. (2002).

4.5 UV-driven inactivation of GluA2 BzF mutants was characterized by a monoexponential peak current reduction

GluA2 receptors harboring BzF in D2 were irreversibly photoinactivated upon UV irradiation, which was characterized by a loss of peak current. All BzF mutants were UV-sensitive. Receptors with BzF-substitutions at the positions S729 and G725 could be inhibited in all functional states (resting, active, and desensitized state; **Figures 35 & 36**). Substitutions at the M721 and Y768 sites resulted in receptor trapping only in particular functional states (**Figure 39**). The rate of trapping could be controlled by varying the UV pulse conditions (**Figures 18 & 19**). Pausing the UV illumination also paused the peak current reduction and thus rundown as a cause of this effect could be eliminated (**Figure 18**). In comparison to the GluA2 Amber mutants harboring BzF, wild-type receptors expressed on the same background were not inactivated upon UV in any states tested, arguing for specificity of BzF-driven crosslinking and eliminating unspecific UV-induced effects. The peak current reduction in wild-type receptors upon 20 s of cumulative UV was only ~13%. It was never monoexponential and was most probably a cause of peak current run-down during long-lasting recordings.

The progress of peak current reduction following photoinactivation of GluA2 BzF mutants was invariably monoexponential, independently of the UV conditions used (**Figures 18, 35, 36**). One exponential component strongly suggests that a single crosslinking event, equivalent to the inactivation of one dimer within the receptor complex, is efficient enough to substantially inactivate the whole receptor. Since every subunit within the tetramer carried a BzF group within D2, four crosslinking reactions were theoretically possible. Given the single-exponential pattern of photoinactivation, subsequent BzF-crosslinking within the tetramer (*i*) could be silent (perhaps within subunits) due to the generation of a non-symmetric dimer arrangement; (*ii*) the non-symmetric arrangement upon inactivation of one dimer could provoke a structural geometry that prevents further crosslinking; or (*iii*) multiple UV-driven crosslinking events could occur

independently. If multiple forms of crosslinking occur, they should do so with the same rate, combining the different crosslinking events into a monoexponential sum. A single crosslink event that generates intersubunit trapping of adjacent subunits seems reasonable on the basis of previous disulfide crosslinking at the S729 and G725 sites (Armstrong et al., 2006; Plested & Mayer, 2009). Also, the biochemical results obtained in this study strongly indicate dimerization of subunits, at least for BzF at the S729 site (see also **Section 4.6**). AMPA receptors are known to adopt three different subconductance levels – small, medium, and large (Rosenmund et al., 1998). This mainly depends on the occupancy of agonist binding sites by glutamate within the receptor LBDs, resulting in higher conductances with more subunits activated. It should be noted, that receptors with two subunits active, have a low open probability and approximately 10% of the conductance of fully active channels, consistent with the ~10% residual activity of S729BzF or G725BzF homomeric mutant receptors following trapping.

Notably, the kinetic properties such as receptor desensitization and activation did not change over the period of photoinactivation with BzF at the S729 or G725 sites (**Figure 21**). AMPA receptors desensitize independently of their subunit occupancy (Robert & Howe, 2003), thus inactivation of one dimer within the receptor complex would still allow sufficient low-conductance activation followed by similar rates of desensitization. Although the rates of desensitization did not change upon exposures to UV, desensitization was not complete following photoinactivation of the GluA2 S729BzF mutant that developed a distinctive steady-state current. This effect strongly depended on the position of the introduced BzF group at the lower D2 lobes (**Figure 22**). The development of the steady-state current was less pronounced or absent with BzF substitutions placed more distal to the clamshell hinge (G725, M721), at positions where the photoactive ketone groups of BzF had to bridge a further distance in order to crosslink to the opposite D2 domain. All three mutants were inactivated by UV in the desensitized state to an extent of ~90%. The differences in their steady-state activation, however, suggest that the geometries following photoinactivation differ generating receptors with different open probabilities. The 6-fold increase in the steady-state level seen for the GluA2 S729 mutant implies inhibition and activation at the same time, a dual effect that would be interesting to investigate further. Also, it cannot be excluded that the big steady-state current seen for the GluA2 S729BzF mutant could arise from a trapped geometry, in which glutamate becomes a partial agonist, preventing complete desensitization. It remains to be tested if the rates of

deactivation and recovery from desensitization change upon exposures of UV, parameters that were difficult to obtain due to the given peak current reduction. Given the strong evidence that several desensitized states might exist also for AMPA receptors (Schauder et al., 2013), trapping of different receptor mutants could also occur at distinct time points during the process of desensitization, proceeding on a time scale not intangible in our experiments.

Last-mentioned, efficient trapping was only achieved with the UVICO lamp, which provided long UV pulses at a tens-of-milliseconds range. Pulses from the short-pulse lamp (SP-20; **Figure 24**) were too short and the illumination by a UV LED (*not shown*; see also **Section 3.4.7**) too dim to promote efficacious trapping on the timescale of the experiments. This observation suggests that abstraction of the hydrogen from nearby C–H bonds by BzF and following insertion (see also **Figure 5**) were inefficient at the S729 site within the short life time of the triplet excited state. Continuous exposures of UV 360 µs did not induce an insertion of BzF at position S729 into the neighbouring subunit – in contrast to the very fast abstraction by Bpa-MTS in the S4 segment of the Shaker potassium channel (Horn et al., 2000), but in common with similar sites in the sodium channel (Ding & Horn, 2001). Long and powerful UV exposures as provided by the UVICO lamp enabled saturation of the BzF excitation cycle, thus resulting in efficient receptor trapping.

4.6 UV-induced photocrosslinking of GluA2 S729 and G725 subunits in live cells

In order to confirm that UV irradiation produced intersubunit crosslinking within the GluA2 S729 and G725 Amber mutants, biochemical experiments were performed. This required several protocol optimization steps. Rescued monomeric GluA2 Amber mutant subunits were detected upon FLAG-tag purification (**Figure 26**). To minimize the dimeric fractions that derived from disulfide formations within the receptor, three cysteines were deleted (**Figure 26**; Lau et al., 2013), NEM was added to the lysis buffer to quench the remaining cysteine residues (**Figure 28**), and the protein samples were run under highly reducing conditions (**Figures 26 & 28**). Wild-type and Amber mutant receptors with three cysteine deletions showed kinetics indistinguishable from their cysteine-containing counterparts (**Figure 30**). The 3 x Cys (–) BzF mutants could also be inactivated with the same rates as receptors with non-modified cysteines, as shown exemplarily for the GuA2 S729 mutant. For both Amber mutants S729 and G725,

strong signals of rescued subunits (at ~100 kDa) were detected in cells that were incubated in a medium containing 1 mM BzF, and unspecific readthrough of the Amber codons in control experiments lacking the UAA was minimal (**Figures 26, 27, 29**). Thus, at least at position S729, incorporation of BzF by the exogenous tRNA was 10- to 20-fold more efficient than that of endogenous amino acids. Similar background levels were seen in other studies employing BzF to crosslink proteins in both bacterial and mammalian cells (Hino et al., 2005; Farrell et al., 2005). Irradiating live cells expressing GluA2 S729BzF with UV generated dimer bands (at ~240 kDa) in a time-dependent fashion, providing strong evidence that BzF groups can crosslink proteins covalently, as previously described for soluble proteins (Chin et al., 2002a; Chin & Schultz, 2002; Farrell et al., 2005; Hino et al., 2005; 2011; Sato et al., 2011). The efficiency of crosslinking was not large (15%). This could be due to several reasons: (*i*) The inhibition seen in functional experiments could be in part due to crosslinking onto neighboring subunits and in part due to intrasubunit recombination of BzF, which would tend to deplete the dimer fraction. As discussed in **Section 4.5**, a single BzF crosslinking event in a mature tetramer might drive a non-symmetric arrangement of the LBD layer, and thus further intrasubunit trapping cannot be fully excluded. This arrangement could also block further crosslinking between subunits, which would also contribute to the small dimer fraction. The situation in this study is analogous to that in some cysteine mutants, for which only two of the four subunits in a complex can crosslink, resulting in incomplete crosslinking (~30%; Lau et al., 2013). (*ii*) Trapping of immature intracellular forms of the receptor, such as dimers, could be further crosslinked by UV. However, for the overexpression intervals used here (72 h), dimers should represent at most a minor fraction of the GluA2 subunits in an entire cell (Shanks et al., 2010). (*iii*) The UV illumination in biochemical experiments was about 100-fold less intense than in electrophysiological recordings. This discrepancy almost certainly meant that crosslinking was incomplete. Trapping intervals longer than 30 minutes produced non-specific dimers in wild-type controls (*not shown*), possibly due to an increased cysteine dimerization from hypoxia or photodamage.

Surprisingly, no dimerization was detected for the GluA2 G725BzF mutant. It gave large glutamate-activated currents in electrophysiological recordings, equally to GluA2 S729BzF (**Section 3.3**). Also, its inactivation behaviour was indistinguishable from the S729BzF mutant (**Figures 18, 19, 35, 36**), and intersubunit crosslinking is also supported by the structural properties (**Figures 14, 22, 37**). The failure to detect dimer fractions of the GluA2 G725BzF

mutant could arise from the low-intensity UV source as described above. In general, the signal-to-noise properties in Western blotting might be too low to detect low levels of produced dimer fractions, which would also explain the missing dimerization for the GluA2 G725BzF mutant.
To improve the yields of rescued GluA2 Amber mutants for biochemical detection, developing alternative genetic targeting methods may help. Minimizing the number of co-transfected plasmids could be an effective approach. Several studies have increased protein expression by using gene clusters of tRNAs (Liu et al., 2007), by engineering vectors that co-express both the tRNA and the cognate synthetase (Wang et al., 2007; Kang et al., 2013; Zhu et al., 2014), or by creating stable cell lines that maintain expression of tRNA or synthetase variants (Sakamoto et al., 2002). Also, using a UV source with a stronger power might boost the dimerization fractions for biochemical detection.

4.7 GluA2 S729AzF mutants showed a “turn-on function” upon exposures of UV

In contrast to BzF at the GluA2 S729 site, incorporation of AzF at the same position failed to induce receptor photoinactivation in electrophysiological recordings. The use of AzF has a variety of limitations, as previously discussed (**Sections 1.2.4 & 4.3**). Given the unpredictable crosslinking pathway of azide groups and their basal effect on receptor desensitization in the absence of UV, the properties of GluA2 S729AzF mutant receptors upon application of UV were tested. Receptors exhibiting fast desensitization kinetics and stable peak current amplitudes were exposed to 12 s (or longer) of cumulative UV in the desensitized state. BzF at the same site and with UV applications during the same functional state produced a well-defined reduction of the peak current (**Figure 18**), indicative of receptor inactivation. Interestingly, S729AzF mutants showed opposed effects upon exposures of UV in the desensitized state. An increase of peak current amplitude was observed, accompanied by a change of desensitization kinetics (~8-fold decrease of the desensitization rate; **Figure 23**). The “turn-on effect” of AzF at the S729 site was further characterized by an immense increase (~3-fold) in the steady-state current, an activating effect that probably resulted from the change in the desensitization rate. With the diverse possibilities of azide groups to react in mind (**Figure 6**), these effects could occur for several reasons: (*i*) The change of the desensitization properties back to a wild-type-like level could be an indication of photodestruction of azide groups, thus altering hydrophobic interactions and

changing effects on receptor desensitization. The UV-driven slowing down of the desensitization rate automatically resulted in an increase in peak current amplitudes, a "turn-on function" that is not surprising, with less receptors within the outside-out patch being in the desensitized state at a given time. (*ii*) Azide groups can form expanded rings upon ambient daylight that very likely react with nucleophiles, another possible explanation for the observed effect. (*iii*) It cannot be fully excluded that an actual specific crosslink was promoted by UV, resulting in insertion into C–H or N–H bonds. However, this light-induced crosslink was silent in this case and did not have the ability to inhibit the receptor in an equal way as for BzF. (*iv*) If ambient daylight was sufficient enough to promote a physical crosslink and thus produced receptors with dramatically changed kinetics, UV could perturb this interaction. In this case, however, no further changes in kinetics should occur upon UV exposure, since azide groups are already recombined not giving any target to UV exposures.

Several studies have used AzF to successfully study protein-protein interactions, mainly due to its advantage of a shorter photoactive side chain compared to BzF (for example Chin et al., 2002b; Takimoto et al., 2009; Zhu et al., 2014). In the framework of this study, however, the limitations of using azide groups were apparent, disqualifying it as an effective crosslinker.

4.8 Receptors with endogenous amino acids at the D2 sites were insensitive to UV

GluA2 Amber mutant receptors incubated in the presence of BzF were invariably inactivated by UV in a monoexponential manner (**Figures 32 & 36**). Large glutamate-activated background currents in the absence of BzF in the cell culture medium for the GluA2 G725 Amber mutant were observed, a site-specific effect that was less pronounced for the S729 site (**Figure 32**). These currents probably derived from unspecific insertion of endogenous amino acids (see also **Figure 31** for the same condition). In contrast to receptors harbouring BzF groups at the G725 site, the unspecific receptor population was insensitive to UV exposures and a monoexponential inactivation was absent (**Figure 32**). Cumulative applications of UV (12 s) in the desensitized state produced a weak reduction in the peak current amplitude (~29% compared to the amplitude of the maximum response), which when fitted with an exponential decay had a time constant ~18-fold slower compared to receptors carrying BzF at the G725 site. The peak current reduction of receptors with unspecific insertions at their Amber codon sites was comparable to wild-type

receptors that were exposed to UV for similar cumulative intervals of UV (**Figure 36**). In general, outside-out patches pulled from cells expressing receptors carrying endogenous amino acids at the introduced stop codon sites, gave currents that were running down, and thus it remained challenging to perform long-lasting electrophysiological recordings. Despite the significant portion of unspecific insertion of endogenous amino acids at Amber codon sites in the absence of BzF, this result strongly confirms the specificity of UAA mutagenesis in AMPA receptors, when every component required is present.

The *Ec*RNA used in this study is aminoacylated by endogenous synthetases in the absence of the UAA as revealed for eGFP (see **Section 4.2**), and also was seen for GluA2 receptors (**Figure 32**). To get an idea about the nature of these endogenous amino acids non-specifically incorporated, the GluA2 L483 Amber mutant was used. Due to its origin deriving from a tyrosine-aminoacylating tRNA (Ye et al., 2008; 2009), it was assumed that the *Ec*RNA might also be unspecifically charged with tyrosine in the absence of the UAA. The produced L483 Amber mutant receptors gave background currents, which were on average equivalent to ~30% of the peak current amplitude obtained for BzF-containing receptors (**Figure 34**). As expected, all outside-out patches recorded from outside-out patches expressing the GluA2 L483 Amber mutant in the absence of BzF gave square current signals (**Figure 34**). Comparing the degree of inhibition of desensitization with the natural substitution mutant GluA2 L483Y, which gave with ~98% a nearly complete block of desensitization, the extent of the block for the L483 Amber mutant was smaller (~60%; **Figure 33**). This result indicates that a probably a mixture of aromatic amino acids is unspecifically incorporated at the D1 interface by the suppressor tRNA.

4.9 Photoinactivation of homomeric S279BzF and G725BzF GluA2 receptors showed only weak state dependence

Employing cysteine mutagenesis in order to study LBD movements during receptor gating provided an outstanding insight into the dynamics of the receptor (Armstrong et al., 2006; Plested & Mayer, 2009). The D2 lobes of the LBD undergo large structural rearrangements following activation by glutamate and different functional states could be trapped with disulfide bonds (Plested & Mayer, 2009). State dependence with cysteines at the GluA2 S729 site was pronounced with sustained inactivation of the receptor in the desensitized and resting state,

where the D2 lobes take positions, close enough for the cysteines to react. In the active state, however, the distance between the reactive side chains of the introduced cysteines was apparently too large to be bridged. Based on these previous results, state-dependent trapping was assessed after introduction of BzF groups at the S729 and G725 sites. For both mutants, application of UV resulted in a monoexponential reduction of the peak current, independently of the state in which the receptor received UV (**Figures 35 & 36**). Trapping of GluA2 subunits in the active state was for both mutants approximately 1.5-2 fold slower compared to receptor inactivation following UV application in the resting or desensitized state. This behavior is not surprising given the fact that the crosslinking chemistry of introduced BzF groups fundamentally differs from bridging cysteines: (*i*) The side chains of BzF are larger compared to those of cysteines, thus per se holding the potential to bridge larger distances; (*ii*) in contrast to cysteine mutagenesis, the reactive ketone groups of BzF do not react with each other, but rather have a large set of possible reaction partners (see **Section 1.2.4**). Both factors probably contributed to BzF crosslinking in all three functional states. Also, it cannot be excluded, that the BzF groups choose different reaction partners depending on the functional state of UV exposure. This could also explain the different extents of receptor inactivation seen for the different functional states tested, in particular for the GluA2 G725BzF mutant that undergoes larger distances for trapping. Here, UV exposure in the active state drove the inhibition of receptors by ~70% compared to the nearly full inhibition in the desensitized or resting states (~90%). In accordance to the previous study by Plested & Mayer (2009), the results presented here confirm that movements of the LBD lobes also occur in the resting state, in the absence of the agonist.

The use of the BzF photocrosslinker turned out to be a convenient strategy to study conformational changes following receptor activation (see also **Section 4.10**). Engineering of further BzF mutants within the D2 lobes and also at the D1 interface would sharpen the existing picture of the LBD movements during receptor gating.

4.10 State-dependent photoinactivation of the GluA2 Y768BzF and M721BzF mutants

Based on the hypothesis, that the different chemistry of disulfide bonds and BzF crosslinking, particularly, the greater length of the BzF side chain, compared to a cysteine, and its multiplicity of possible targets, underlies the lack of state dependence for the S729BzF and G725BzF

mutants, state dependence with BzF was expected more likely at sites, that move to greater extents. Incorporation of BzF at the M721 site resulted in efficient receptor photoinactivation in the desensitized state, whereas UV exposures within the active state did not induce any changes in the peak current amplitude (**Figure 39**). A further site within Helix K, Y768, showed a pronounced state-dependent receptor inactivation following UV, in inverse functional states compared to the M721BzF mutant (**Figure 39**). The state dependence observed in the Y768BzF and M721BzF mutants allows to map putative crosslinking events onto structural templates of functional states, with two caveats. (*i*) The exact geometry of BzF-trapping is unknown, given potential crosslinking sites in any of the four subunits in the complex, and (*ii*) precise models of the tetramer of LBDs in either the active or desensitized states are lacking. Inactivation of M721BzF mutant receptors was most efficient in the desensitized state, which is inconsistent with the putative desensitized dimer crystal structure (Armstrong et al., 2006). In this structure, the ketone radical cannot approach closer than 13 Å from the nearest backbone in the opposing subunit (**Figure 37**). Considering the fact that multiple desensitized states might exist also for AMPA receptors (Schauder et al., 2013), intersubunit crosslinking of subunits during this functional state could be possible. On the other hand, intrasubunit recombination of BzF groups cannot be fully excluded, since GluA2 M721BzF was relatively poor at inactivating heteromeric receptors (**Figure 42 & Section 4.11**). Also, no multimeric bands were detected in biochemical studies for the M721BzF mutant (**Figure 40**) that, however, could be due to low receptor expression levels.

In the desensitized dimer structure (Armstrong et al., 2006), the BzF side chain at position Y768 can be arranged so that the oxygen radical comes within 4 Å of the Cβ of Val666, with possibility of the necessary coplanarity (Dormán & Prestwich, 1994; **Figure 37**), but notably, functional crosslinking was negligible during receptor desensitization, suggesting that such an arrangement is not often obtained in the desensitized state. Crosslinking within subunits seems likely for Y768BzF, given that this mutant was potently and selectively photoinactivated in the active state, although the BzF side chain is poorly placed to reach neighboring subunits in this conformation (**Figure 37**), or the antagonist-bound crystal structure of the full-length receptor. The Y768BzF mutant expressed readily, but largely failed to dimerize in biochemical experiments, also with state-dependent treatment of the cell during the UV application (**Figure 40**). Therefore, state dependence likely arose from deformation of the lower lobe of the LBD

upon desensitization, reducing intrasubunit crosslinking for the 768BzF mutant, whilst increasing opportunities for M721BzF to recombine. Such a deformation, perhaps resembling movements of the lower lobe deduced from molecular dynamics simulations (Yao et al., 2013), might also explain the common regulation of gating and desensitization by spatially distinct point mutations in the lower lobe of the LBD (Carbone & Plested, 2012). Changes in D2 conformation are also expected if AMPA receptor LBDs must accommodate twisting (relative to the TMD) on the scale of that seen in kainate receptors (Schauder et al., 2013). Further screening of sites within lower lobe of iGluRs should help to resolve this picture.
Overall, these results confirm the feasibility of the method to investigate receptor structure and dynamis.

4.11 Photoinactivation of heteromeric GluA1/GluA2 receptors carrying BzF groups within the A2 subunits

The majority of AMPA receptors within a targeted cell could be inactivated within ~10 s, independent of their functional state. Given the monoexponential UV-driven inactivation of homomeric GluA2 receptors, it was reasoned that one produced crosslink by one of the four BzF groups within the receptor might be enough to silence the whole receptor. In consideration of this fact, similar single-exponential characteristics of photoinactivation were expected for heteromeric GluA2/GluA1 receptor complexes with only one of the subunits (GluA2) carrying the photoactive UAA. As expected, receptors incorporating naïve subunits were also inactivated with monoexponential time courses of peak current reduction upon exposures of UV. Hereby, the rates of inactivation for heteromeric GluA1/GluA2 S729BzF or GluA1/GluA2 G725BzF receptors were undistinguishable from those observed for heteromers (**Figure 41**). This observation is consistent with the assumption that the monoexponential behaviour of receptor inactivation is due to the silencing of one dimer pair. Heteromeric AMPA receptors dominated in these co-expression experiments, indicating that BzF-containing subunits are as well expressed as wild-type subunits. Heteromeric receptors with BzF at positions 725 or 729 in GluA2 showed a smaller peak current reduction than homomeric complexes. The possibility cannot be excluded that trapping induces a conformation in which glutamate remains a partial agonist, or that only the subunits containing BzF groups were inactivated through intrasubunit crosslinking. However,

photoinactivation did not change the IV relation (which depends on polyamine block and subunit composition), rendering unlikely the possibility that a subpopulation of receptors with a particular subunit stoichiometry is preferentially trapped. Partially inactivated receptors should activate with subconductance openings, which might be expected to show different block by polyamines. However, such an effect might be too small to detect and unravelling the responses of a mixture of receptors with distinct conductances, given that unmodified AMPA receptors also activate with subconductances (Carbone & Plested, 2012; Rosenmund et al., 1998), could prove challenging. UV exposures on heteromeric receptors harboring BzF at position M721 within the GluA2 subunit resulted in a poor inactivation (~30%) compared to the homomeric counterparts, which shows that intra-subunit recombination of BzF cannot be excluded. Biochemical experiments following photoinactivation by UV light would make a contribution into the understanding of the molecular process of crosslinking of heteromeric receptors.

5 FUTURE PERSPECTIVES – Possible applications of UAA mutagenesis

This study has proven that genetically encoded unnatural amino acid mutagenesis followed by UV-driven receptor inactivation is achievable in ligand-gated ion channels, and a range of applications are offered by this technique. A better understanding of the chemistry of BzF crosslinking, in particular the investigation of its reaction partners within the AMPA receptor, would provide a useful tool to identify interaction sites between proteins. A plausible approach to identify protein-protein interactions is the application of mass spectrometry. Various studies have applied this technique to confirm specific incorporation of AzF and BzF at Amber codon sites introduced to proteins (Chin et al., 2002b; Liu et al., 2007), and attempts were made to map UV-induced intra- and intermolecular crosslinks of AzF or BzF groups (Forné et al., 2012; Berg et al., 2014). However, these studies are still in the fledgling stages with major challenges such as large amounts of data due to multiple partner candidates of BzF during photocrosslinking to overcome. Once optimized, the nature of the produced crosslink could be used to identify protein-protein interaction sites between AMPA receptors and their auxiliary subunits, sites that are not identified up to now.

One major advantage of using UAAs in combination with UV activation is the insensitivity towards lipid buried sites, allowing optical control directly in the membrane. So far, the molecular dynamics of AMPA receptors during activation were mainly attacked from the receptor´s extracellular domains, namely its LBDs, by means of cysteine mutagenesis (Armstrong et al., 2006; Plested & Mayer, 2009; Lau et al., 2013). However, the characteristics of the membrane-spanning ion channel, in particular its nature of conformational changes during gating, remain unclear. Specific sites within the ion channel could be replaced by Amber stop codons for BzF similarly to LBD sites shown in this study. Distinct pore conformations and modulation of the spermine block during the different functional states can be studied upon exposures to UV. Also, as already mentioned, there is still a lack of knowledge regarding the interaction sites between AMPA receptors with their modulatory proteins, which exert control over channel gating. The definition of the molecular structure of these interaction sites would

contribute to fundamental understanding of the functioning of glutamate receptors during the activation pathway.

A further major application of BzF crosslinking is the inactivation of native receptors. Several methods have been used to inactivate glutamate receptors *in* vivo (including RNAi and ANQX; Adesnik et al., 2005; Tracy et al., 2011). Despite notable advantages (for example, targeting exclusively surface receptors, in the case of ANQX), these methods either lack cellular specificity, or develop slowly (over hours or days). The majority of AMPA receptors within a targeted cell could be inactivated within ~10 s, independent of their functional state. Receptors incorporating naïve subunits were also inactivated, so overexpression of one BzF-containing subtype could target native heteromultimeric channels on a wild-type background, complementing "molecular replacement" approaches (Granger et al., 2012).
The possible applications of unnatural amino acid mutagenesis mentioned could provide novel insights into iGluR ion channel functioning and their interaction with auxiliary subunits, with implications for the activity of native channels.

Bibliography

Adesnik, H., Nicoll, R.A., and England, P.M. (2005). Photoinactivation of native AMPA receptors reveals their real-time trafficking. Neuron *48*, 977-985.

Agard, N.J., Prescher, J.A., and Bertozzi, C.R. (2004). A strain-promoted [3+2] azide-alkyne cycloaddition for covalent modification of biomolecules in living systems. Journal of the American Chemical Society *126*, 15046-15047.

Aiyar, A., Xiang, Y., and Leis, J. (1996). Site-directed mutagenesis using overlap extension PCR. Methods in molecular biology *57*, 177-191.

Al Rahim, M., and Hossain, M.A. (2013). Genetic deletion of NP1 prevents hypoxic-ischemic neuronal death via reducing AMPA receptor synaptic localization in hippocampal neurons. Journal of the American Heart Association *2*, e006098.

Alt, A., Nisenbaum, E.S., Bleakman, D., and Witkin, J.M. (2006). A role for AMPA receptors in mood disorders. Biochemical pharmacology *71*, 1273-1288.

Ambrogelly, A., Palioura, S., and Soll, D. (2007). Natural expansion of the genetic code. Nature chemical biology *3*, 29-35.

Anggono, V., and Huganir, R.L. (2012). Regulation of AMPA receptor trafficking and synaptic plasticity. Current opinion in neurobiology *22*, 461-469.

Araki, K., Meguro, H., Kushiya, E., Takayama, C., Inoue, Y., and Mishina, M. (1993). Selective expression of the glutamate receptor channel delta 2 subunit in cerebellar Purkinje cells. Biochemical and biophysical research communications *197*, 1267-1276.

Armstrong, N., and Gouaux, E. (2000). Mechanisms for activation and antagonism of an AMPA-sensitive glutamate receptor: crystal structures of the GluR2 ligand binding core. Neuron *28*, 165-181.

Armstrong, N., Jasti, J., Beich-Frandsen, M., and Gouaux, E. (2006). Measurement of conformational changes accompanying desensitization in an ionotropic glutamate receptor. Cell *127*, 85-97.

Armstrong, N., Sun, Y., Chen, G.Q., and Gouaux, E. (1998). Structure of a glutamate-receptor ligand-binding core in complex with kainate. Nature *395*, 913-917.

Ayalon, G., Segev, E., Elgavish, S., and Stern-Bach, Y. (2005). Two regions in the N-terminal domain of ionotropic glutamate receptor 3 form the subunit oligomerization interfaces that

control subtype-specific receptor assembly. The Journal of biological chemistry *280*, 15053-15060.

Ayalon, G., and Stern-Bach, Y. (2001). Functional assembly of AMPA and kainate receptors is mediated by several discrete protein-protein interactions. Neuron *31*, 103-113.

Bahring, R., Bowie, D., Benveniste, M., and Mayer, M.L. (1997). Permeation and block of rat GluR6 glutamate receptor channels by internal and external polyamines. The Journal of physiology *502 (Pt 3)*, 575-589.

Beene, D.L., Brandt, G.S., Zhong, W., Zacharias, N.M., Lester, H.A., and Dougherty, D.A. (2002). Cation-pi interactions in ligand recognition by serotonergic (5-HT3A) and nicotinic acetylcholine receptors: the anomalous binding properties of nicotine. Biochemistry *41*, 10262-10269.

Beene, D.L., Dougherty, D.A., and Lester, H.A. (2003). Unnatural amino acid mutagenesis in mapping ion channel function. Current opinion in neurobiology *13*, 264-270.

Beene, D.L., Price, K.L., Lester, H.A., Dougherty, D.A., and Lummis, S.C. (2004). Tyrosine residues that control binding and gating in the 5-hydroxytryptamine3 receptor revealed by unnatural amino acid mutagenesis. The Journal of neuroscience : the official journal of the Society for Neuroscience *24*, 9097-9104.

Bellone, C., and Luescher, C. (2006). Cocaine triggered AMPA receptor redistribution is reversed in vivo by mGluR-dependent long-term depression. Nature neuroscience *9*, 636-641.

Berg, M., Michalowski, A., Palzer, S., Rupp, S., and Sohn, K. (2014). An in vivo photo-cross-linking approach reveals a homodimerization domain of Aha1 in S. cerevisiae. PloS one *9*, e89436.

Bianco, A., Townsley, F.M., Greiss, S., Lang, K., and Chin, J.W. (2012). Expanding the genetic code of Drosophila melanogaster. Nature chemical biology *8*, 748-750.

Boulter, J., Hollmann, M., O'Shea-Greenfield, A., Hartley, M., Deneris, E., Maron, C., and Heinemann, S. (1990). Molecular cloning and functional expression of glutamate receptor subunit genes. Science *249*, 1033-1037.

Bowers, M.S., Chen, B.T., and Bonci, A. (2010). AMPA receptor synaptic plasticity induced by psychostimulants: the past, present, and therapeutic future. Neuron *67*, 11-24.

Bowie, D., and Mayer, M.L. (1995). Inward rectification of both AMPA and kainate subtype glutamate receptors generated by polyamine-mediated ion channel block. Neuron *15*, 453-456.

Bowie, D. (2002). External anions and cations distinguish between AMPA and kainate receptor gating mechanisms. The Journal of physiology *539*, 725-733.

Bradford, M.M. (1976). A rapid and sensitive method for the quantitation of microgram quantities of protein utilizing the principle of protein-dye binding. Analytical biochemistry *72*, 248-254.

Burnashev, N., Monyer, H., Seeburg, P.H., and Sakmann, B. (1992). Divalent ion permeability of AMPA receptor channels is dominated by the edited form of a single subunit. Neuron *8*, 189-198.

Butterfield, D.A., and Pocernich, C.B. (2003). The glutamatergic system and Alzheimer's disease: therapeutic implications. CNS drugs *17*, 641-652.

Carbone, A.L., and Plested, A.J. (2012). Coupled control of desensitization and gating by the ligand binding domain of glutamate receptors. Neuron *74*, 845-857.

Chang, Y., and Weiss, D.S. (2002). Site-specific fluorescence reveals distinct structural changes with GABA receptor activation and antagonism. Nature neuroscience *5*, 1163-1168.

Chen, L., Chetkovich, D.M., Petralia, R.S., Sweeney, N.T., Kawasaki, Y., Wenthold, R.J., Bredt, D.S., and Nicoll, R.A. (2000). Stargazin regulates synaptic targeting of AMPA receptors by two distinct mechanisms. Nature *408*, 936-943.

Chen, P.R., Groff, D., Guo, J., Ou, W., Cellitti, S., Geierstanger, B.H., and Schultz, P.G. (2009). A facile system for encoding unnatural amino acids in mammalian cells. Angewandte Chemie *48*, 4052-4055.

Chin, J.W. (2014). Expanding and Reprogramming the Genetic Code of Cells and Animals. Annual review of biochemistry.

Chin, J.W., Cropp, T.A., Anderson, J.C., Mukherji, M., Zhang, Z., and Schultz, P.G. (2003a). An expanded eukaryotic genetic code. Science *301*, 964-967.

Chin, J.W., Cropp, T.A., Chu, S., Meggers, E., and Schultz, P.G. (2003b). Progress toward an expanded eukaryotic genetic code. Chem Biol *10*, 511-519.

Chin, J.W., Martin, A.B., King, D.S., Wang, L., and Schultz, P.G. (2002a). Addition of a photocrosslinking amino acid to the genetic code of Escherichia coli. Proceedings of the National Academy of Sciences of the United States of America *99*, 11020-11024.

Chin, J.W., Santoro, S.W., Martin, A.B., King, D.S., Wang, L., and Schultz, P.G. (2002b). Addition of p-azido-L-phenylalanine to the genetic code of Escherichia coli. Journal of the American Chemical Society *124*, 9026-9027.

Chin, J.W., and Schultz, P.G. (2002). In vivo photocrosslinking with unnatural amino acid mutagenesis. Chembiochem: a European journal of chemical biology *3*, 1135-1137.

Choi, D.W., and Rothman, S.M. (1990). The role of glutamate neurotoxicity in hypoxic-ischemic neuronal death. Annu Rev Neurosci *13*, 171-182.

Christensen, J.K., Paternain, A.V., Selak, S., Ahring, P.K., and Lerma, J. (2004). A mosaic of functional kainate receptors in hippocampal interneurons. The Journal of neuroscience: the official journal of the Society for Neuroscience *24*, 8986-8993.

Christie, L.A., Russell, T.A., Xu, J., Wood, L., Shepherd, G.M., and Contractor, A. (2010). AMPA receptor desensitization mutation results in severe developmental phenotypes and early postnatal lethality. Proceedings of the National Academy of Sciences of the United States of America *107*, 9412-9417.

Clayton, A., Siebold, C., Gilbert, R.J., Sutton, G.C., Harlos, K., McIlhinney, R.A., Jones, E.Y., and Aricescu, A.R. (2009). Crystal structure of the GluR2 amino-terminal domain provides insights into the architecture and assembly of ionotropic glutamate receptors. Journal of molecular biology *392*, 1125-1132.

Coin, I., Perrin, M.H., Vale, W.W., and Wang, L. (2011). Photo-cross-linkers incorporated into G-protein-coupled receptors in mammalian cells: a ligand comparison. Angewandte Chemie *50*, 8077-8081.

Coleman, S.K., Moykkynen, T., Cai, C., von Ossowski, L., Kuismanen, E., Korpi, E.R., and Keinanen, K. (2006). Isoform-specific early trafficking of AMPA receptor flip and flop variants. The Journal of neuroscience: the official journal of the Society for Neuroscience *26*, 11220-11229.

Collingridge, G.L., and Lester, R.A. (1989). Excitatory amino acid receptors in the vertebrate central nervous system. Pharmacological reviews *41*, 143-210.

Colquhoun, D., Jonas, P., and Sakmann, B. (1992). Action of brief pulses of glutamate on AMPA/kainate receptors in patches from different neurones of rat hippocampal slices. The Journal of physiology *458*, 261-287.

Cornish, V.W., Benson, D.R., Altenbach, C.A., Hideg, K., Hubbell, W.L., and Schultz, P.G. (1994). Site-specific incorporation of biophysical probes into proteins. Proceedings of the National Academy of Sciences of the United States of America *91*, 2910-2914.

Das, U., Kumar, J., Mayer, M.L., and Plested, A.J. (2010). Domain organization and function in GluK2 subtype kainate receptors. Proceedings of the National Academy of Sciences of the United States of America *107*, 8463-8468.

Davis, L., and Chin, J.W. (2012). Designer proteins: applications of genetic code expansion in cell biology. Nature reviews. Molecular cell biology *13*, 168-182.

Dedkova, L.M., Fahmi, N.E., Golovine, S.Y., and Hecht, S.M. (2003). Enhanced D-amino acid incorporation into protein by modified ribosomes. Journal of the American Chemical Society *125*, 6616-6617.

DiGregorio, D.A., Rothman, J.S., Nielsen, T.A., and Silver, R.A. (2007). Desensitization properties of AMPA receptors at the cerebellar mossy fiber granule cell synapse. The Journal of neuroscience: the official journal of the Society for Neuroscience *27*, 8344-8357.

Ding, S, and Horn, R. (2001). Slow photo-cross-linking kinetics of benzophenone-labeled voltage sensors of ion channels. Biochemistry *40*, 10707-10716.

Dingledine, R., Borges, K., Bowie, D., and Traynelis, S.F. (1999). The glutamate receptor ion channels. Pharmacological reviews *51*, 7-61.

Dormán, G., and Prestwich, G.D. (1994). Benzophenone photophores in biochemistry. Biochemistry *33*, 5661-5673.

Dougherty, D.A. (2000). Unnatural amino acids as probes of protein structure and function. Current opinion in chemical biology *4*, 645-652.

Drees, B.L. (1999). Progress and variations in two-hybrid and three-hybrid technologies. Current opinion in chemical biology *3*, 64-70.

Edwards, H., and Schimmel, P. (1990). A bacterial amber suppressor in Saccharomyces cerevisiae is selectively recognized by a bacterial aminoacyl-tRNA synthetase. Molecular and cellular biology *10*, 1633-1641.

Edwards, H., Trezeguet, V., and Schimmel, P. (1991). An Escherichia coli tyrosine transfer RNA is a leucine-specific transfer RNA in the yeast Saccharomyces cerevisiae. Proceedings of the National Academy of Sciences of the United States of America *88*, 1153-1156.

Ellman, J., Mendel, D., Anthony-Cahill, S., Noren, C.J., and Schultz, P.G. (1991). Biosynthetic method for introducing unnatural amino acids site-specifically into proteins. Methods in enzymology *202*, 301-336.

England, P.M. (2004). Unnatural amino acid mutagenesis: a precise tool for probing protein structure and function. Biochemistry *43*, 11623-11629.

England, P.M., Lester, H.A., Davidson, N., and Dougherty, D.A. (1997). Site-specific, photochemical proteolysis applied to ion channels in vivo. Proceedings of the National Academy of Sciences of the United States of America *94*, 11025-11030.

Erdmann, A., Edmann, U., Martens, A., Müller, O., and Paul., A. (2005). Neurobiology, Westermann Druck GmbH Braunschweig, Germany, *page 26 ff.*

Escher, E., and Schwyzer, R. (1974). p-Nitrophenylalanine, p-azidophenylalanine, m-azidophenylalanine, and o-nitro-p-azido-phenylalanine as photoaffinity labels. FEBS letters *46*, 347-350.

Fagegaltier, D., Hubert, N., Yamada, K., Mizutani, T., Carbon, P., and Krol, A. (2000). Characterization of mSelB, a novel mammalian elongation factor for selenoprotein translation. The EMBO journal *19*, 4796-4805.

Farrell, I.S., Toroney, R., Hazen, J.L., Mehl, R.A., and Chin, J.W. (2005). Photo-cross-linking interacting proteins with a genetically encoded benzophenone. Nature methods *2*, 377-384.

Fields, S., and Song, O. (1989). A novel genetic system to detect protein-protein interactions. Nature *340*, 245-246.

Forné, I., Ludwigsen, J., Imhof, A., Becker, P.B., and Mueller-Planitz, F. (2012). Probing the conformation of the ISWI ATPase domain with genetically encoded photoreactive crosslinkers and mass spectrometry. Molecular and cellular proteomics *11*, M111.012088.

Furukawa, H., Singh, S.K., Mancusso, R., and Gouaux, E. (2005). Subunit arrangement and function in NMDA receptors. Nature *438*, 185-192.

Galardy, R.E., Craig, L.C., and Printz, M.P. (1973). Benzophenone triplet: a new photochemical probe of biological ligand-receptor interactions. Nature: New biology *242*, 127-128.

Gallivan, J.P., and Dougherty, D.A. (1999). Cation-π interactions in structural biology. Proceedings of the National Academy of Sciences of the United States of America *96*, 9459-9464.

Garcia, G., 3rd, Chiara, D.C., Nirthanan, S., Hamouda, A.K., Stewart, D.S., and Cohen, J.B. (2007). [3H]Benzophenone photolabeling identifies state-dependent changes in nicotinic acetylcholine receptor structure. Biochemistry *46*, 10296-10307.

Gautier, A., Nguyen, D.P., Lusic, H., An, W., Deiters, A., and Chin, J.W. (2010). Genetically encoded photocontrol of protein localization in mammalian cells. Journal of the American Chemical Society *132*, 4086-4088.

Granger, A.J., Shi, Y., Lu, W., Cerpas., M., and Nicoll, R.A. (2013). LTP requires a reserve pool of glutamate receptors independent of subunit type. Nature *493*, 495-500.

Greger, I.H., Khatri, L., Kong, X., and Ziff, E.B. (2003). AMPA receptor tetramerization is mediated by Q/R editing. Neuron *40*, 763-774.

Greger, I.H., Khatri, L., and Ziff, E.B. (2002). RNA editing at arg607 controls AMPA receptor exit from the endoplasmic reticulum. Neuron *34*, 759-772.

Greiss, S., and Chin, J.W. (2011). Expanding the genetic code of an animal. Journal of the American Chemical Society *133*, 14196-14199.

Groff, D., Chen, P.R., Peters, F.B., and Schultz, P.G. (2010). A genetically encoded epsilon-N-methyl lysine in mammalian cells. Chembiochem: a European journal of chemical biology *11*, 1066-1068.

Grunbeck, A., Huber, T., Abrol, R., Trzaskowski, B., Goddard, W.A., 3rd, and Sakmar, T.P. (2012). Genetically encoded photo-cross-linkers map the binding site of an allosteric drug on a G protein-coupled receptor. ACS chemical biology *7*, 967-972.

Grunbeck, A., Huber, T., Sachdev, P., and Sakmar, T.P. (2011). Mapping the ligand-binding site on a G protein-coupled receptor (GPCR) using genetically encoded photocrosslinkers. Biochemistry *50*, 3411-3413.

Hamill, O.P., Marty, A., Neher, E., Sakmann, B., and Sigworth, F.J. (1981). Improved patch-clamp techniques for high-resolution current recording from cells and cell-free membrane patches. Pflugers Archiv: European journal of physiology *391*, 85-100.

Hardingham, G.E., Fukunaga, Y., and Bading, H. (2002). Extrasynaptic NMDARs oppose synaptic NMDARs by triggering CREB shut-off and cell death pathways. Nature neuroscience *5*, 405-414.

Hino, N., Hayashi, A., Sakamoto, K., and Yokoyama, S. (2006). Site-specific incorporation of non-natural amino acids into proteins in mammalian cells with an expanded genetic code. Nature protocols *1*, 2957-2962.

Hino, N., Okazaki, Y., Kobayashi, T., Hayashi, A., Sakamoto, K., and Yokoyama, S. (2005). Protein photo-cross-linking in mammalian cells by site-specific incorporation of a photoreactive amino acid. Nature methods *2*, 201-206.

Hino, N., Oyama, M., Sato, A., Mukai, T., Iraha, F., Hayashi, A., Kozuka-Hata, H., Yamamoto, T., Yokoyama, S., and Sakamoto, K. (2011). Genetic incorporation of a photo-crosslinkable amino acid reveals novel protein complexes with GRB2 in mammalian cells. Journal of molecular biology *406*, 343-353.

Hjelmstad, G.O., Isaac, J.T., Nicoll, R.A., and Malenka, R.C. (1999). Lack of AMPA receptor desensitization during basal synaptic transmission in the hippocampal slice. Journal of neurophysiology *81*, 3096-3099.

Hollmann, M., Hartley, M., and Heinemann, S. (1991). Ca2+ permeability of KA-AMPA--gated glutamate receptor channels depends on subunit composition. Science *252*, 851-853.

Hollmann, M., and Heinemann, S. (1994). Cloned glutamate receptors. Annu Rev Neurosci *17*, 31-108.

Hollmann, M., O'Shea-Greenfield, A., Rogers, S.W., and Heinemann, S. (1989). Cloning by functional expression of a member of the glutamate receptor family. Nature *342*, 643-648.

Horn, R., Ding, S., Gruber, H.J. (2000). Immobilizing the moving parts of voltage-gated ion channels. The Journal of general physiology *116*, 461-476.

Huang, L.Y., Umanah, G., Hauser, M., Son, C., Arshava, B., Naider, F., and Becker, J.M. (2008). Unnatural amino acid replacement in a yeast G protein-coupled receptor in its native environment. Biochemistry *47*, 5638-5648.

Huber, T., Naganathan, S., Tian, H., Ye, S., and Sakmar, T.P. (2013). Unnatural amino acid mutagenesis of GPCRs using amber codon suppression and bioorthogonal labeling. Methods in enzymology *520*, 281-305.

Jin, R., Banke, T.G., Mayer, M.L., Traynelis, S.F., and Gouaux, E. (2003). Structural basis for partial agonist action at ionotropic glutamate receptors. Nature neuroscience *6*, 803-810.

Jin, R., Horning, M., Mayer, M.L., and Gouaux, E. (2002). Mechanism of activation and selectivity in a ligand-gated ion channel: structural and functional studies of GluR2 and quisqualate. Biochemistry *41*, 15635-15643.

Jin, R., Singh, S.K., Gu, S., Furukawa, H., Sobolevsky, A.I., Zhou, J., Jin, Y., and Gouaux, E. (2009). Crystal structure and association behaviour of the GluR2 amino-terminal domain. The EMBO journal *28*, 1812-1823.

Johnston, M.V., Trescher, W.H., Ishida, A., and Nakajima, W. (2001). Neurobiology of hypoxic-ischemic injury in the developing brain. Pediatric research *49*, 735-741.

Jones, M.V., and Westbrook, G.L. (1996). The impact of receptor desensitization on fast synaptic transmission. Trends in neurosciences *19*, 96-101.

Kang, J.Y., Kawaguchi. D., Coin, I., Xiang, Z., O`Leary, D.D., Slesinger, P.A., and Wang, L. (2013). In vivo expression of a light-activatable potassium channel using unnatural amino acids. Neuron *80*, 358-370.

Kauer, J.C., Erickson-Viitanen, S., Wolfe, H.R.Jr., and DeGrado, W.F. (1986). p-Benzoyl-L-phenylalanine, a new photoreactive amino acid. Photolabeling of calmodulin with a synthetic calmodulin-binding peptide.The Journal of biological chemistry *261*, 10695-10700.

Keana, J.F.W., and Cai, S.X. (1990). New Reagents for Photoaffinity Labeling: Synthesis and photolysis of functionalized perfluorophenyl azides. Journal of organic chemistry *55*, 3640-3647.

Kearney, P.C., Zhang, H., Zhong, W., Dougherty, D.A., and Lester, H.A. (1996). Determinants of nicotinic receptor gating in natural and unnatural side chain structures at the M2 9' position. Neuron *17*, 1221-1229.

Keinänen, K., Wisden, W., Sommer, B., Werner, P., Herb, A., Verdoorn, T.A., Sakmann, B., and Seeburg, P.H. (1990). A family of AMPA-selective glutamate receptors. Science *249*, 556-560.

Kiick, K.L., Saxon, E., Tirrell, D.A., and Bertozzi, C.R. (2002). Incorporation of azides into recombinant proteins for chemoselective modification by the Staudinger ligation. Proceedings of the National Academy of Sciences of the United States of America *99*, 19-24.

Kirshenbaum, K., Carrico, I.S., and Tirrell, D.A. (2002). Biosynthesis of proteins incorporating a versatile set of phenylalanine analogues. Chembiochem: a European journal of chemical biology *3*, 235-237.

Kiskin, N.I., Krishtal, O.A., and Tsyndrenko, A. (1986). Excitatory amino acid receptors in hippocampal neurons: kainate fails to desensitize them. Neuroscience letters *63*, 225-230.

Klippenstein, V., Ghisi, V., Wietstruk, M., and Plested, A.J. (2014). Photoinactivation of glutamate receptors by genetically encoded unnatural amino acids. The Journal of neuroscience: the official journal of the Society for Neuroscience *34*, 980-991.

Knowles, J.R. (1972). Photogenerated reagents for biological receptor-site labeling. Accounts of chemical research *5*, 155-160.

Koh, D.S., Burnashev, N., and Jonas, P. (1995). Block of native Ca(2+)-permeable AMPA receptors in rat brain by intracellular polyamines generates double rectification. The Journal of physiology *486 (Pt 2)*, 305-312.

Koike, M., Tsukada, S., Tsuzuki, K., Kijima, H., and Ozawa, S. (2000). Regulation of kinetic properties of GluR2 AMPA receptor channels by alternative splicing. The Journal of neuroscience: the official journal of the Society for Neuroscience *15*, 2166-2174.

Kolb, H.C., and Sharpless, K.B (2003). The growing impact of click chemistry on drug discovery. Drug discovery today *8*, 1128-1137.

Kozak, M. (2005). Regulation of translation via mRNA structure in prokaryotes and eukaryotes. Gene *361*, 13-37.

Kuner, T., Seeburg, P.H., and Guy, H.R. (2003). A common architecture for K+ channels and ionotropic glutamate receptors? Trends in neurosciences *26*, 27-32.

Kurose, T., Pashmforoush, M., Yoshimasa, Y., Carroll, R., Schwartz, G.P., Burke, G.T., Katsoyannis, P.G., and Steiner, D.F. (1994). Cross-linking of a B25 azidophenylalanine insulin derivative to the carboxyl-terminal region of the alpha-subunit of the insulin receptor. Identification of a new insulin-binding domain in the insulin receptor. The Journal of biological chemistry *269*, 29190-29197.

Kuusinen, A., Abele, R., Madden, D.R., and Keinanen, K. (1999). Oligomerization and ligand-binding properties of the ectodomain of the alpha-amino-3-hydroxy-5-methyl-4-isoxazole propionic acid receptor subunit GluRD. The Journal of biological chemistry *274*, 28937-28943.

Lang, K., Davis, L., Torres-Kolbus, J., Chou, C., Deiters, A., and Chin, J.W. (2012). Genetically encoded norbornene directs site-specific cellular protein labelling via a rapid bioorthogonal reaction. Nature chemistry *4*, 298-304.

Lau, A.Y., and Roux, B. (2011). The hidden energetics of ligand binding and activation in a glutamate receptor. Nature structural & molecular biology *18*, 283-287.

Lau, A.Y., Salazar, H., Blachowicz, L., Ghisi, V., Plested, A.J., and Roux, B. (2013). A conformational intermediate in glutamate receptor activation. Neuron *79*, 492-503.

Laube, B., Kuhse, J., and Betz, H. (1998). Evidence for a tetrameric structure of recombinant NMDA receptors. The Journal of neuroscience: the official journal of the Society for Neuroscience *18*, 2954-2961.

Lee, H.S., Guo, J., Lemke, E.A., Dimla, R.D., and Schultz, P.G. (2009). Genetic incorporation of a small, environmentally sensitive, fluorescent probe into proteins in Saccharomyces cerevisiae. Journal of the American Chemical Society *131*, 12921-12923.

Leveille, F., El Gaamouch, F., Gouix, E., Lecocq, M., Lobner, D., Nicole, O., and Buisson, A. (2008). Neuronal viability is controlled by a functional relation between synaptic and

extrasynaptic NMDA receptors. FASEB journal: official publication of the Federation of American Societies for Experimental Biology *22*, 4258-4271.

Li, F., Xiong, Y., Wang, J., Cho, H.D., Tomita, K., Weiner, A.M., and Steitz, T.A. (2002). Crystal structures of the Bacillus stearothermophilus CCA-adding enzyme and its complexes with ATP or CTP. Cell *111*, 815-824.

Li, L., Zhong, W., Zacharias, N., Gibbs, C., Lester, H.A., and Dougherty, D.A. (2001). The tethered agonist approach to mapping ion channel proteins--toward a structural model for the agonist binding site of the nicotinic acetylcholine receptor. Chem Biol *8*, 47-58.

Li, Q., Zhang, Y., Sheng, Y., Huo, R., Sun, B., Teng, X., Li, N., Zhu, J.X., Yang, B.F., and Dong, D.L. (2012). Large T-antigen up-regulates Kv4.3 K(+) channels through Sp1, and Kv4.3 K(+) channels contribute to cell apoptosis and necrosis through activation of calcium/calmodulin-dependent protein kinase II. The Biochemical journal *441*, 859-867.

Liu, C.C., and Schultz, P.G. (2010). Adding new chemistries to the genetic code. Annual review of biochemistry *79*, 413-444.

Liu, D.R., and Schultz, P.G. (1999). Progress toward the evolution of an organism with an expanded genetic code. Proceedings of the National Academy of Sciences of the United States of America *96*, 4780-4785.

Liu, W., Brock, A., Chen, S., Chen, S., and Schultz, P.G. (2007). Genetic incorporation of unnatural amino acids into proteins in mammalian cells. Nature methods *4*, 239-244.

Loh, P.G., and Song, H. (2010). Structural and mechanistic insights into translation termination. Current opinion in structural biology *20*, 98-103.

Lomeli, H., Sprengel, R., Laurie, D.J., Kohr, G., Herb, A., Seeburg, P.H., and Wisden, W. (1993). The rat delta-1 and delta-2 subunits extend the excitatory amino acid receptor family. FEBS letters *315*, 318-322.

Longstaff, D.G., Larue, R.C., Faust, J.E., Mahapatra, A., Zhang, L., Green-Church, K.B., and Krzycki, J.A. (2007). A natural genetic code expansion cassette enables transmissible biosynthesis and genetic encoding of pyrrolysine. Proceedings of the National Academy of Sciences of the United States of America *104*, 1021-1026.

Lu, W., Shi, Y., Jackson, A.C., Bjorgan, K., During, M.J., Sprengel, R., Seeburg, P.H., and Nicoll, R.A. (2009). Subunit composition of synaptic AMPA receptors revealed by a single-cell genetic approach. Neuron *62*, 254-268.

Lummis, S.C., Beene, D.L., Lee, L.W., Lester, H.A., Broadhurst, R.W., and Dougherty, D.A. (2005a). Cis-trans isomerization at a proline opens the pore of a neurotransmitter-gated ion channel. Nature *438*, 248-252.

Lummis, S.C., D, L.B., Harrison, N.J., Lester, H.A., and Dougherty, D.A. (2005b). A cation-pi binding interaction with a tyrosine in the binding site of the GABAC receptor. Chem Biol *12*, 993-997.

Lummis, S.C., Harrison, N.J., Wang, J., Ashby, J.A., Millen, K.S., Beene, D.L., and Dougherty, D.A. (2012). Multiple Tyrosine Residues Contribute to GABA Binding in the GABA(C) Receptor Binding Pocket. ACS chemical neuroscience *3*, 186-192.

Lummis, S.C., McGonigle, I., Ashby, J.A., and Dougherty, D.A. (2011). Two amino acid residues contribute to a cation-pi binding interaction in the binding site of an insect GABA receptor. The Journal of neuroscience: the official journal of the Society for Neuroscience *31*, 12371-12376.

MacBeath, G. (2002). Protein microarrays and proteomics. Nature genetics *32 Suppl*, 526-532.

Malinow, R., and Malenka, R.C. (2002). Ampa Receptor trafficking And synaptic plasticity. Annual Review of Neuroscience *25*, 103-126.

Mayer, M.L., and Armstrong, N. (2004). Structure and function of glutamate receptor ion channels. Annual review of physiology *66*, 161-181.

Mayer, M.L., and Vyklicky, L., Jr. (1989). Concanavalin A selectively reduces desensitization of mammalian neuronal quisqualate receptors. Proceedings of the National Academy of Sciences of the United States of America *86*, 1411-1415.

Meguro, H., Mori, H., Araki, K., Kushiya, E., Kutsuwada, T., Yamazaki, M., Kumanishi, T., Arakawa, M., Sakimura, K., and Mishina, M. (1992). Functional characterization of a heteromeric NMDA receptor channel expressed from cloned cDNAs. Nature *357*, 70-74.

Menniti, F.S., Lindsley, C.W., Conn, P.J., Pandit, J., Zagouras, P., and Volkmann, R.A. (2013). Allosteric modulators for the treatment of schizophrenia: targeting glutamatergic networks. Current topics in medicinal chemistry *13*, 26-54.

Miller, W.T., and Kaiser, E.T. (1988). Probing the peptide binding site of the cAMP-dependent protein kinase by using a peptide-based photoaffinity label. Proceedings of the National Academy of Sciences of the United States of America *85*, 5429-5433.

Miller, J.C., Silverman, S.K., England, P.M., Dougherty, D.A., and Lester, H.A. (1998). Flash decaging of tyrosine sidechains in an ion channel. Neuron *20*, 619-624.

Milstein, A.D., Zhou, W., Karimzadegan, S., Bredt, D.S., and Nicoll, R.A. (2007). TARP subtypes differentially and dose-dependently control synaptic AMPA receptor gating. Neuron *55*, 905-918.

Moens, U., Seternes, O.M., Johansen, B., and Rekvig, O.P. (1997). Mechanisms of transcriptional regulation of cellular genes by SV40 large T- and small T-antigens. Virus genes *15*, 135-154.

Mori, H., and Ito, K. (2006). Different modes of SecY-SecA interactions revealed by site-directed in vivo photo-cross-linking. Proceedings of the National Academy of Sciences of the United States of America *103*, 16159-16164.

Moriyoshi, K., Masu, M., Ishii, T., Shigemoto, R., Mizuno, N., and Nakanishi, S. (1991). Molecular cloning and characterization of the rat NMDA receptor. Nature *354*, 31-37.

Mosbacher, J., Schoepfer, R., Monyer, H., Burnashev, N., Seeburg, P.H., and Ruppersberg, J.P. (1994). A molecular determinant for submillisecond desensitization in glutamate receptors. Science *266*, 1059-1062.

Mukai, T., Kobayashi, T., Hino, N., Yanagisawa, T., Sakamoto, K., and Yokoyama, S. (2008). Adding l-lysine derivatives to the genetic code of mammalian cells with engineered pyrrolysyl-tRNA synthetases. Biochemical and biophysical research communications *371*, 818-822.

Musazzi, L., Milanese, M., Farisello, P., Zappettini, S., Tardito, D., Barbiero, V.S., Bonifacino, T., Mallei, A., Baldelli, P., Racagni, G.*, et al.* (2010). Acute stress increases depolarization-evoked glutamate release in the rat prefrontal/frontal cortex: the dampening action of antidepressants. PloS one *5*, e8566.

Myasnikov, A.G., Simonetti, A., Marzi, S., and Klaholz, B.P. (2009). Structure-function insights into prokaryotic and eukaryotic translation initiation. Current opinion in structural biology *19*, 300-309.

Naganathan, S., Grunbeck, A., Tian, H., Huber, T., and Sakmar, T.P. (2013). Genetically-encoded molecular probes to study G protein-coupled receptors. Journal of visualized experiments: JoVE.

Nakagawa, T., Cheng, Y., Ramm, E., Sheng, M., and Walz, T. (2005). Structure and different conformational states of native AMPA receptor complexes. Nature *433*, 545-549.

Neumann, H., Peak-Chew, S.Y., and Chin, J.W. (2008). Genetically encoding N(epsilon)-acetyllysine in recombinant proteins. Nature chemical biology *4*, 232-234.

Nicoll, R.A. (2006). Auxiliary Subunits Assist AMPA-Type Glutamate Receptors. Science *311*, 1253-1256.

Nirenberg, M.W., Matthaei, J.H., and Jones, O.W. (1962). An intermediate in the biosynthesis of polyphenylalanine directed by synthetic template RNA. Proceedings of the National Academy of Sciences of the United States of America *48*, 104-109.

Noren, C.J., Anthony-Cahill, S.J., Griffith, M.C., and Schultz, P.G. (1989). A general method for site-specific incorporation of unnatural amino acids into proteins. Science *244*, 182-188.

Noren, C.J., Anthony-Cahill, S.J., Suich, D.J., Noren, K.A., Griffith, M.C., and Schultz, P.G. (1990). In vitro suppression of an amber mutation by a chemically aminoacylated transfer RNA prepared by runoff transcription. Nucleic acids research *18*, 83-88.

Nowak, M.W., Gallivan, J.P., Silverman, S.K., Labarca, C.G., Dougherty, D.A., and Lester, H.A. (1998). In vivo incorporation of unnatural amino acids into ion channels in Xenopus oocyte expression system. Methods in enzymology *293*, 504-529.

Nowak, M.W., Kearney, P.C., Sampson, J.R., Saks, M.E., Labarca, C.G., Silverman, S.K., Zhong, W., Thorson, J., Abelson, J.N., Davidson, N.*, et al.* (1995). Nicotinic receptor binding site probed with unnatural amino acid incorporation in intact cells. Science *268*, 439-442.

Otis, T., Zhang, S., and Trussell, L.O. (1996a). Direct measurement of AMPA receptor desensitization induced by glutamatergic synaptic transmission. The Journal of neuroscience: the official journal of the Society for Neuroscience *16*, 7496-7504.

Otis, T.S., Wu, Y.C., and Trussell, L.O. (1996b). Delayed clearance of transmitter and the role of glutamate transporters at synapses with multiple release sites. The Journal of neuroscience: the official journal of the Society for Neuroscience *16*, 1634-1644.

Padgett, C.L., Hanek, A.P., Lester, H.A., Dougherty, D.A., and Lummis, S.C. (2007). Unnatural amino acid mutagenesis of the GABA(A) receptor binding site residues reveals a novel cation-pi interaction between GABA and beta 2Tyr97. The Journal of neuroscience: the official journal of the Society for Neuroscience *27*, 886-892.

Palzer, S., Bantel, Y., Kazenwadel, F., Berg, M., Rupp, S., and Sohn, K. (2013). An expanded genetic code in Candida albicans to study protein-protein interactions in vivo. Eukaryotic cell *12*, 816-827.

Panchenko, V.A., Glasser, C.R., and Mayer, M.L. (2001). Structural similarities between glutamate receptor channels and K(+) channels examined by scanning mutagenesis. The Journal of general physiology *117*, 345-360.

Paoletti, P., Bellone, C., and Zhou, Q. (2013). NMDA receptor subunit diversity: impact on receptor properties, synaptic plasticity and disease. Nature reviews Neuroscience *14*, 383-400.

Paoletti, P., and Neyton, J. (2007). NMDA receptor subunits: function and pharmacology. Current opinion in pharmacology *7*, 39-47.

Parrish, A.R., She, X., Xiang, Z., Coin, I., Shen, Z., Briggs, S.P., Dillin, A., Wang, L. (2012). Expanding the genetic code of Caenorhabditis elegans using bacterial aminoacyl-tRNA synthetase/tRNA pairs. ACS chemical biology *7*, 1292-1302.

Partin, K.M., Bowie, D., and Mayer, M.L. (1995). Structural determinants of allosteric regulation in alternatively spliced AMPA receptors. Neuron *14*, 833-843.

Partin, K.M., Fleck, M.W., and Mayer, M.L. (1996). AMPA receptor flip/flop mutants affecting deactivation, desensitization, and modulation by cyclothiazide, aniracetam, and thiocyanate. The Journal of neuroscience: the official journal of the Society for Neuroscience *16*, 6634-6647.

Pless, S.A., Galpin, J.D., Niciforovic, A.P., and Ahern, C.A. (2011). Contributions of counter-charge in a potassium channel voltage-sensor domain. Nature chemical biology *7*, 617-623.

Pless, S.A., Galpin, J.D., Niciforovic, A.P., Kurata, H.T., and Ahern, C.A. (2013). Hydrogen bonds as molecular timers for slow inactivation in voltage-gated potassium channels. eLife *2*, e01289.

Plested, A.J., and Mayer, M.L. (2009). AMPA receptor ligand binding domain mobility revealed by functional cross linking. The Journal of neuroscience: the official journal of the Society for Neuroscience *29*, 11912-11923.

Pohlsgaard, J., Frydenvang, K., Madsen, U., and Kastrup, J.S. (2011). Lessons from more than 80 structures of the GluA2 ligand-binding domain in complex with agonists, antagonists and allosteric modulators. Neuropharmacology *60*, 135-150.

Prescott, C., Weeks, A.M., Staley, K.J., and Partin, K.M. (2006). Kynurenic acid has a dual action on AMPA receptor responses. Neuroscience letters *402*, 108-112.

Puddifoot, C.A., Chen, P.E., Schoepfer, R., and Wyllie, D.J. (2009). Pharmacological characterization of recombinant NR1/NR2A NMDA receptors with truncated and deleted carboxy termini expressed in Xenopus laevis oocytes. British journal of pharmacology *156*, 509-518.

Robert, A., and Howe, J.R. (2003). How AMPA Receptor Desensitization Depends on Receptor Occupancy. The Journal of neuroscience: the official journal of the Society for Neuroscience *23*, 847-858.

Robert, A., Armstrong, N., Gouaux, J.E., and Howe, J.R. (2005). AMPA receptor binding cleft mutations that alter affinity, efficacy, and recovery from desensitization. The Journal of neuroscience: the official journal of the Society for Neuroscience *25*, 3752-3762.

Rodnina, M.V., and Wintermeyer, W. (2009). Recent mechanistic insights into eukaryotic ribosomes. Current opinion in cell biology *21*, 435-443.

Rosenmund, C., Stern-Bach, Y., and Stevens, C.F. (1998). The tetrameric structure of a glutamate receptor channel. Science *280*, 1596-1599.

Rothman, J.S., Cathala, L., Steuber, V., and Silver, R.A. (2009). Synaptic depression enables neuronal gain control. Nature *457*, 1015-1018.

Rozov, A., Jerecic, J., Sakmann, B., and Burnashev, N. (2001). AMPA receptor channels with long-lasting desensitization in bipolar interneurons contribute to synaptic depression in a novel feedback circuit in layer 2/3 of rat neocortex. The Journal of neuroscience: the official journal of the Society for Neuroscience *21*, 8062-8071.

Rubio, M.D., Drummond, J.B., and Meador-Woodruff, J.H. (2012). Glutamate receptor abnormalities in schizophrenia: implications for innovative treatments. Biomolecules & therapeutics *20*, 1-18.

Ryu, K., Yokoyama, M., Yamashita, M., and Hirano, T. (2012). Induction of excitatory and inhibitory presynaptic differentiation by GluD1. Biochemical and biophysical research communications *417*, 157-161.

Sakamoto, K., Hayashi, A., Sakamoto, A., Kiga, D., Nakayama, H., Soma, A., Kobayashi, T., Kitabatake, M., Takio, K., Saito, K., Shirouzu, M., Hirao, I., and Yokoyama, S. (2002). Site-specific incorporation of an unnatural amino acid into proteins in mammalian cells. Nucleic acids research *30*, 4692-4699.

Sakimura, K., Bujo, H., Kushiya, E., Araki, K., Yamazaki, M., Yamazaki, M., Meguro, H., Warashina, A., Numa, S., and Mishina, M. (1990). Functional expression from cloned cDNAs of glutamate receptor species responsive to kainate and quisqualate. FEBS letters *272*, 73-80.

Sakmann, B., and Neher, E. (1984). Patch clamp techniques for studying ionic channels in excitable membranes. Annual review of physiology *46*, 455-472.

Saks, M.E., Sampson, J.R., Nowak, M.W., Kearney, P.C., Du, F., Abelson, J.N., Lester, H.A., and Dougherty, D.A. (1996). An engineered Tetrahymena tRNAGln for in vivo incorporation of unnatural amino acids into proteins by nonsense suppression. The Journal of biological chemistry *271*, 23169-23175.

Salussolia, C.L., Corrales, A., Talukder, I., Kazi, R., Akgul, G., Bowen, M., and Wollmuth, L.P. (2011). Interaction of the M4 segment with other transmembrane segments is required for surface expression of mammalian alpha-amino-3-hydroxy-5-methyl-4-isoxazolepropionic acid (AMPA) receptors. The Journal of biological chemistry *286*, 40205-40218.

Sato, S., Mimasu, S., Sato, A., Hino, N., Sakamoto, K., Umehara, T., and Yokoyama, S. (2011). Crystallographic study of a site-specifically cross-linked protein complex with a genetically incorporated photoreactive amino acid. Biochemistry *50*, 250-257.

Schauder, D.M., Kuybeda, O., Zhang, J., Klymko, K., Bartesaghi, A., Borgnia, M.J., Mayer, M.L., and Subramaniam, S. (2013). Glutamate receptor desensitization is mediated by changes in quaternary structure of the ligand binding domain. Proceedings of the National Academy of Sciences of the United States of America *110*, 5921-5926.

Schmid, S.M., and Hollmann, M. (2008). To gate or not to gate: are the delta subunits in the glutamate receptor family functional ion channels? Molecular neurobiology *37*, 126-141.

Schorge, S., and Colquhoun, D. (2003). Studies of NMDA receptor function and stoichiometry with truncated and tandem subunits. The Journal of neuroscience: the official journal of the Society for Neuroscience *23*, 1151-1158.

Schwenk, J., Harmel, N., Brechet, A., Zolles, G., Berkefeld, H., Muller, C.S., Bildl, W., Baehrens, D., Huber, B., Kulik, A., Kloecker, N., Schulte, U., and Fakler, B. (2012). High-resolution proteomics unravel architecture and molecular diversity of native AMPA receptor complexes. Neuron *74*, 621-633.

Schwenk, J., Harmel, N., Zolles, G., Bildl, W., Kulik, A., Heimrich, B., Chisaka, O., Jonas, P., Schulte, U., Fakler, B., and Kloecker, N. (2009). Functional proteomics identify cornichon proteins as auxiliary subunits of AMPA receptors. Science *323*, 1313-1319.

Schwyzer, R., and Caviezel, M. (1971). p-Azido-L-phenylalanine: a photo-affinity 'probe' related to tyrosine. Helvetica chimica acta *54*, 1395-1400.

Shanks, N.F., Maruo, T., Farina, A.N., Ellisman, M.H., and Nakagawa, T. (2010). Contribution of the global subunit structure and stargazin on the maturation of AMPA receptors. The Journal of neuroscience: the official journal of the Society for Neuroscience *30*, 2728-2740.

Shen, B., Xiang, Z., Miller, B., Louie, G., Wang, W., Noel, J.P., Gage, F.H., and Wang, L. (2011). Genetically encoding unnatural amino acids in neural stem cells and optically reporting voltage-sensitive domain changes in differentiated neurons. Stem cells *29*, 1231-1240.

Sheng, M., and Sala, C. (2001). PDZ domains and the organization of supramolecular complexes. Annu Rev Neurosci *24*, 1-29.

Shepherd, J.D., and Huganir, R.L. (2007). The cell biology of synaptic plasticity: AMPA receptor trafficking. Annual review of cell and developmental biology *23*, 613-643.

Shoelsen, S.E., Lee, J., Lynch, C.S., Backer, J.M., and Pilch, P.F (1993). BpaB25 insulins. Photoactivatable analogues that quantitatively cross-link, radiolabel, and activate the insulin receptor. The Journal of biological chemistry *268*, 4085-4091.

Sobolevsky, A.I., Rosconi, M.P., and Gouaux, E. (2009). X-ray structure, symmetry and mechanism of an AMPA-subtype glutamate receptor. Nature *462*, 745-756.

Sommer, B., Burnashev, N., Verdoorn, T.A., Keinanen, K., Sakmann, B., and Seeburg, P.H. (1992). A glutamate receptor channel with high affinity for domoate and kainate. The EMBO journal *11*, 1651-1656.

Sommer, B., Keinanen, K., Verdoorn, T.A., Wisden, W., Burnashev, N., Herb, A., Kohler, M., Takagi, T., Sakmann, B., and Seeburg, P.H. (1990). Flip and flop: a cell-specific functional switch in glutamate-operated channels of the CNS. Science *249*, 1580-1585.

Sommer, B., Kohler, M., Sprengel, R., and Seeburg, P.H. (1991). RNA editing in brain controls a determinant of ion flow in glutamate-gated channels. Cell *67*, 11-19.

Spalloni, A., Nutini, M., and Longone, P. (2013). Role of the N-methyl-d-aspartate receptors complex in amyotrophic lateral sclerosis. Biochimica et biophysica acta *1832*, 312-322.

Srinivasan, G., James, C.M., and Krzycki, J.A. (2002). Pyrrolysine encoded by UAG in Archaea: charging of a UAG-decoding specialized tRNA. Science *296*, 1459-1462.

Stern-Bach, Y., Bettler, B., Hartley, M., Sheppard, P.O., O'Hara, P.J., and Heinemann, S.F. (1994). Agonist selectivity of glutamate receptors is specified by two domains structurally related to bacterial amino acid-binding proteins. Neuron *13*, 1345-1357.

Stern-Bach, Y., Russo, S., Neuman, M., and Rosenmund, C. (1998). A point mutation in the glutamate binding site blocks desensitization of AMPA receptors. Neuron *21*, 907-918.

Sun, Y., Olson, R., Horning, M., Armstrong, N., Mayer, M., and Gouaux, E. (2002). Mechanism of glutamate receptor desensitization. Nature *417*, 245-253.

Takimoto, J.K., Adams, K.L., Xiang, Z., and Wang, L. (2009). Improving orthogonal tRNA-synthetase recognition for efficient unnatural amino acid incorporation and application in mammalian cells. Molecular bioSystems *5*, 931-934.

Tanaka, Y., Bond, M.R., and Kohler, J.J. (2008). Photocrosslinkers illuminate interactions in living cells. Molecular bioSystems *4*, 473-480.

Thermo Fisher Scientific, Inc. (2009). Light sources and conditions for photoactivation of aryl azide crosslinking and labeling reagents. Handbook TR0011.2.

Thibodeaux, G.N., Liang, X., Moncivais, K., Umeda, A., Singer, O., Alfonta, L., and Zhang, Z.J. (2010). Transforming a pair of orthogonal tRNA-aminoacyl-tRNA synthetase from Archaea to function in mammalian cells. PloS one *5*, e11263.

Tichelaar, W., Safferling, M., Keinanen, K., Stark, H., and Madden, D.R. (2004). The Three-dimensional Structure of an Ionotropic Glutamate Receptor Reveals a Dimer-of-dimers Assembly. Journal of molecular biology *344*, 435-442.

Tong, Y., Brandt, G.S., Li, M., Shapovalov, G., Slimko, E., Karschin, A., Dougherty, D.A., and Lester, H.A. (2001). Tyrosine decaging leads to substantial membrane trafficking during modulation of an inward rectifier potassium channel. The Journal of general physiology *117*, 103-118.

Torrice, M.M., Bower, K.S., Lester, H.A., and Dougherty, D.A. (2009). Probing the role of the cation-pi interaction in the binding sites of GPCRs using unnatural amino acids. Proceedings of the National Academy of Sciences of the United States of America *106*, 11919-11924.

Tracy, T.E., Yan, J.J., and Chen, L. (2011). Acute knockdown of AMPA receptors reveals a trans-synaptic signal for presynaptic maturation. The EMBO journal *30*, 1577-1592.

Traynelis, S.F., Wollmuth, L.P., McBain, C.J., Menniti, F.S., Vance, K.M., Ogden, K.K., Hansen, K.B., Yuan, H., Myers, S.J., and Dingledine, R. (2010). Glutamate receptor ion channels: structure, regulation, and function. Pharmacological reviews *62*, 405-496.

Trussell, L.O., and Fischbach, G.D. (1989). Glutamate receptor desensitization and its role in synaptic transmission. Neuron *3*, 209-218.

Trussell, L.O., Zhang, S., and Raman, I.M. (1993). Desensitization of AMPA receptors upon multiquantal neurotransmitter release. Neuron *10*, 1185-1196.

Turcatti, G., Nemeth, K., Edgerton, M.D., Meseth, U., Talabot, F., Peitsch, M., Knowles, J., Vogel, H., and Chollet, A. (1996). Probing the structure and function of the tachykinin neurokinin-2 receptor through biosynthetic incorporation of fluorescent amino acids at specific sites. The Journal of biological chemistry *271*, 19991-19998.

von Engelhardt, J., Mack, V., Sprengel, R., Kavenstock, N., Li, K.W., Stern-Bach, Y., Smit, A.B., Seeburg, P.H., and Monyer, H. (2010). CKAMP44: a brain-specific protein attenuating short-term synaptic plasticity in the dentate gyrus. Science *327*, 1518-1522.

Walsh, C.T., Garneau-Tsodikova, S., and Gatto, G.J., Jr. (2005). Protein posttranslational modifications: the chemistry of proteome diversifications. Angewandte Chemie *44*, 7342-7372.

Wang, F., Robbins, S., Guo, J., Shen, W., and Schultz, P.G. (2010). Genetic incorporation of unnatural amino acids into proteins in Mycobacterium tuberculosis. PloS one *5*, e9354.

Wang, L., Brock, A., Herberich, B., and Schultz, P.G. (2001). Expanding the genetic code of Escherichia coli. Science *292*, 498-500.

Wang, L., and Schultz, P.G. (2001). A general approach for the generation of orthogonal tRNAs. Chem Biol *8*, 883-890.

Wang, L., and Schultz, P.G. (2004). Expanding the genetic code. Angewandte Chemie *44*, 34-66.

Wang, L., Xie, J., and Schultz, P.G. (2006). Expanding the genetic code. Annual review of biophysics and biomolecular structure *35*, 225-249.

Wang, W., Takimoto, J.K., Louie, G.V., Baiga, T.J., Noel, J.P., Lee, K.F., Slesinger, P.A., and Wang, L. (2007). Genetically encoding unnatural amino acids for cellular and neuronal studies. Nature neuroscience *10*, 1063-1072.

Watson, J.D. (1964). The Synthesis of Proteins Upon Ribosomes. Bulletin de la Societe de chimie biologique *46*, 1399-1425.

Wenthold, R.J., Petralia, R.S., Blahos, J., II, and Niedzielski, A.S. (1996). Evidence for multiple AMPA receptor complexes in hippocampal CA1/CA2 neurons. The Journal of neuroscience: the official journal of the Society for Neuroscience *16*, 1982-1989.

Wenthold, R.J., Yokotani, N., Doi, K., and Wada, K. (1992). Immunochemical characterization of the non-NMDA glutamate receptor using subunit-specific antibodies. Evidence for a hetero-oligomeric structure in rat brain. The Journal of biological chemistry *267*, 501-507.

Weston, M.C., Gertler, C., Mayer, M.L., and Rosenmund, C. (2006a). Interdomain interactions in AMPA and kainate receptors regulate affinity for glutamate. The Journal of neuroscience: the official journal of the Society for Neuroscience *26*, 7650-7658.

Weston, M.C., Schuck, P., Ghosal, A., Rosenmund, C., and Mayer, M.L. (2006b). Conformational restriction blocks glutamate receptor desensitization. Nature structural & molecular biology *13*, 1120-1127.

Williams, K. (1997). Modulation and block of ion channels: a new biology of polyamines. Cellular signalling *9*, 1-13.

Woese, C.R., Olsen, G.J., Ibba, M., and Soll, D. (2000). Aminoacyl-tRNA synthetases, the genetic code, and the evolutionary process. Microbiology and molecular biology reviews: MMBR *64*, 202-236.

Wollmuth, L.P., and Sobolevsky, A.I. (2004). Structure and gating of the glutamate receptor ion channel. Trends in neurosciences *27*, 321-328.

Yamazaki, M., Araki, K., Shibata, A., and Mishina, M. (1992). Molecular cloning of a cDNA encoding a novel member of the mouse glutamate receptor channel family. Biochemical and biophysical research communications *183*, 886-892.

Yanagisawa, T., Ishii, R., Fukunaga, R., Kobayashi, T., Sakamoto, K., and Yokoyama, S. (2008). Multistep engineering of pyrrolysyl-tRNA synthetase to genetically encode N(epsilon)-(o-azidobenzyloxycarbonyl) lysine for site-specific protein modification. Chemistry and biology *15*, 1187-1197.

Yang, F., Moss, L.G., and Phillips, G.N., Jr. (1996). The molecular structure of green fluorescent protein. Nature biotechnology *14*, 1246-1251.

Yao, Y., Belcher, J., Berger, A.J., Mayer, M.L., and Lau, A.Y. (2013). Conformational analysis of NMDA receptor GluN1, GluN2, and GluN3 ligand-binding domains reveals subtype-specific characteristics. Structure *21*, 1788-1799.

Ye, S., Huber, T., Vogel, R., and Sakmar, T.P. (2009). FTIR analysis of GPCR activation using azido probes. Nature chemical biology *5*, 397-399.

Ye, S., Kohrer, C., Huber, T., Kazmi, M., Sachdev, P., Yan, E.C., Bhagat, A., RajBhandary, U.L., and Sakmar, T.P. (2008). Site-specific incorporation of keto amino acids into functional G protein-coupled receptors using unnatural amino acid mutagenesis. The Journal of biological chemistry *283*, 1525-1533.

Ye, S., Riou, M., Carvalho, S., and Paoletti, P. (2013). Expanding the genetic code in Xenopus laevis oocytes. Chembiochem: a European journal of chemical biology *14*, 230-235.

Ye, S., Zaitseva, E., Caltabiano, G., Schertler, G.F., Sakmar, T.P., Deupi, X., and Vogel, R. (2010). Tracking G-protein-coupled receptor activation using genetically encoded infrared probes. Nature *464*, 1386-1389.

Young, T.S., Ahmad, I., Brock, A., and Schultz, P.G. (2009). Expanding the genetic repertoire of the methylotrophic yeast Pichia pastoris. Biochemistry *48*, 2643-2653.

Zhang, Z., Alfonta, L., Tian, F., Bursulaya, B., Uryu, S., King, D.S., and Schultz, P.G. (2004). Selective incorporation of 5-hydroxytryptophan into proteins in mammalian cells. Proceedings of the National Academy of Sciences of the United States of America *101*, 8882-8887.

Zhu, H., and Snyder, M. (2003). Protein chip technology. Current opinion in chemical biology *7*, 55-63.

Zhu, J.J., Esteban, J.A., Hayashi, Y., and Malinow, R. (2000). Postnatal synaptic potentiation: delivery of GluR4-containing AMPA receptors by spontaneous activity. Nature neuroscience *3*, 1098-1106.

Zhu, S., Riou, M., Yao, C.A., Carvalho, S., Rodriguez, P.C., Bensaude, O., Paoletti, P., and Ye, S. (2014). Genetically encoding a light switch in an ionotropic glutamate receptor reveals subunit-specific interfaces. Proceedings of the National Academy of Sciences of the United States of America *111*, 6081-6086.

Ziff, E.B. (2007). TARPs and the AMPA receptor trafficking paradox. Neuron *53*, 627-633.

Affidavit

“I, Viktoria Klippenstein, certify under penalty of perjury by my own signature that I have composed the thesis on the topic “Photoinactivation of Glutamate Receptors by Genetically Encoded Unnatural Amino Acids” independently and without assistance from third parties. I used no other aids and resources than those listed.

All points based literally or in spirit on publications or presentations of other authors are, as such, indicated in proper citations (see "uniform requirements for manuscripts (URM)" the ICMJE www.icmje.org). The sections on methodology (in particular practical work, laboratory requirements, statistical processing) and results (in particular images, graphics and tables) correspond to the URM (see above) and are entirely my responsibility.

My interest in any publications related to this dissertation corresponds to those that are specified in the following joint declaration with the responsible person and supervisor Prof. Dr. Christian Rosenmund. All publications resulting from this thesis correspond to the URM (see above) and I am responsible for this correspondence.

The importance of this affidavit and the criminal consequences of a false affidavit (sections 156,161 of the Criminal Code) are known to me and I understand the rights and responsibilities stated therein.

Date Signature

Cirriculum vitae

Mein Lebenslauf wird aus datenschutzrechtlichen Gruenden in der elektronischen Version meiner Arbeit nicht veroeffentlicht.

List of publications

Viktoria Klippenstein contributed to the following publications:

In the framework of her Master´s thesis:

- Klugmann M, **Klippenstein V**, Spanagel R, Leweke FM, Schneider M (*2011*) Cannabinoid exposure in pubertal rats increases spontaneous ethanol consumption and NMDA receptor associated protein levels. *Int J Neuropsychopharmacol. 14: 505–517*

In the framework of her PhD thesis:

- **Klippenstein V**, Ghisi V, Wietstruk M, Plested AJR (*2014*) Photoinactivation of glutamate receptors by genetically encoded unnatural amino acids. *Journal of Neuroscience 34(3): 980-91*

Together with Dr. Andrew Plested, Viktoria Klippenstein designed the published project. She was responsible for the practical performance of the experiments. All electrophysiological measurements were perfomed by Viktoria Klippenstein. She had technical assistance for cloning (Markus Wietstruk) and for Western blotting (Dr. Valentina Ghisi). Viktoria Klippenstein is entirely responsible for the data analysis. The design of graphs and the writing of the publication was carried out by Viktoria Klippenstein and Dr. Andrew Plested.

Signature of the doctoral candidate

Acknowledgements

I want to sincerely thank my project supervisor Dr. Andrew Plested for his guidance, his patience, and his enthusiasm. Throughout the last four years, he always had the ability to motivate me even when things were not running as desired. He has been a good scientific role model and contributed greatly to my development as a scientist.

I would also like to thank Prof. Dr. Christian Rosenmund for being my PhD supervisor and for facilitating the doctoral examinaion procedure.

Thanks to the Cluster of Excellence "NeuroCure" for the financial support and to the PhD graduate school "Medical Neurosciences" of the Chrité Universitätsmedizin for the fellowship.

Sincere thanks to the members of my annual PhD committee meetings, Prof. Dr. Stephan Sigrist, Dr. Jens Peter von Kries, and Dr. Hector Salazar, for the valuable discussions and suggestions on my work.

Many thanks to Prof. Thomas Sakmar and Dr. Xishin Ye for the gift of the tRNA / tRNA-synthetase pairs.

I would like to thank Dr. Chris Ahern and Dr. Sam Goodchild for their great advice and helpful comments on the project.

Thanks to Prof. Dr. Thomas Jentsch for allowing me to use the confocal microscope. Thanks to his lab members, who reliably perfomed the DNA sequencing.

Many thanks to Dr. Björn Schröder for the loan of the UVICO lamp.

I want to acknowledge Marcus Wietstruk for his outstanding help in making mutants and for mastering every molecular biological challenge.

Sincere thanks to Dr. Valentina Ghisi for perfoming the Western blots.

I want to sincerely thank everyone else from the team, JB, Milla, Hector, Anna, Vera, Miriam, Carissa, Mette – for all the support, for the wonderful atmosphere in the office, for all the laughter, and their friendship. I will miss all of them a lot.

Thanks to my lovely friends outside the lab, Ann-So, Yalda, Alex, Johannes and Dennis, who have always been laughing and crying with me.

Above all, I would sincerely like to thank my family for giving me so much energy and love. Ich habe Euch sehr lieb!